S. Sritharan, S. Aaleti, D. J. Thomas

Seismic Analysis and Design of Precast Concrete Jointed Wall Systems

ISU-ERI-Ames Report ERI-07404
Submitted to the
Precast/Prestressed Concrete Institute

DECEMBER 2007

Final

REPORT

IOWA STATE UNIVERSITY
OF SCIENCE AND TECHNOLOGY

Department of Civil, Construction and Environmental Engineering

Seismic Analysis and Design of Precast Concrete Jointed Wall Systems

by

Sri Sritharan
Associate Professor

Sriram Aaleti
Graduate Research Assistant

Derek J. Thomas
Former Graduate Student

ISU-ERI-Ames Report ERI-07404

A Final Report to the Precast/Prestressed Concrete

Department of Civil, Construction and Environmental Engineering
Iowa State University
Ames, IA 50011

December 2007

Intentionally blank

ABSTRACT

This report, which was produced as a part of research project undertaken to assist with codification of the jointed precast wall systems designed with unbonded post-tensioning for seismic regions, presents a simplified analysis and a design method for jointed wall systems. Prior to establishing the analysis and design methods, the performance of the jointed wall system included in the PRESSS (PREcast Seismic Structural System) test building is summarized using the test data that has been carefully processed to reflect the suitable initial conditions. Next, results from tests completed on the material and U-shaped flexural plate (UFP) connectors that were used as the primary energy dissipation elements in the PRESSS jointed wall system are presented and a force-displacement response envelope suitable for this connector that may be used in the design if jointed wall systems is recommended.

Section analysis of flexural concrete members designed with jointed connections and unbonded reinforcement cannot be performed using conventional methods because the strain compatibility condition between steel and concrete does not exist at the section level. Therefore, suitable approximations must be made to simplify the design and analysis methods for such members. The simplified analysis procedure presented in this report makes an approximation on variation in the neutral axis depth as a function of the base rotation and enables characterization of jointed wall behavior under monotonic loading. The validation of this analysis procedure is presented using the data from the PRESSS wall system. The applicability of the proposed analysis procedure for single precast walls designed with unbonded post-tensioning is also demonstrated using the wall tests completed at Lehigh University.

Finally, a design methodology is introduced for the jointed precast wall systems, which is also equally applicable to single precast walls that may be designed with unbonded post-tensioning. This design methodology is based on the guidelines originally proposed as part of the PRESSS program with significant enhancements to a number of critical issues. The application of this design method is also demonstrated using design examples.

ACKNOWLEDGEMENTS

The research described in this report was funded by the Precast/Prestressed Concrete Institute (PCI) in order to support codification effort of the precast wall systems with unbonded post-tensioning. The authors would like to thank Mr. Paul Johal and Mr. Jason J. Krohn of PCI for their contribution towards coordination of this project. Additionally, the authors thank Dr. Neil M. Hawkins, Professor Emeritus at the University of Illinois at Urbana-Champaign, and Dr. S. K. Ghosh of SK Ghosh Associates Inc. for their assistance during the course of this project. Dax Kuhfuss, Brett Pleima and Rick Snyder are current or former undergraduate students at Iowa State University and their assistance with data reduction of the jointed wall system reported in Chapter 2 are gratefully acknowledged.

Conclusions, opinions and recommendations expressed in this report are those of the authors alone, and should not be construed as being endorsed by the financial sponsor.

TABLE OF CONTENTS

Intentionally blank

CHAPTER 1: INTRODUCTION

1.1 General

Concrete structural walls provide a cost effective means to resist seismic lateral loads and thus they are frequently used as the primary lateral load resisting system in reinforced concrete buildings. Structural walls with high flexural stiffness typically assists with limiting interstory drifts in buildings, consequently reducing structural and non-structural damage during seismic events. Superior performance of buildings that consisted of structural walls was evident in several past seismic events (Fintel, 1974; Fintel, 1991; Fintel 1995). The concrete structural walls can be of cast-in-place concrete or of precast concrete. With the added benefits of prefabrication, precast walls make an excellent choice for resisting lateral loads in concrete buildings. However, the application of precast systems is generally limited in seismic regions due to the lack of research information, which, in turn, has imposed constraints in the current design codes. This chapter presents an introductory discussion on the performance of the structural walls in past earthquakes, the concept of precast unbonded jointed wall systems for seismic regions, and the scope of research presented in this report.

1.2 Past Performance of Precast Structures with Structural Walls

Significant structural damage to concrete frame buildings and precast structures has been observed in moderate to large earthquakes that have occurred from 1960 to 1999. Fintel (1991), who examined the structural damage of buildings after several of these earthquakes, reported based on earthquake damage observed until the late1980s that there was not a single concrete building with structural walls that experienced any significant damage. Thomas and Sritharan (2004) conducted a detailed literature review on the seismic performance of precast structures with structural walls during the seismic events that occurred between 1960 and 1990. The most damaging recent earthquakes, which alerted the engineering community to closely examine the seismic behavior of precast structures, were the 1994 Northridge earthquake in California, the 1995 Kobe earthquake in Japan, and the 1999 Kocaeli earthquake in Turkey.

In the 1994 Northridge earthquake, several precast concrete parking structures performed poorly, causing significant structural damage (see Figure 2.1). The primary cause for this damage was not any inherent deficiency in precast concrete elements, but was due to the use of poor connection details between precast elements and not ensuring deformation compatibility between the earthquake force resisting system and gravity frames in the structures that contribute to sustaining the gravity loads. A post-earthquake investigation of the structural damage following the Northridge earthquake revealed that the lateral load resisting precast shear walls remained uncracked, while precast concrete elements of the floor system collapsed (Ghosh, 2001).

Figure 1.1 Collapse of the second level of the Northridge Fashion Center parking garage constructed using precast post-tensioned technology (Photo Credit: J. Dewey, USGS).

A positive aspect of all the devastation caused by the 1995 Kobe earthquake was good performance of several precast and prestressed concrete structures. Apartment buildings in Japan are typically two-to-five stories in height, and some of these buildings also include precast concrete walls as the primary elements to resist both the gravity and lateral loads. None of these buildings that included the precast walls experienced any damage in the Kobe earthquake (see an example in Figure 1.2), while cracking of concrete members was observed

in cast-in-place concrete buildings. In the 1999 Kocaeli earthquake, a few apartment buildings with large precast wall panels connected in vertical and horizontal directions were found to have performed more than adequately amidst significant devastation (see Figure 1.3).

(a) Example 1 (b) Example 2

Figure 1.2 Precast concrete structures that sustained no structural damage when subjected to the 1995 Kobe earthquakes in Japan (Ghosh, 2001).

Figure 1.3 Precast concrete building that sustained no damage when subjected to the 1999 Kocaeli earthquake in Turkey (Ghosh, 2001).

1.3 Limitations of Precast Concrete Application in Seismic Regions

There are several limitations that restrict the use of precast concrete in seismic regions. The primary limitation stems from poor performance of precast concrete frame buildings in the past seismic events. Although the poor performance of buildings was largely attributed to the use of substandard materials, poor construction practices, and insufficient design of connections, it had contributed to the decline of designers' confidence in the use of precast concrete in seismic design (Park, 1995).

Stringent provisions in the model building codes of the United States (e.g., the Uniform Building Code (1997); the NEHRP Recommended Provisions (Building Seismic Safety Council, 1997); and the International Building Code (2003)) also limit the applications of precast concrete in seismic regions. Typically, these building codes require that the precast seismic systems be shown by analysis and tests to have lateral load resisting characteristics that are equal or superior to those of monolithic cast-in-place reinforced concrete systems. This requirement has led to the development of a design concept known as the 'cast-in-place emulation' (Ghosh 2002; Vernu and Sritharan, 2004; and ACI Committee 318, 2005). To develop precast systems using the cast-in-place emulation, the current building codes propose two alternative designs: 1) structural systems that use "wet joints"; and 2) structural systems based on "dry joints". In precast structural systems with wet joints, the connections are established using in-situ concrete to achieve the cast-in-place emulation (Vernu and Sritharan, 2004). However, these systems do not have all of the economical advantages of precast concrete technology because of the use of in-situ concrete. Furthermore, precast concrete systems that emulate the cast-in-place concrete systems have joints that are typically proportioned with sufficient strength to avoid inelastic deformations within these joints. Plastic hinges in these systems are forced to develop in the precast members, which does not lead to an economical design. Dry joints in precast buildings are typically established through bolting, welding, or by other mechanical means. The behavior of precast concrete systems with dry joints differs from that of the emulation systems because the dry joints create natural discontinuities in the structure. The dry joints are often inherently less stiff than the precast members, and thus the deformations tend to concentrate at these joints.

The aforementioned limitations of precast concrete systems have created opportunities for development of innovative precast concrete seismic structural systems that may be quite different from the emulation types in term of concept and behavior (Nakaki et al. 1999). Also, it is apparent that such new structural systems with an established set of design guidelines will promote the confidence in the designers to use the precast concrete option for seismic design.

1.4 The PRESSS Program

In response to the recognized need to overcome the limitations for the use of precast concrete in seismic regions, the PRESSS (PREcast Seismic Structural Systems) program was initiated in the early 1990's in the United States. Through this program, researchers envisioned to fulfill two primary objectives: (1) to develop comprehensive and rational design recommendations based on fundamental and basic research data which will emphasize the viability of precast construction in various seismic zones, and (2) to develop new materials, concepts and technologies for precast construction suitable for seismic application (Priestley 1991).

As part of the PRESSS program, several precast structural component tests were conducted at different institutions around the country, followed by seismic testing of a five-story precast concrete building at the University of California at San Diego (UCSD). These tests, which promoted the use of unbonded prestressing, were aimed to 1) demonstrate the viability of precast concrete design for regions of moderate to high seismicity; 2) establish dependable seismic performance for properly designed precast concrete structural systems; 3) emphasize the advantages of seismic performance of precast concrete structural systems over the equivalent reinforced concrete or steel structural systems; 4) demonstrate the adequate details of precast gravity frames, which are not part of the precast building system(s) resisting lateral seismic forces; 5) establish predictability of behavior of precast concrete buildings using state-of-the-art analytical tools; and 6) develop design guidelines for precast concrete structures in seismic zones, which can be incorporated into the model building codes.

The precast structural wall systems investigated as a part of the PRESSS program were the unbonded post-tensioned single walls and unbonded post-tensioned jointed wall systems. The unbonded post-tensioned single walls were primarily studied through analytical means by researchers at Lehigh University (Kurama et al., 1999a; Kurama et al., 1999b; Kurama et al., 2002). They have recently tested several unbonded post-tensioned precast single walls with horizontal joints under simulated lateral seismic loading (Perez et al., 2004). A jointed precast wall system with unbonded post-tensioning was included in the PRESSS test building (Nakaki et al., 1999; Priestley et al., 1999; and Sritharan et al., 2002), which is the focus of this report. However, the analysis and design chapters included in this report are applicable for single walls designed with unbonded post-tensioning tendons. Selected experimental results from Perez et al. (2004) are used in Chapter 4 to validate the proposed analysis procedure for these types of walls.

1.4.1 Jointed Precast Concrete Wall System

In a jointed wall system, two or more single precast walls designed with unbonded post-tensioning are connected to each other with the help of special connectors along the vertical joints, as shown in Figure 1.4. The post-tensioning steel in each wall may be distributed symmetrically along its length or concentrated at the center of the wall. The basic concept of the wall system is that it allows the walls to rock individually at the base when the wall system is subjected to lateral loads and return them to their original position after the event has concluded.

The post-tensioning steel is typically designed to remain elastic under the design-level earthquake loading. As a result, it provides the restoring force needed for the jointed wall to re-center when the applied lateral load is removed, thereby minimizing its residual displacements. The restoring capacity of the jointed wall depends on the amount of post-tensioning steel, the number of vertical connectors, initial prestressing force, and the cyclic behavior of the vertical connector. The vertical connectors dissipate seismic energy by experiencing inelastic deformations under the applied earthquake loads. Therefore, the jointed wall systems have the ability to dissipate energy with minimal damage and little residual

displacements. The shear transfer from the wall to the foundation at the base utilizes a friction mechanism.

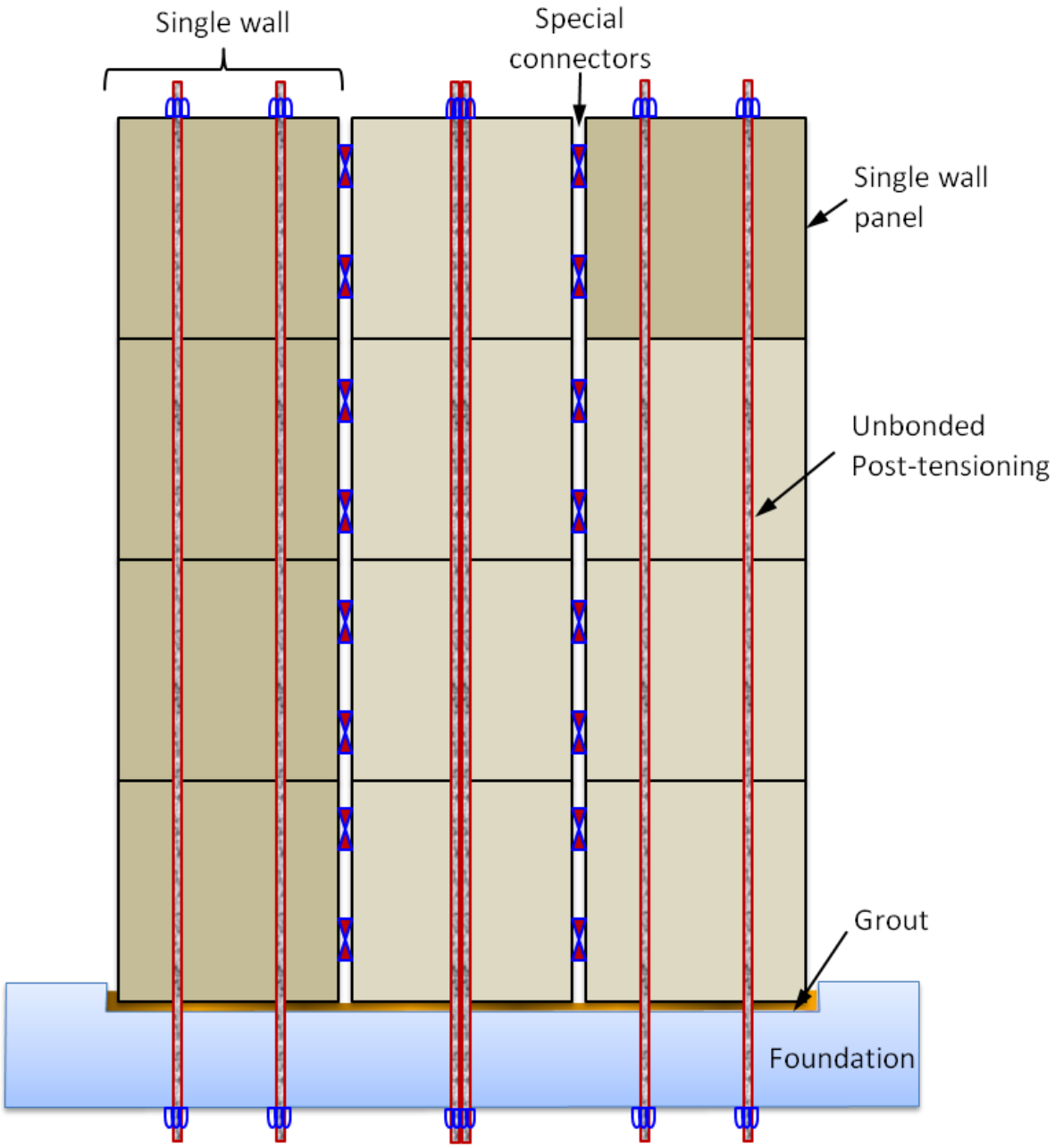

Figure 1.4 The concept of the jointed precast wall system.

In the PRESSS test building, a two-wall jointed system was included as the primary lateral load resisting system parallel to a building axis (see Figure 1.5). Its seismic response was excellent under simulated in-plane seismic loading. At the design-level earthquake load

testing, the wall system experienced a lateral displacement of up to 8.34 in., which corresponded to a drift of 1.85%. At the next level of testing with an input motion 1.5 times the design level event, a maximum lateral wall displacement of 11.53 in., corresponding to a drift of 2.56%, was measured. As intended in the design, flexural cracking concentrated at the base of the walls, thereby minimizing the damage experienced by the wall system during the entire test. Some hairline cracks, which developed within the first story of the structure at the design level testing, completely closed upon unloading of the lateral loads. Minor, easily repairable crushing of cover concrete occurred at the compression ends of the leading wall base over a height of about 6 in. when subjected to the maximum lateral drift of 2.56%. More complete results of this test are reported in Chapter 2.

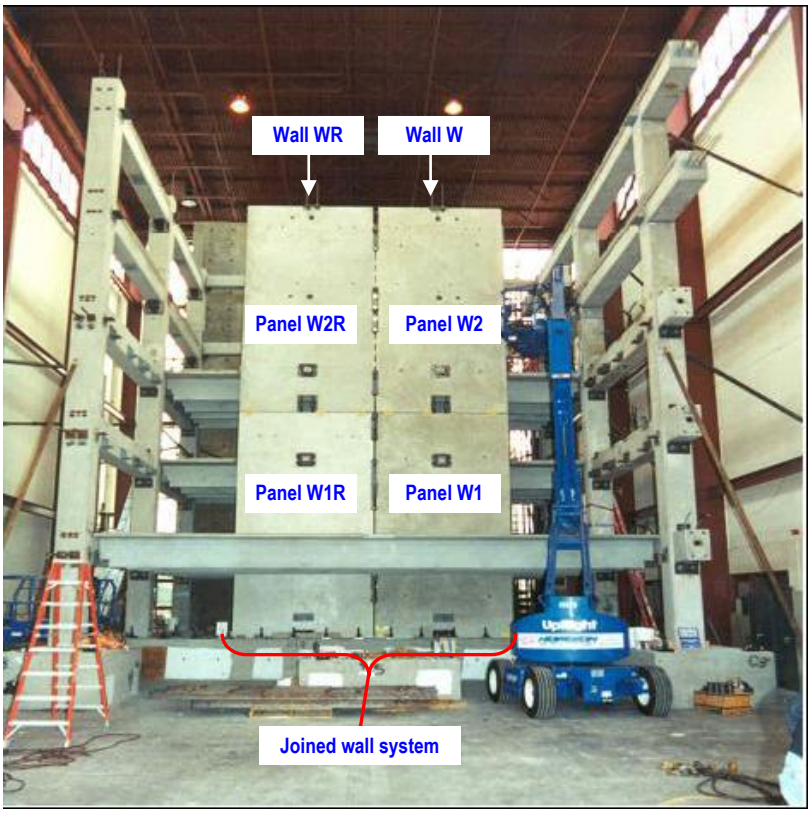

Figure 1.5 The two-wall jointed system included in the PRESSS building.

At the end of the PRESSS research program, design guidelines were proposed by Stanton and Nakaki (2002) for several precast frame connections and the jointed wall system

included in the PRESSS test building. In a subsequent study, the validation of the proposed design guidelines for precast hybrid frames and jointed wall systems was conducted by researchers at Iowa State University (Celik and Sritharan, 2004; Thomas and Sritharan, 2004). As part of this investigation, several shortcomings in the design guidelines proposed for the jointed wall system were reported by Thomas and Sritharan (2004). They also found that the design guidelines as proposed by Stanton and Nakaki would not lead to economical design. This finding was confirmed by Ghosh of S. K. Ghosh Associates, Inc., who created design examples based on the proposed design guidelines. Following the publication of the design guidelines, an effort was undertaken by the Precast/Prestressed Concrete Institute (PCI) to codify the precast jointed wall system for seismic design. Professor Neil Hawkins and Dr. S. K. Ghosh have been responsible for this effort on behalf of PCI. The codification process is executed through ACI Innovation Task Group 5 (ITG-5), with an intention that the group will publish the following two documents to be referenced in the ACI Building Standards:

- ITG 5.1: *Acceptance Criteria for Special Unbonded Post-Tensioned Precast Structural Walls Based on Validation Testing* (ACI Innovation Task Group 5, 2007), and
- ITG 5.2: *Special Unbonded Post-Tensioned Precast Structural Walls*.

1.5 Research Tasks

The research project presented in this report was initiated in support of the codification effort undertaken by PCI, with the scope of understanding the jointed wall behavior in the PRESSS building and improving its design guidelines so that the jointed precast wall systems can be designed cost effectively. The different tasks of the research undertaken in this project are as follows:

- **Processing of experimental data** — Although the wall direction test data were examined preliminarily (Priestley et al. 1999), they have not been carefully processed. In order to provide the test information needed for the codification process, processing of all wall direction test data must be completed. Several inverse triangular tests and pseudodynamic tests with intensity increasing up to 1.5xEQIII were conducted in the

wall direction. In each test, two sets of data were collected. Actuator forces and data from instrumentation used for control purposes made up the first set while the second set consisted of data from the remaining instrumentation. Both data files were recorded as independent files for each test with initial values being "as recorded" at the beginning of the test. In this task, all data are biased to reflect the appropriate initial values based on the zero load/zero displacement condition and the data collected during the previous test(s). Data processing in the wall direction includes biasing of data files obtained from all wall direction tests, and synchronizing the two data files collected during each test. A database is also created to help extract the appropriate test information for the current and future research projects. A revised set of test results for the wall direction response of the PRESSS building are reported based on the processed data.

- **Testing of UFP Connectors** — It was identified that understanding the strain hardening behavior of the wall system as a function of lateral displacement is of significant importance. Of potential sources for uncertainties, the contribution of the stainless steel U-plates to hardening behavior of the wall system is the least understood because inelastic behavior of stainless steel is dependent on the strain history. Therefore, the strain hardening behavior of the U-plates in the PRESSS building is quantified using cyclic component tests.

- **Characterizing behavior of precast wall systems designed with unbonded prestressing** — An analysis method suitable for examining monotonic behavior of jointed precast wall systems and single precast walls designed with unbonded post-tension is sought. The jointed connections introduce strain incompatibility between the steel and concrete at the section level, which makes the lateral load analysis of flexural members with jointed connections impossible using the conventional methods. Recognizing this challenge, this task establishes a simplified analysis method with validation using available experimental data.

- **Design of jointed wall systems** — Using the jointed wall test data and the analysis method established in the previous task, this task establishes an improved seismic design method for joint wall systems. In this process, the following design issues, which are inadequately quantified in the current version of the design guidelines, are addressed: 1) determining the design moments of individual walls in a jointed wall system; 2) estimating the neutral axis depth as a function of drift; 3) improving the design of the post-tensioning tendon through realistic estimates of the tendon elongations at the design drift; and 4) including the connector force in the design of intermediate walls in a jointed wall system consisting of more than two walls. In addition, the application of the design method is demonstrated using design examples.

1.6 Report Layout

This report contains six chapters including the introduction presented in Chapter 1. Chapter 2 provides a summary of data processing completed for the PRESSS building in the test wall direction of testing and performance of the precast jointed wall based on the processed test data. Chapter 3 presents the experimental results from the UFP connector tests and proposes a force-displacement curve that may be used in the design of wall systems containing this connector. A simplified analysis method suitable for establishing monotonic behavior of jointed precast wall systems and single precast walls designed with unbonded post-tensioning is presented in Chapter 4. Chapter 5 presents a design method suitable for unbonded post-tensioned jointed wall systems together with two design examples. Finally, Chapter 5 provides a summary of the report, along with the conclusions drawn from this research study.

Intentionally blank

CHAPTER 2: PROCESSING OF EXPERIMENTAL DATA

2.1 Introduction

To evaluate the seismic performance of the jointed precast wall system in the in-plane direction, the PRESSS building was subjected to several inverse triangular tests and pseudodynamic tests. The preliminary results obtained from these tests were previously presented on a test by test basis by Priestley et al. (1999) and Conley et al. (2002). Since then the test data have been carefully processed and a summary of the relevant test results are presented in this chapter.

2.2 Data Processing

In each wall direction test of the PRESSS building, two sets of data were collected. As noted previously, actuator forces and data from instrumentation that were used for controlling of the tests made up the first set while the second set consisted of data from the remaining instrumentation (see Sritharan et al. (2002) for details of instrumentation). All data files were recorded as independent files with initial values being "as recorded" at the beginning of each test. Consequently, all data files from the different tests were biased to reflect the appropriate initial values with respect to the zero load/zero displacement condition and the data collected during the previous test(s). Consequently, the data sets from each test were synchronized. A database containing the processed data was created to help extract the appropriate test information for the remainder of the research presented in the subsequent chapters.

Table 2.1 summarizes the significant tests in the wall direction, the bias scan used for each test, the corrected peak values of the lateral displacement at the top of the wall. As can be seen in this table, the jointed wall experienced a maximum lateral displacement of 11.530 in., corresponding to an average interstory drift of 2.56%. This lateral drift was achieved for an earthquake representing 150% of a design-level earthquake. At the design-earthquake, the jointed wall produced a maximum lateral displacement of 8.343 in. with a corresponding

average drift of 1.85%. The corrected peak values of the base shear force and base moment obtained for all significant tests are listed in Table 2.2.

Table 2.1 A summary of the significant tests conducted in the wall direction of the PRESSS building and corrected peak displacements.

Test No.	Description	Bias Scan	Peak 5th Floor Displacement (in.)	
			Max	Min
025	0.25EQ1	initial scan of 0.25EQ1 test	0.200	-0.198
032	0.5EQ1	initial scan of 0.25EQ1 test	0.332	-0.417
033	1.0EQ1(1)	initial scan of 0.25EQ1 test	1.221	-0.509
034	IT1(1)	initial scan of 0.25EQ1 test	1.247	-1.236
036	IT1(2)	initial scan of IT1(2) test	1.244	-1.248
038	1.0EQ1(2)	initial scan of IT1(2) test	1.751	-0.626
039	-1.0EQ1	initial scan of IT1(2) test	0.879	-1.635
040	1.0EQ2	initial scan of IT1(2) test	3.020	-1.539
041	IT2	initial scan of IT1(2) test	3.084	-2.905
046	-1.0EQ2	initial scan of IT1(2) test	1.356	-2.905
047	1.0EQ3	initial scan of IT1(2) test	2.022	-1.399
049	1.0EQ3mod	initial scan of IT1(2) test	2.130	-0.050
050	1.0EQ3mod2	initial scan of IT1(2) test	2.151	0.107
051	1.0EQ3mod5-10	initial scan of IT1(2) test	8.343	-2.582
052	IT3(1)	initial scan of IT1(2) test	8.337	-7.937
054	IT3(2)	initial scan of IT1(2) test	8.340	-7.943
055	-1.5EQ3mod5-10	initial scan of IT1(2) test	7.395	-11.530

2.3 Base Moment vs. Lateral Displacement Response

Using the database containing the corrected data for various tests summarized in Table 2.1, the key test results obtained for the PRESSS building in the wall direction are presented in this and subsequent sections. Figure 2.1 shows the base moment vs. lateral displacement response of the PRESSS building in the wall direction for all tests summarized in Table 2.1.

In addition to the jointed wall, the precast gravity columns and framing action resulting from the interaction between the seismic frames and precast floors contributed to the moment resistance depicted in Figure 2.1. Thomas and Sritharan (2004) estimated the different contributions to the moment resistance in the wall direction of testing and concluded that about 77% of the resistance was provided by the wall system, 5% by the gravity columns and 17% by the aforementioned framing action at large lateral displacements. Furthermore, they found that the moment resisted by the leading wall of the PRESSS jointed wall system was about twice that of the trailing wall.

Table 2.2 Corrected peak values of the base shear forces and base moments obtained for the wall direction tests of the PRESSS building.

Test No.	Description	Peak Base Shear Force (Kips)		Peak Base Moment (Kip-in.)	
		Max	Min	Max	Min
025	0.25EQ1	83.2	-89.7	28162	-31598
032	0.5EQ1	142.1	-122.2	41040	-47108
033	1.0EQ1(1)	315.1	-177.4	61188	-56274
034	IT(1)	186.4	-178.7	62637	-61969
036	IT(2)	173.0	-165.0	59465	-62249
038	1.0EQ1(2)	285.2	-146.3	67062	-44556
039	-1.0EQ1	145.0	-295.5	42962	-66521
040	1.0EQ2	295.7	-260.2	75051	-63149
041	IT2	221.6	-192.6	74700	-74773
046	-1.0EQ2	261.7	-301.5	56971	-73130
047	1.0EQ3	300.8	-219.5	61057	-50607
049	1.0EQ3mod	213.6	-93.6	60389	-14244
050	1.0EQ3mod2	257.2	-101.0	61205	-14542
051	1.0EQ3mod5-10	306.6	-323.5	92896	-68786
052	IT3(1)	301.6	-230.6	94213	-91826
054	IT3(2)	279.2	-267.6	94043	-93209
055	-1.5EQ3mod5-10	465.9	-356.9	89600	-102069

As indicated by the shape of the base moment vs. lateral displacement response in Figure 2.1, the hysteretic response of the jointed wall in the PRESSS building was stable and dependable, confirming the excellent seismic performance observed for the wall system. It was reported previously that the jointed wall possessed a negligible amount of residual drift at the end of each pseudodynamic test to earthquake loading (Priestley et al. 1999). The corrected data revealed that the residual displacements recorded at the fifth floor level immediately following the peak lateral displacement cycles were 1.54 in. and 2.90 in. for the design-level and 150% of the design-level earthquakes, respectively. While these displacements corresponded to average inter-story drifts of 0.34% and 0.64%, the average drifts recorded at the end of these tests were, respectively, 0.1% and 0.03 % in spite of using input motions with short durations. This observation suggests that a structural system upon unloading from the maximum lateral displacement does not have to achieve the zero displacement-zero moment condition in the immediate half-cycle for that system to eventually recenter at the end of the earthquake motion.

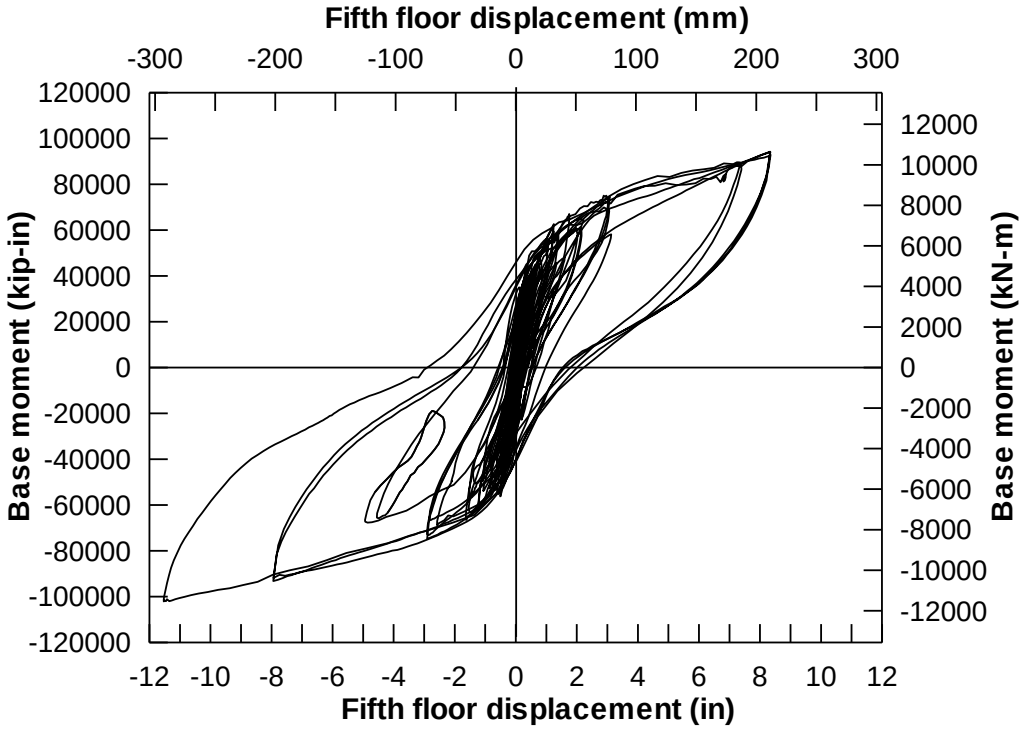

Figure 2.1 Seismic response of the PRESSS building in the wall direction of testing.

2.4 Wall Uplift

Although the jointed wall consisted of four precast panels (see Figure 1.5), the flexural deformation of the wall system was concentrated at the wall base-to-foundation interface with walls experiencing only a few flexural cracks at the first story level. Displacement transducers positioned at the wall bases recorded the concentrated deformation at the base of the walls. Figures 2.2 to 2.3 show two examples of the recorded wall uplifts as a function of top floor displacement for all significant tests summarized in Table 2.1, while Figure 2.4 depicts the displacements recorded by one transducer during Tests 51 and 55 as a function of pseudotime. Interpolations of data recorded by different transducers indicated that the maximum uplifts of 1.85 in. and 2.66 in. occurred at the toe of the trailing wall, which was expected to undergo larger uplift than the leading wall.

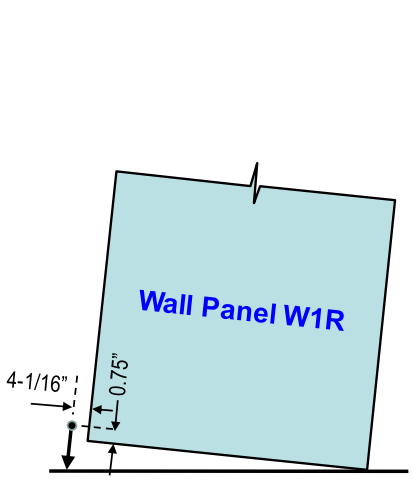

(a) Gauge location

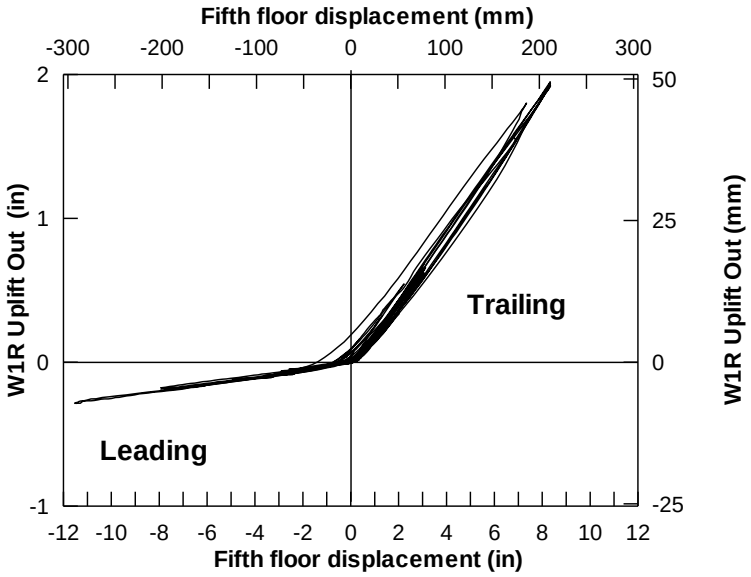

(b) Recorded response

Figure 2.2 Recorded wall uplift near a wall base as a function of top floor displacement.

The vertical and horizontal movements between the wall panels were also monitored at 2.5 story height of the building, where horizontal interfaces between the precast wall panels were located. The connection between the wall panels at this interface was established using 1 in. thick grout and four interlock reinforcement couplers at the toes of the wall panels. The vertical movement monitored between the wall panels near the centerline of the building was negligible. The device placed to monitor the vertical displacement between the inner faces of

the panels recorded a maximum value of 0.08 in. until the end of Test 51. However, this movement increased up to 0.35 in. during the remainder of the tests (see Figure 2.5).

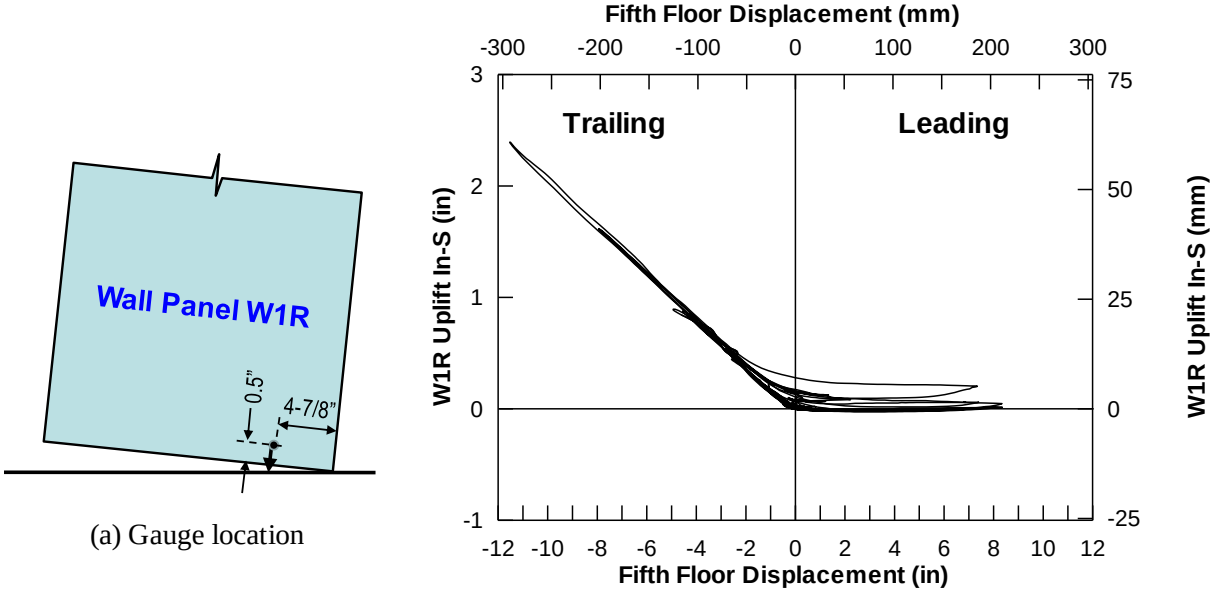

(a) Gauge location

(b) Recorded response

Figure 2.3 Recorded wall uplift near a wall base as a function of top floor displacement.

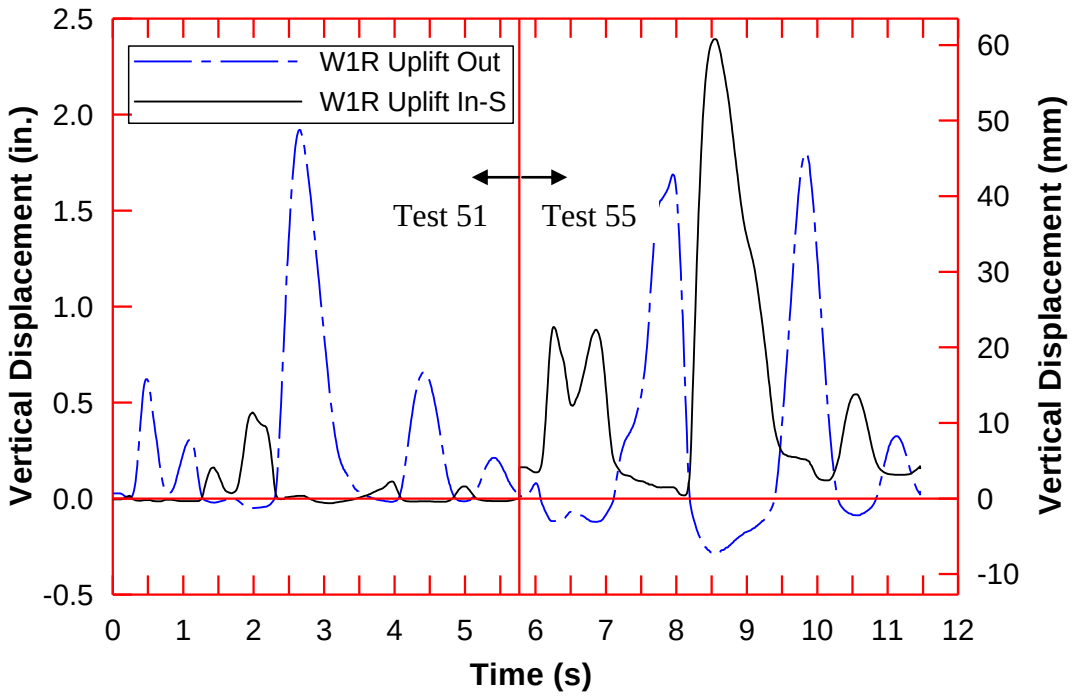

Figure 2.4 Recorded wall uplift near a wall base as a function of pseudotime.

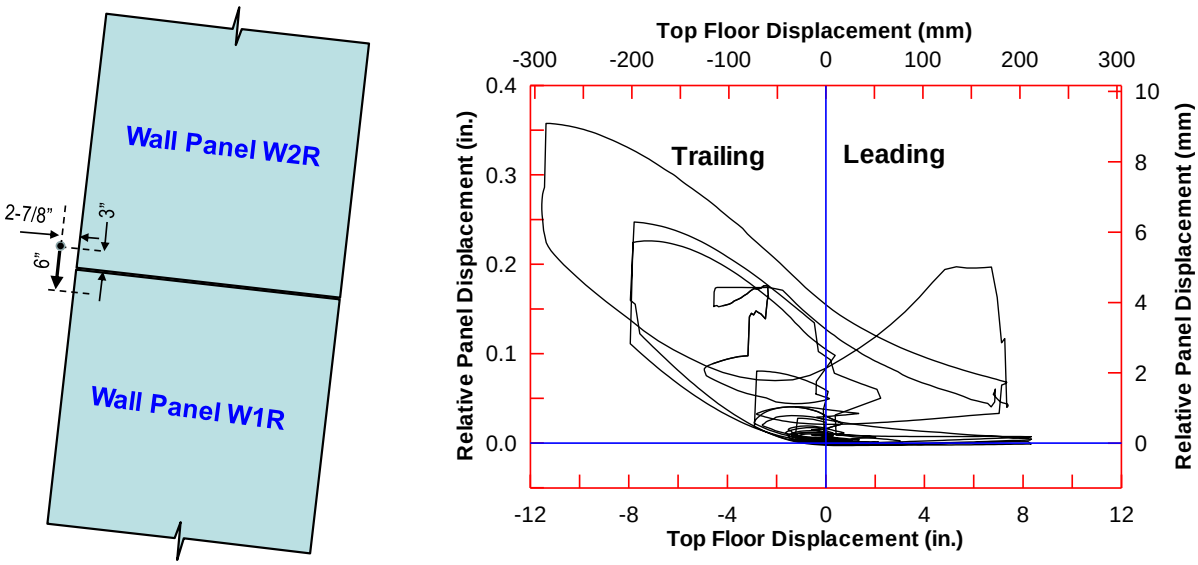

(a) Gauge location

(a) Recorded response

Figure 2.5 Recorded relative vertical displacement between panels at 2.5 story height.

It must be noted that the high relative panel displacements shown at large lateral displacements may be questionable because a similar trend was not observed for displacements recorded by a device closer to the opposite edges of the same panels. Also note that when the wall WR acted as the leading wall, this particular device should have continued to record insignificant displacements, which is not the case towards the end of the test.

2.5 Deformation of the Connectors

The vertical deformation that the UFP connectors experienced between the walls in the vertical joint was monitored using two displacement transducers near the base and at the top of the wall. Figures 2.6 and 2.7 depict the corrected data obtained from these displacement transducers, which shows that the vertical displacement demand imposed on the connectors was almost linearly proportional to the fifth floor lateral displacement. These figures along with Figure 2.8, which shows a time history plot for two tests, indicate that the UFP connectors underwent a maximum displacement of 2.7 in the direction parallel to the side face of the wall panels. As expected, this displacement closely matches the maximum uplift estimated above for the trailing wall.

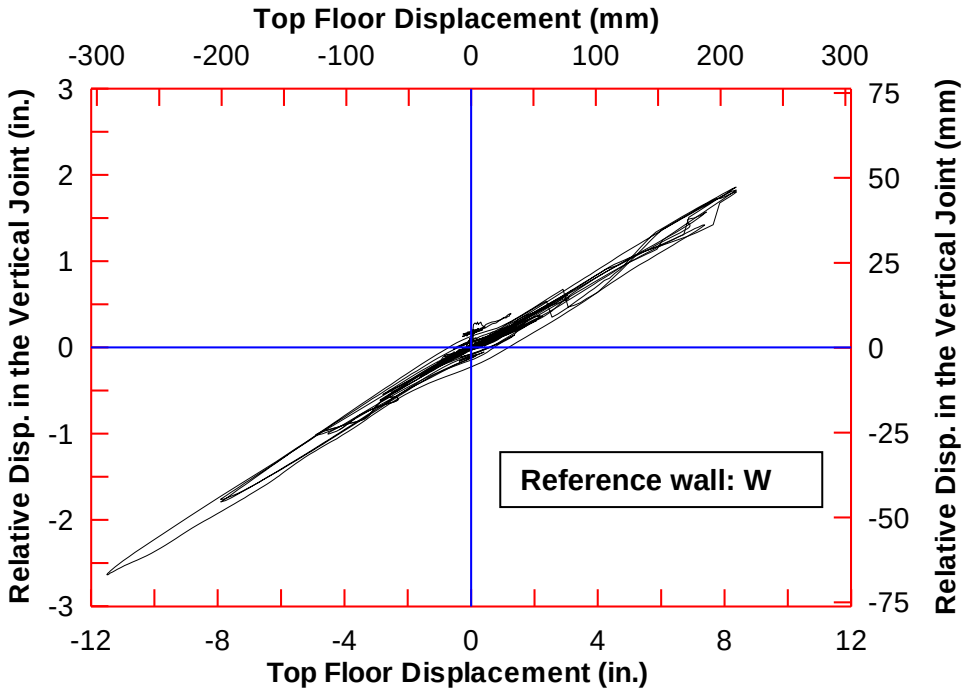

Figure 2.6 Relative displacements recorded between walls in the vertical joint near the base to quantify the displacements imposed on UFPs.

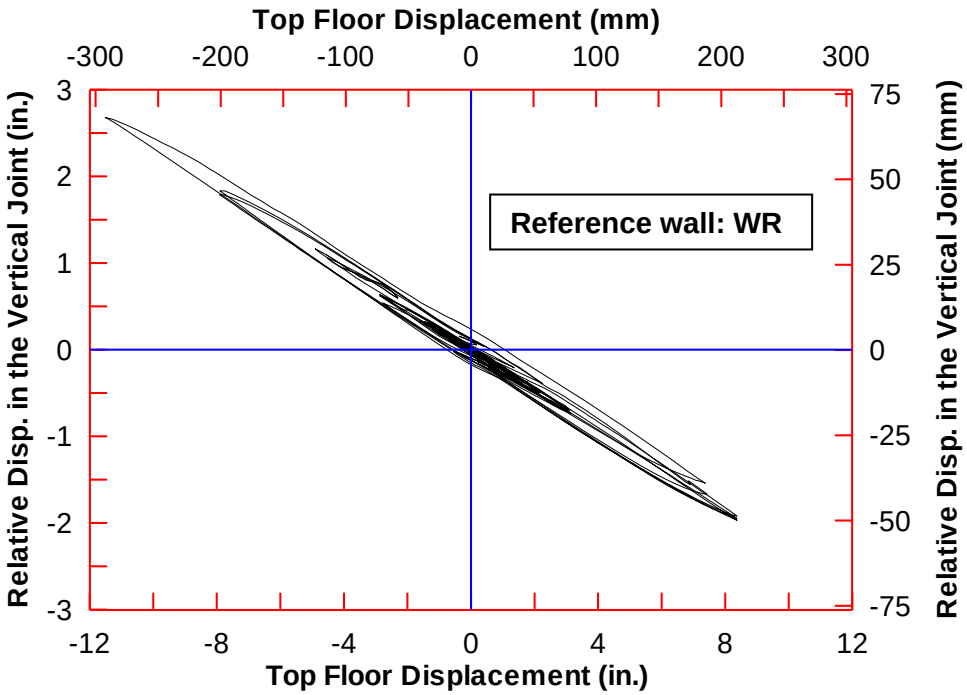

Figure 2.7 Relative displacements recorded between walls in the vertical joint at the top to quantify the displacements imposed on UFPs.

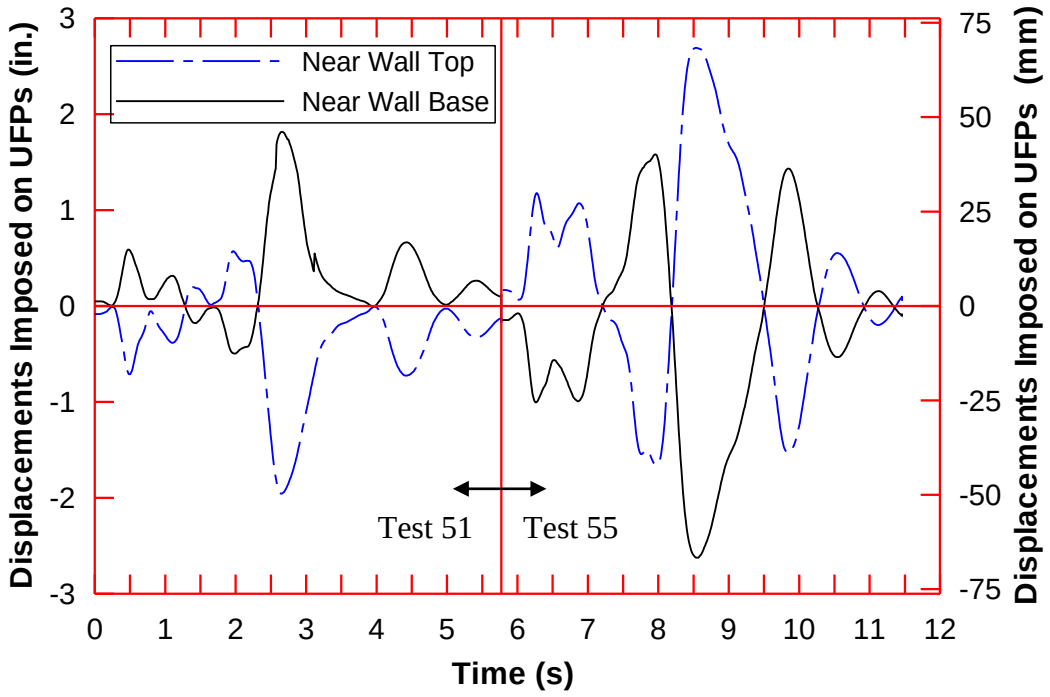

Figure 2.8 Relative displacements recorded between walls in the vertical joint as a function of pseudotime.

2.6 Demand on the Post-Tensioning Bars

The unbonded post-tensioning in each wall was provided using four 1-in. diameter Dywidag bars. Gauges mounted onto these bars monitored the strain demand starting prior to applying the initial prestress. On average, the bars carried an initial prestressing strain of 1641 microstrain, equaling prestressing of 47.3 ksi (or 37.1 kips) before the start of the seismic test. This is about 10% lower than the target design value of 41 kips, which was established assuming that the prestressing bars should yield at a design drift 2 percent. Prestressing to the walls was applied about a week before the seismic test. The loss of prestressing during the period between after anchoring the bars and before the start of the test was negligible, but strain fluctuations of about 2% were observed.

Figures 2.9 and 2.10 show strains recorded on two different prestressing bars for all the tests listed in Table 2.1. It is seen that prestressing bars were subjected to as high as 4500 microstrain. Given that ASTM standards define yield strain for the prestressing bar at 7000

microstrain (Naaman, 2004), the prestressing bars in the jointed wall system are considered not to have experienced yielding. The uni-axial tension tests performed on the prestressing bars defined the proportional limit, which defines the strain at which the stress-strain response of the bar deviates from linearity, at 5086 microstrain. Therefore, it is concluded that prestressing bars in the jointed wall system of the PRESSS building did not experience any losses due to material nonlinearity developing in the prestressing bars. A confirmation for this conclusion is that the strains in the prestressing bars at the end of the wall direction seismic test were the same as those recorded at the beginning of the test.

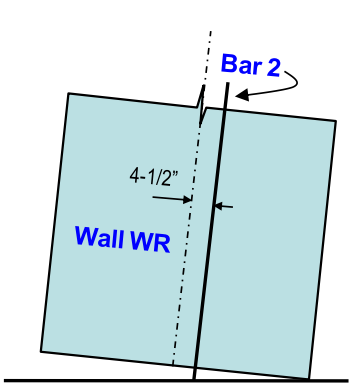

(a) Bar location

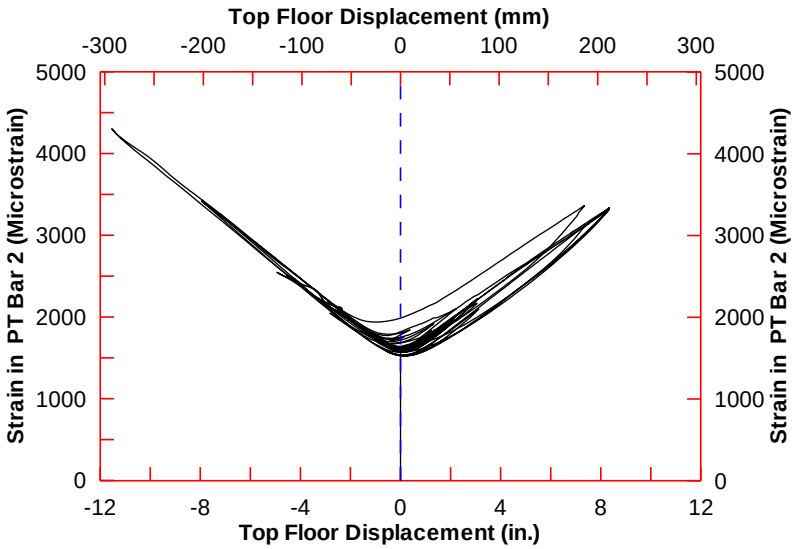

(b) Measured strains

Figure 2.9 Variation in strain in a prestressing bar as a function of top floor displacement.

2.7 Strain in the Confinement Steel

A few strain gauges were also mounted on the confinement reinforcement placed at the wall ends near the base and an example is shown in Figure 2.11 from a gauge located at 9 in. above the wall base. Although limited success was achieved in recording the strain demands on the confinement reinforcement, the recorded data indicated that strains imposed on the confinement reinforcement did not cause significant yielding of this reinforcement. This finding is consistent with the test observations in that no damage to the confinement

reinforcement or significant spalling of cover concrete was observed during the wall direction testing of the PRESSS building.

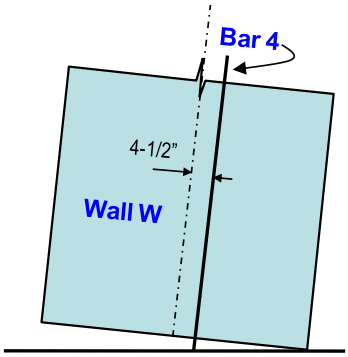

(a) Bar location

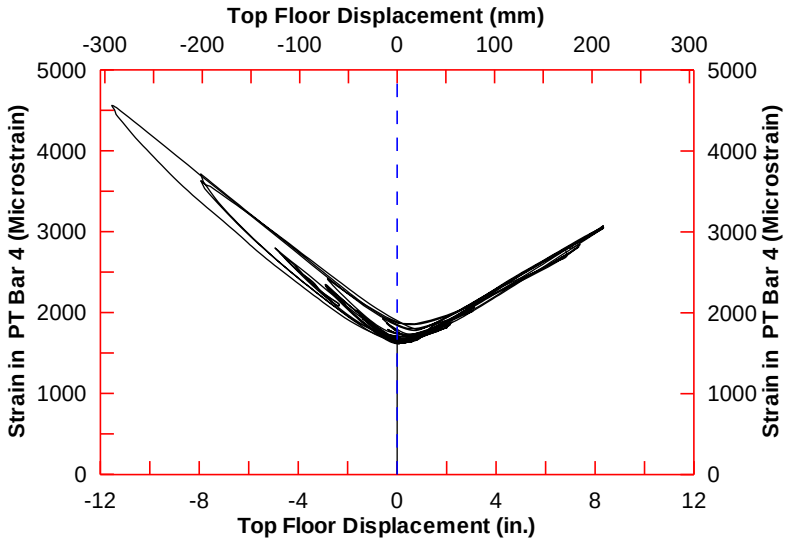

(b) Measured strains

Figure 2.10 Variation in strain in a prestressing bar as a function of top floor displacement.

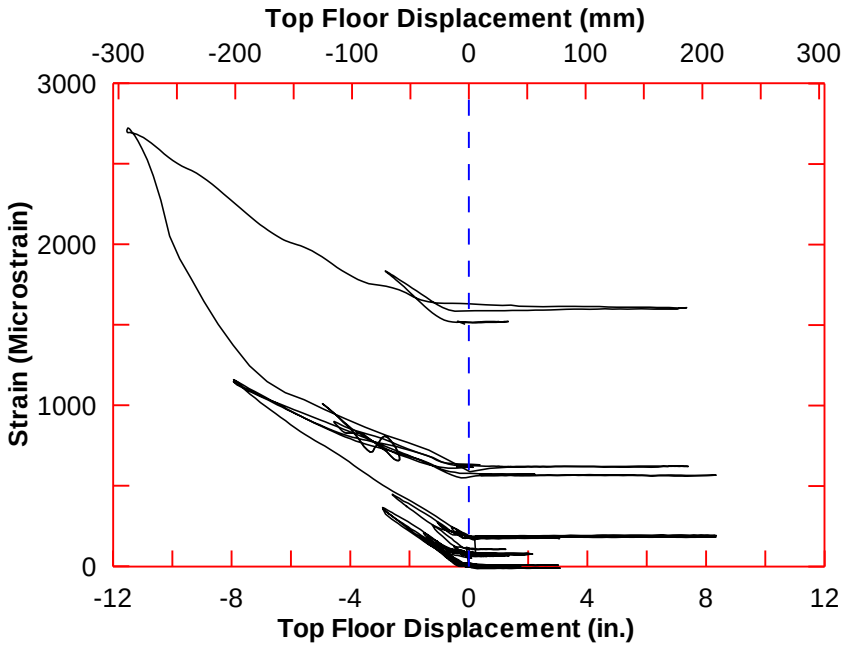

Figure 2.11 Recorded confinement strain demand as a function of top floor displacement.

2.8 Strain in the Horizontal Straps

The wall panels at the mid height of the first story was secured with two, 3/8-in. thick, 4 in.-wide Grade 60 steel plates, whose primary function was to provide resistance if the walls were to move away from each other in the direction parallel to the direction of loading. Gauges mounted on the outside surfaces of the straps monitored the strain demands. Measured strains in the straps were less than 200 microstrains, confirming that these traps could have been eliminated from the jointed wall system.

2.9 Equivalent Viscous Damping

Using the test data obtained from IT(1), IT2, IT3(1) and -1.5EQ3mod5-10, the amount of energy dissipated by the PRESSS building in the wall direction was quantified (using Eq. 5.3), where the majority of the energy dissipation was provided by the UFP connectors. As shown in Figure 2.12, the energy dissipation was estimated in terms of equivalent viscous damping using the inverse triangular tests except for -1.5EQ3mod5-10. In the latter case, the damping was calculated using the hysteresis loop obtained using the most dominant half-cycle of response that induced a lateral displacement of -11.53 in. at the top floor of the building (see Figure 2.1). Table 2.3 summarizes the calculated damping for the four different levels of testing. The hysteretic response of the building corresponding to the peak lateral displacements recorded at intensities comparable to the design-level earthquake and beyond produced an equivalent viscous damping of 18%, which is 45% greater than the assumed viscous damping of 12.4% at a design drift of 2%. Note that the drift assumed in the design was maximum interstory drift not the maximum average story drift. However, due to concentration of cracks at the base, the measured responses of the walls at the peak lateral displacements confirmed that the maximum average interstory and the maximum story drift were almost identical for the jointed wall system.

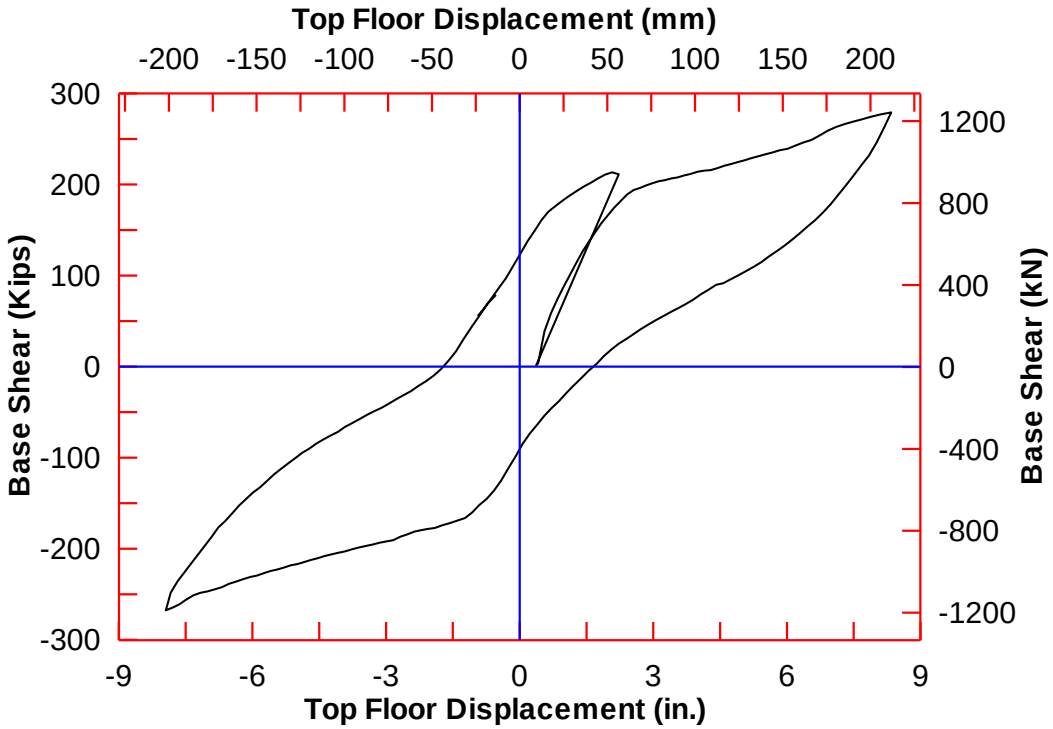

Figure 2.12 An example of a hysteretic loop obtained during the wall direction inverse triangle load test of the PRESSS building. (This loop was established between Tests 52 and 54 identified in Table 2.1).

Table 2.3 Computed equivalent viscous damping for the PRESSS building in the wall direction of testing.

Test	Maximum lateral displacement at the fifth floor (in.)	Maximum average drift (%)	Equivalent viscous damping (%)
IT1 (Test 34)	1.25	0.28	9.63
IT2 (Test 41)	3.08	0.68	11.66
IT3 (Test 52)	8.33	1.85	18.26
1.5EQ3 (Test 55)	11.53	2.56	17.79

Intentionally blank

CHAPTER 3: QUANTIFICATION OF CONNECTOR RESPONSE

3.1 Introduction

The performance of the UFP connectors included in the wall system of the PRESSS building was excellent. However, establishing the contribution of the connectors through component testing was identified to be a critical step to quantify the actual contribution of the jointed precast wall system designed with UFP connectors as well as to improve design efficiency of this system. When forming the U shape of the connector, the plates are bent over a small radius and therefore, stainless steel is preferred over mild steel for the UFPs in order to avoid any premature damage to them during manufacturing. Since stainless steel experiences isotropic hardening under cyclic loading, the contribution of the UFP becomes dependent on previous strain history. Consequently, quantifying the contribution of the connector response using a displacement history that UFPs may experience during seismic loading is an important step.

To quantify the behavior of the UFP connector, experimental tests were performed similar to those completed at the University of California at San Diego (UCSD) in conjunction with the PRESSS building test (Conley et al. 2002). Included in the tests at Iowa State University (ISU) are three uniaxial tensile tests of the material and two cyclic tests of the UFP connectors.

3.2 Uniaxial Tests

Three tensile test coupons were machined from 3/8-in thick 304 stainless steel, the same thickness and material used for the UFPs, to meet ASTM standards for tension testing of metallic materials (ASTM Committee E-28, 1991). The required dimensions of the test coupons are shown in Figure 3.1, while Table 3.1 provides the actual dimensions of the coupons as measured prior to testing.

The stress-strain curves obtained from the uniaxial tests are shown in Figure 3.2. The extensometer measuring strains was removed prematurely during testing of both Specimens 1 and 2 since the specimens began necking long before the ultimate failure actually occurred (the actual elongation of the specimens was over 30%). During testing of Specimen 3 the extensometer reading was taken to a strain of over 0.371 in/in. Also included in Figure 3.2 is a stress-strain curve obtained from the uniaxial testing of UFP coupons at UCSD. The comparison between the ISU and UCSD test data indicate that the material strength of the ISU coupon was about 2% weaker than the material tested at UCSD (Conley et al., 2002). The UCSD test represented the UFP connectors actually used in the PRESSS test building.

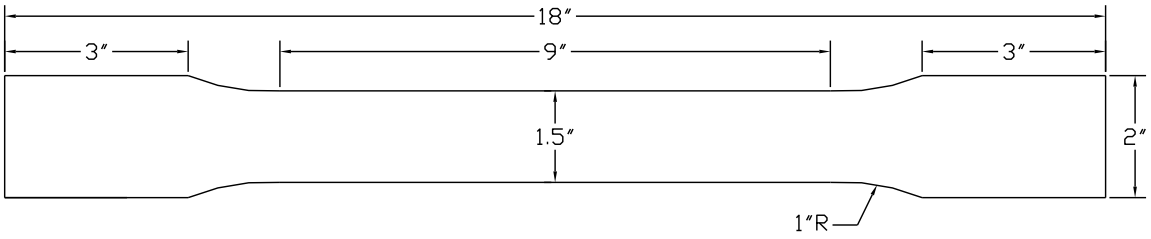

Figure 3.1 Dimensions of test coupon chosen for the uniaxial tensile tests

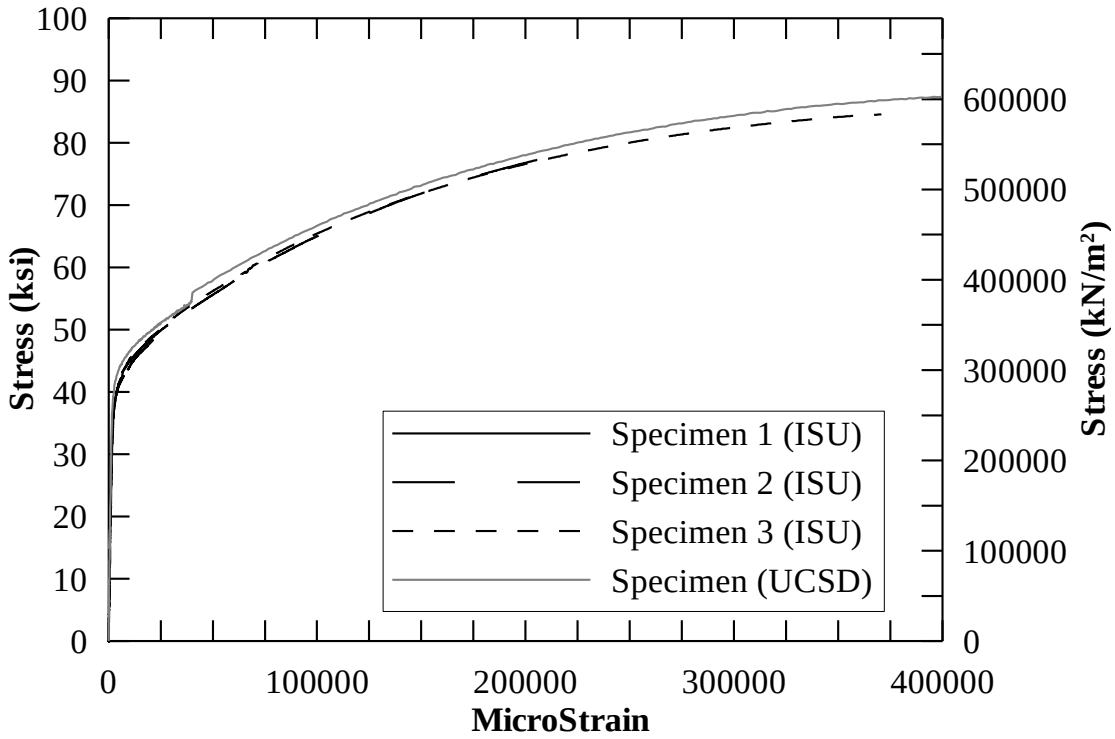

Figure 3.2 Measured stress-strain response of UFP coupons under uniaxial tension.

Table 3.1 Measured width and thickness of the tension test coupons

	Width (in.)	Thickness (in.)
Specimen 1	1.498	0.393
Specimen 2	1.498	0.397
Specimen 3	1.498	0.396

3.3 Cyclic Testing

Two sets of UFP were subjected to cyclic loading. Similar to the UCSD cyclic tests, the test setup used two 3-in. wide UFP sections that were welded between 4-in square tubing sections and a 0.75-in. thick plate as detailed in Figure 3.3. The test rig allowed the UFPs to be subjected to relative vertical displacements of up to ± 3.5 in. and the structural tubing provided stiff boundaries to simulate the stiff wall panels in a jointed wall system. The test rig was then placed in a MTS uniaxial fatigue test machine and was gripped at each end by a plate welded between the two UFPs at the top and a rod connected to the square tubing at the bottom. The cyclic tests on the UFPs were performed by regulating the MTS fatigue machine by displacements.

The first UFP (U1) was tested under gradually increasing displacement cycles shown in Figure 3.4. This test sequence was similar to that used for the UFP cyclic test at UCSD (Conley et al., 2002). During testing at a displacement of 2-in., the test rig began to slip out of the top grip that may be seen in Figure 3.3. The force-displacement hysteresis response of U1 that was obtained prior to experiencing slip in the top grip (i.e., U1-1) can be seen in Figure 3.5.

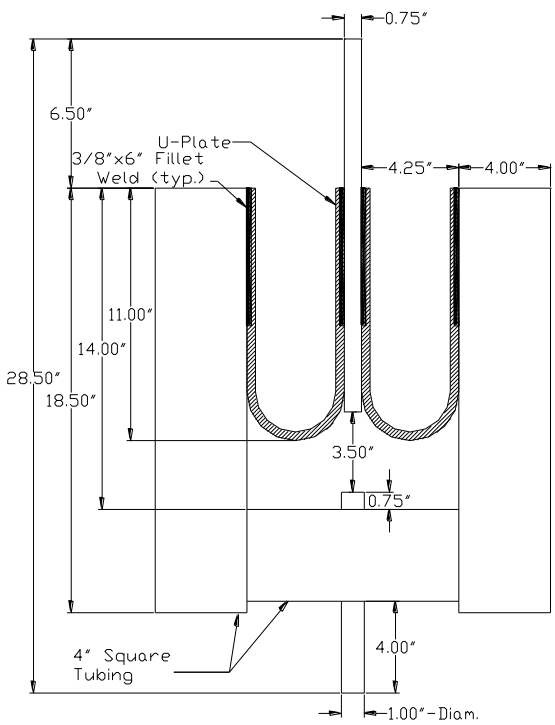

(a) A schematic showing dimensions

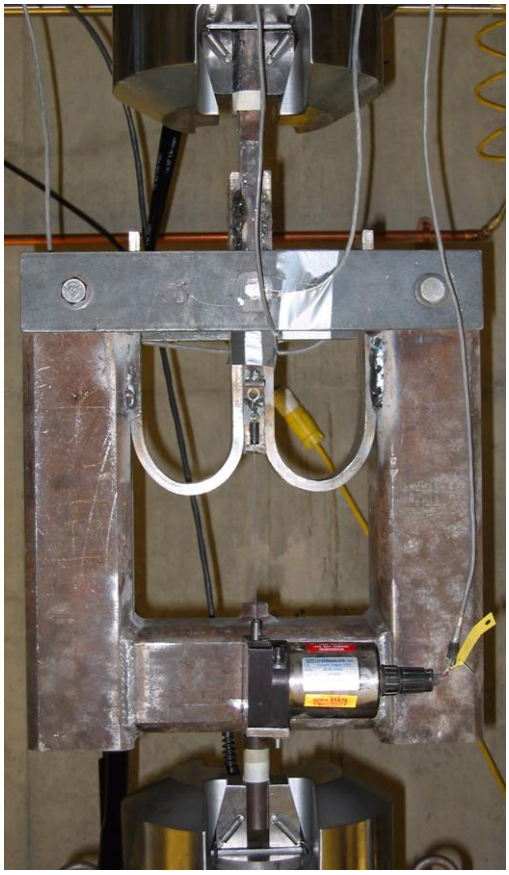

(b) A picture showing the actual test

Figure 3.3 Test setup used for cyclic testing of UFP connectors

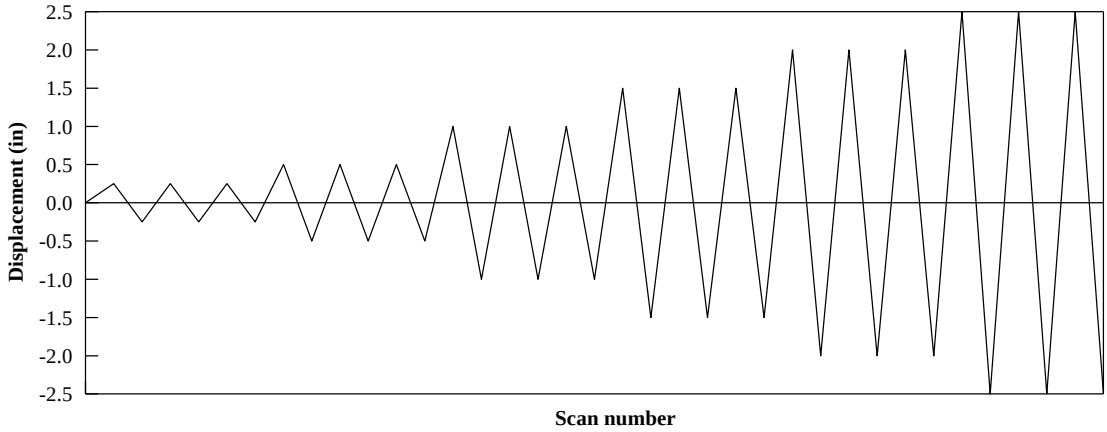

Figure 3.4 Displacement history applied to U1.

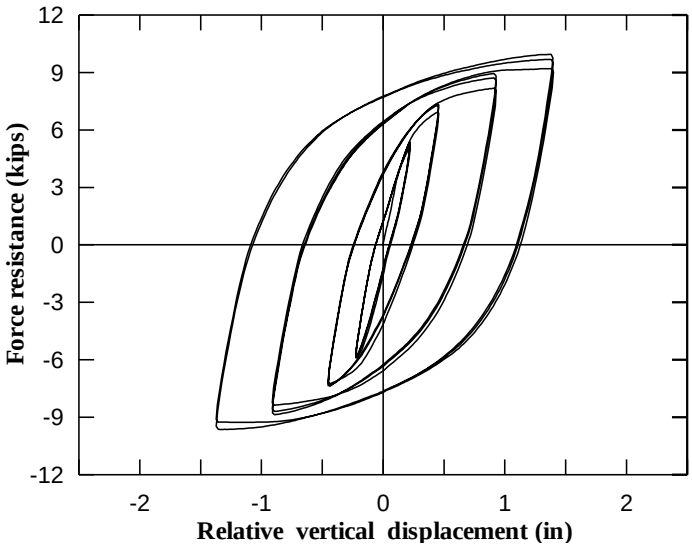

Figure 3.5 Force-displacement hysteresis response of U1 prior to experiencing slip at the top grip (i.e., U1-1).

To eliminate slipping at the grip, the thickness of the gripping region of the plate located at the top of the test rig was increased. Then the UFP test rig, still containing U1, was returned to zero displacement and was tested again for the entire displacement history provided in Figure 3.4. The hysteresis response obtained for the second test of U1, referred to as U1-2, is reproduced in Figure 3.6. It is noted that force resistance obtained for U1-2 for displacements up to 2 in. are greater than those obtained for U1-1 at the same displacements. This observation was expected due to isotropic hardening characteristics of the stainless steel and confirms the dependency of the force-displacement response of the stainless steel UFPs on the previous strain history.

A new pair of UFPs was used in the second cyclic test that was subjected to a displacement history similar to that the UFPs experienced during testing of the jointed wall system in the PRESSS building. The displacement history for the second test was established using displacement device W1VCS included in the PRESSS building, which measured the relative displacement along the vertical joint between the two walls near the base (see Figure 3.7). The main purpose of choosing the displacement history based on the PRESSS building test was to sufficiently account for the influence of strain history in establishing a suitable force-displacement envelope response for the UFP connector.

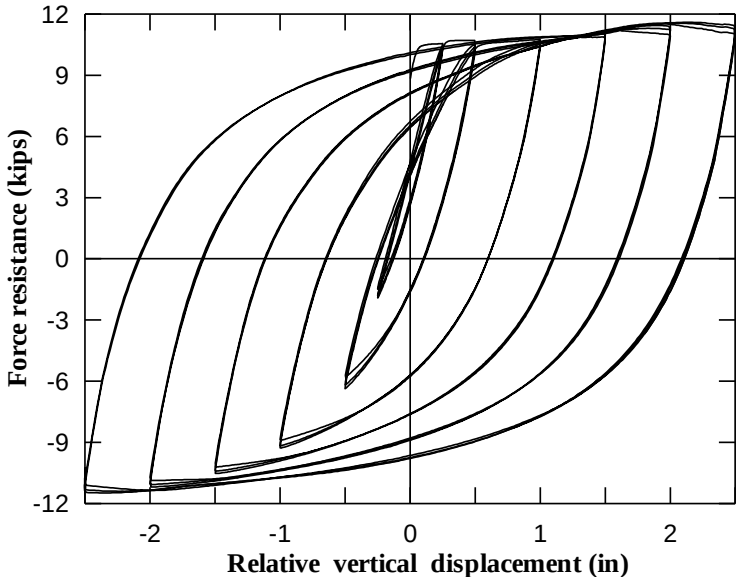

Figure 3.6 Force-displacement hysteresis response of U1-2.

Recorded displacements from displacement device W1VCS was previously presented in a different form in Figures 2.6 and 2.8, whereas Figure 3.8a shows the entire displacement history produced by this device for all tests summarized in Table 2.1. Using the peaks from Figure 3.8a, the target displacement load history shown in Figure 3.8b was established for the second cyclic test. As with testing of U1, the second UFP (U2) was also tested twice. After completing the first test on U-2 for the displacement history depicted in Figure 3.8b, the relative displacement of the UFP was returned to zero and the test was repeated using the same displacement sequence. The two tests were referred to U2-1 and U2-2, respectively, and the corresponding hysteresis responses are shown in Figures 3.9 and 3.10, respectively. The primary reasons for performing U2-2 was to yet again examine the influence of the past strain history on the response of the UFP connector and to investigate the potential damage to UFPs resulting from experiencing an excessive number of large-amplitude displacement cycles and subsequent low cycle fatigue.

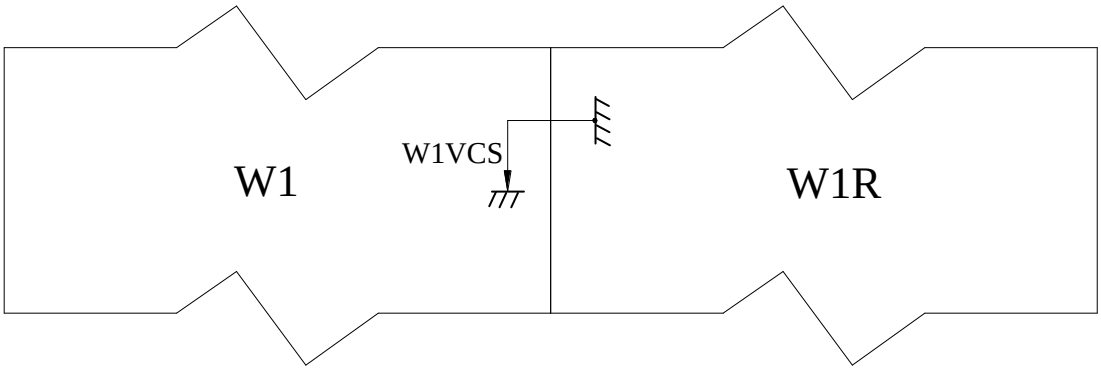

Figure 3.7 Location of displacement device W1VCS in the PRESSS wall system

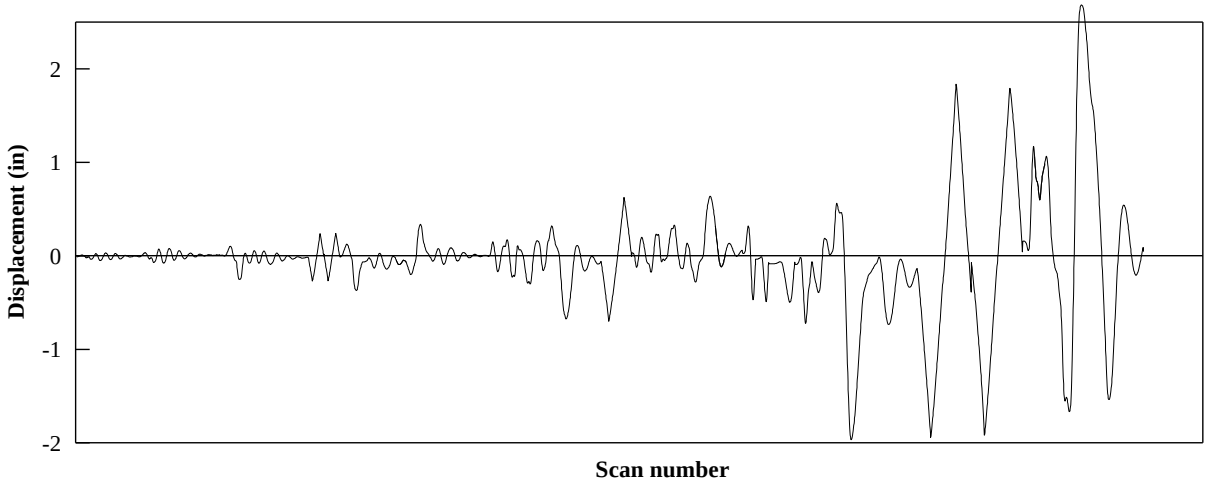

(a) Measured displacements by device W1VCS in the PRESSS test building

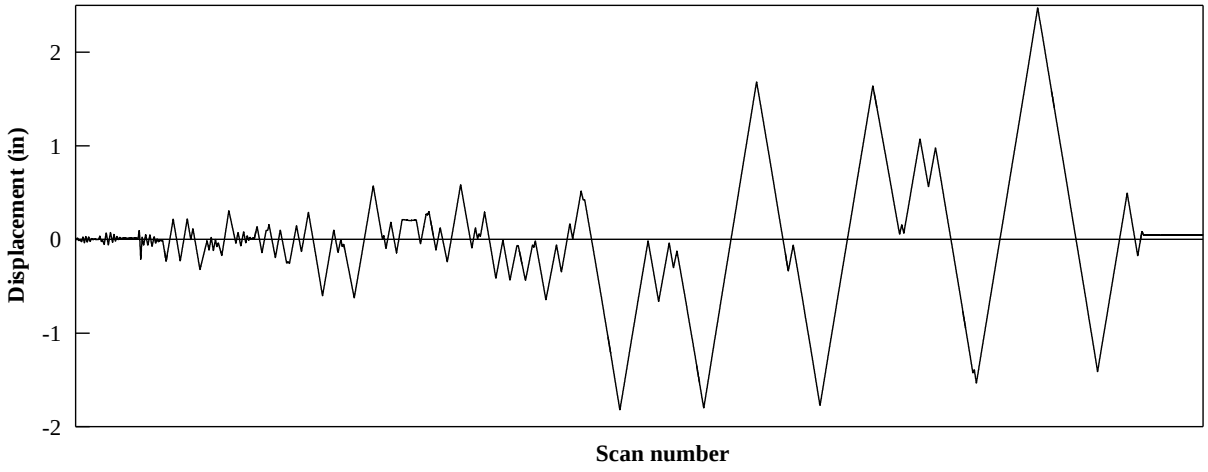

(b) Target displacement sequence chosen for testing of U2

Figure 3.8 Displacement histories of UFPs

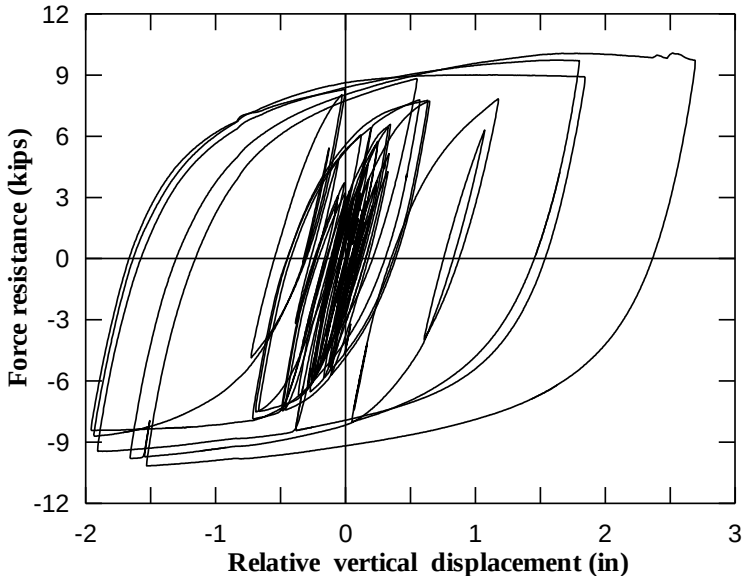

Figure 3.9 Force-displacement hysteresis response obtained for U2-1.

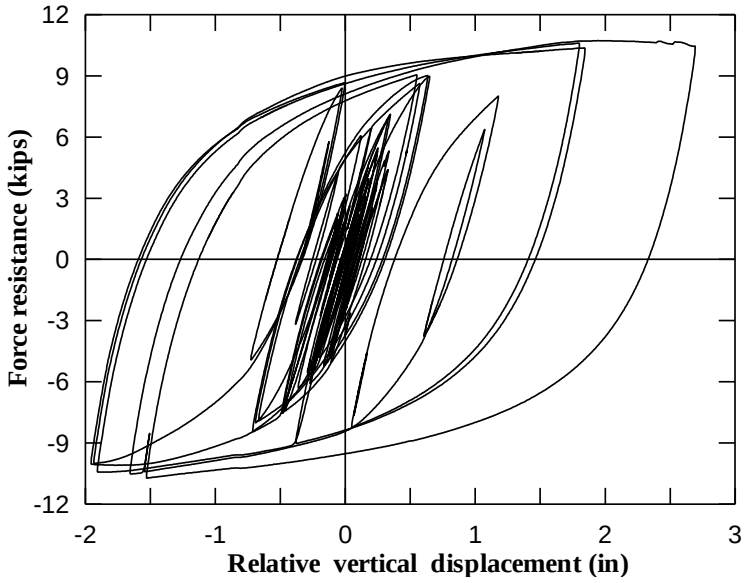

Figure 3.10 Force-displacement hysteresis response obtained for U2-2.

The condition of the UFPs at the end of the second test was good and showed no indication of cracking or any other damage, except for the fact that their original shape was distorted. The force resistance exhibited during U2-2 testing was generally higher than U1-1 at a given displacement. The percentage increase at the peak displacements of the different cycles varied between about 2 to 17 percent. Such a variation is not desirable for predicting

the behavior of the wall system under earthquake loading. However, the performance of the connector in terms experiencing the effects of multiple earthquakes was excellent.

3.4 Proposed Force-Displacement Response

In order to apply the above results in the design process at the prototype scale, the following points must be recognized. First, the test rig used two 3-in. deep UFPs while the actual depth of UFPs could be 7 in. or deeper. Assuming that depth of the UFPs to be used at the prototype scale is 7 in. (as used in the PRESSS building), the corresponding force resistance may be obtained by using a multiplication factor of 7/6. Second, as previously mentioned, the stainless steel tested under monotonic loading at ISU was slightly weaker than those tested at UCSD (see Figure 3.2). A further confirmation of the difference in the material strength is evident in Figure 3.11, which compares a response envelope from the UFP cyclic tests conducted at UCSD (Conley et al., 2002) with that obtained from U1-1 test completed at ISU. Note that both of these tests were conducted under similar displacement histories and that the envelope of U1-1 had been adjusted to account for the difference in the depth of the UFP connectors. Based on these observations, it was concluded that the UFPs used in the PRESSS test building was approximately 8.8% stronger than the UFPs used in the tests at ISU.

Considering the small differences in material strengths and isotropic hardening of the material, the force-displacement response envelope shown in Figure 3.12 is recommended for design. This envelope that represents the expected performance of a 7-in. deep UFP connector made out of 3/8 in. thick 304 stainless steel was derived based on the response envelope of test U2-1 (see Figure 3.9) with enhancements to account for the difference in the depth of the connector and 8.8% material strength difference observed between the ISU and UCSD tests. In this approach, it is assumed that the load history shown in Figure 3.8b adequately accounts for the expected effects of strain history on the response of the UFP connector to be used in practical applications. Because of these assumptions, it should be realized that the force-displacement response shown in Figure 3.12 is an accurate representation of the envelope response of the UFP connectors used in the jointed wall system of the PRESSS test building.

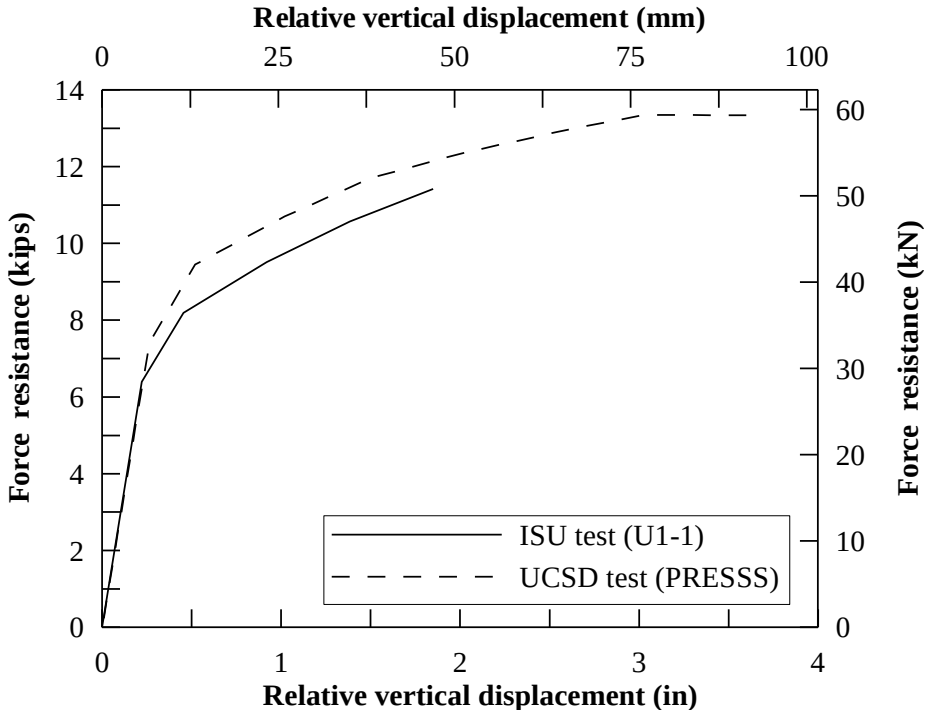

Figure 3.11 Comparison of UFP force-displacement response envelopes obtained from two different tests subjected to identical cyclic loading.

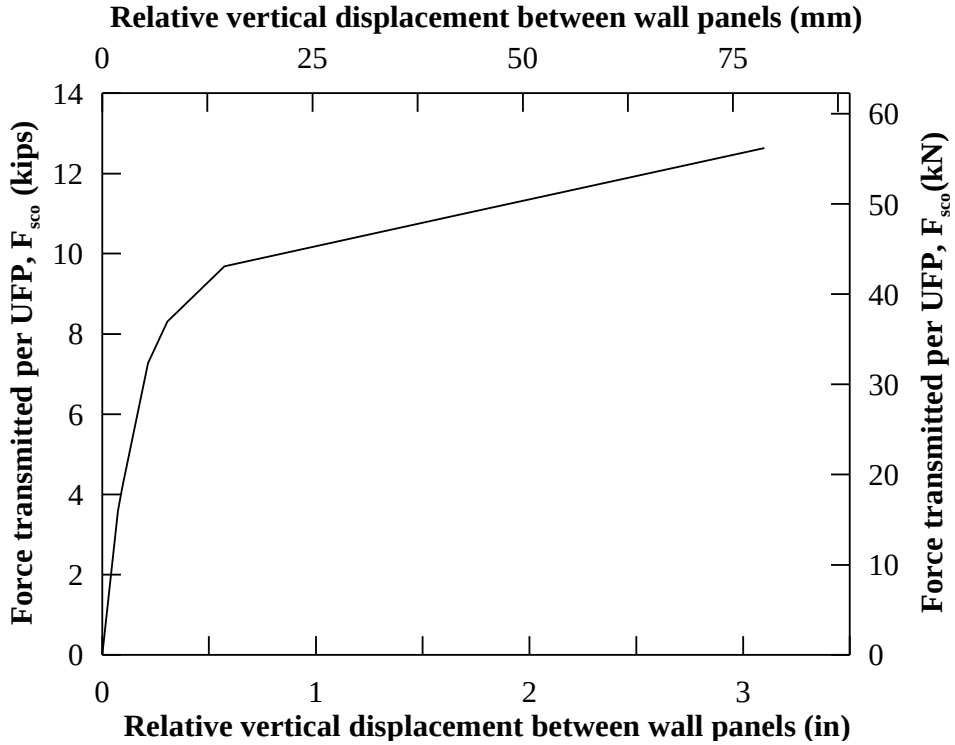

Figure 3.12 Recommended force-displacement response for a 7-in deep UFP connector made from /8 in. thick 304 stainless steel.

CHAPTER 4: AN ANALYSIS PROCEDURE WITH VALIDATION

4.1 Introduction

An analysis method suitable for examining monotonic behavior of unbonded jointed precast wall systems and single precast walls is presented and its accuracy is verified using available test data. By reversing the design guidelines presented for the jointed wall systems by Stanton and Nakaki (2002), Thomas and Sritharan (2004) established an analysis procedure, which they referred to as the PRESSS analysis procedure. Following identifications of shortcomings in this approach, they proposed the modified PRESSS analysis procedure. The modifications included the use of a constant neutral axis depth for wall section analysis regardless of the rotation at the base of each wall and an effective concrete confinement factor of 1.6 for defining the concrete strength. The appropriateness of these modifications was satisfactorily demonstrated using the PRESSS test data obtained in the wall direction of testing. Considering that this modified analysis procedure does not allow the variation of confined concrete strength to be modeled as a function of the amount of confinement reinforcement, further improvements to the analysis procedure are incorporated to account for the confinement effects of concrete more accurately. In addition, a trilinear approximation is introduced for the variation of the neutral axis depth as a function of the wall base rotation. This concept was shown to be appropriate for jointed hybrid frame connections by Celik and Sritharan (2004). With these modifications, the procedure hereafter will be referred to as the simplified analysis procedure because of its reduced complexity in comparison to the Monolithic Beam Analogy (MBA) method procedure introduced for jointed precast connections (Pampanin et al. (2001); Thomas and Sritharan (2004)).

Following a step-by-step presentation of the analysis procedure in the next section, validation of the simplified analysis procedure is presented using test data obtained from the jointed precast wall system used in the PRESSS building and several single unbonded wall tests conducted at the ATLSS Research Center. Results from the simplified analysis procedure are combined with the results obtained from the MBA method of analysis presented elsewhere for precast jointed wall systems (Sritharan and Thomas (2003); Thomas and

Sritharan (2004)) to establish the improved design guidelines for precast jointed wall systems in Chapter 5.

4.2 Simplified Analysis Procedure

To analyze a jointed wall system (or a single wall) with unbonded post-tensioning steel (see Fig. 4.1), a non-iterative procedure is presented in this section by establishing a relationship between the neutral axis depth and the base rotation for each wall in the wall system. This relationship is based on the neutral axis depth estimated at a base rotation of 2% and is found from an iterative procedure involving the force equilibrium and geometric compatibility conditions. According to the design guidelines presented by Stanton and Nakaki (2002), the following assumptions are made in the analysis procedure:

1. The walls are provided with adequate out-of-plane bracing, preventing them from experiencing torsional and out-of-plane deformations.
2. The dimensions and material properties of the walls and connectors are known.
3. The fiber grout pad located at the interface between the wall and the foundation does not experience any strength degradation.
4. All walls will undergo the same lateral deformation at every floor level due to the rigid floor assumption.
5. The wall base has enough friction resistance, such that the wall will not undergo any relative lateral movement at the base with respect to the foundation.
6. The connectors and the post-tension steel anchors remain fully effective for the entire analysis.
7. All vertical joints in a jointed wall system have the same number of connectors.

Presented below are descriptions of the different steps of the proposed analysis procedure. It is expected that the analysis of the individual walls be performed in the following order: 1) the leading wall; 2) intermediate walls starting with that adjacent to the leading wall towards that located next to the trailing wall; and 3) the trailing wall.

Step 1: Define Dimensions, Reinforcement Details, and Material Properties

The following variables are defined in this step.

System Dimensions

h_w = height of the wall system,

t_w = thickness of each wall,

L_s= total length of the wall system,

n = number of walls in the jointed system, and

$l_w = (L_s / n)$ = length of each wall.

Post-tensioning Steel

A_{pt} = area of a post-tensioning tendon,

n_{pt} = number of post-tensioning tendons in each wall,

h_u = unbonded length of the post-tensioning tendon,

$x_{pt,i}$ = location of the i^{th} post-tension tendon from the rocking edge of the wall,

E_p = modulus of elasticity of the post-tensioning tendon,

f_{p0} = initial stress in the post-tensioning tendon,

f_{py} = yield strength of the post-tensioning tendon, and

$A_{p,total}$ (= $n_{pt} A_{pt}$) = total area of post-tensioning steel in each wall.

Confinement Details

A_s = area of confinement steel (which may be taken as $0.5(A_{sx}+A_{sy})$,

A_{sx} = area of confinement steel in the x-direction

A_{sy} = area of confinement steel in the y-direction

s = spacing of the confinement reinforcement,

l_{cr} = length of confinement area, and

f_y = yield strength of the mild steel reinforcement.

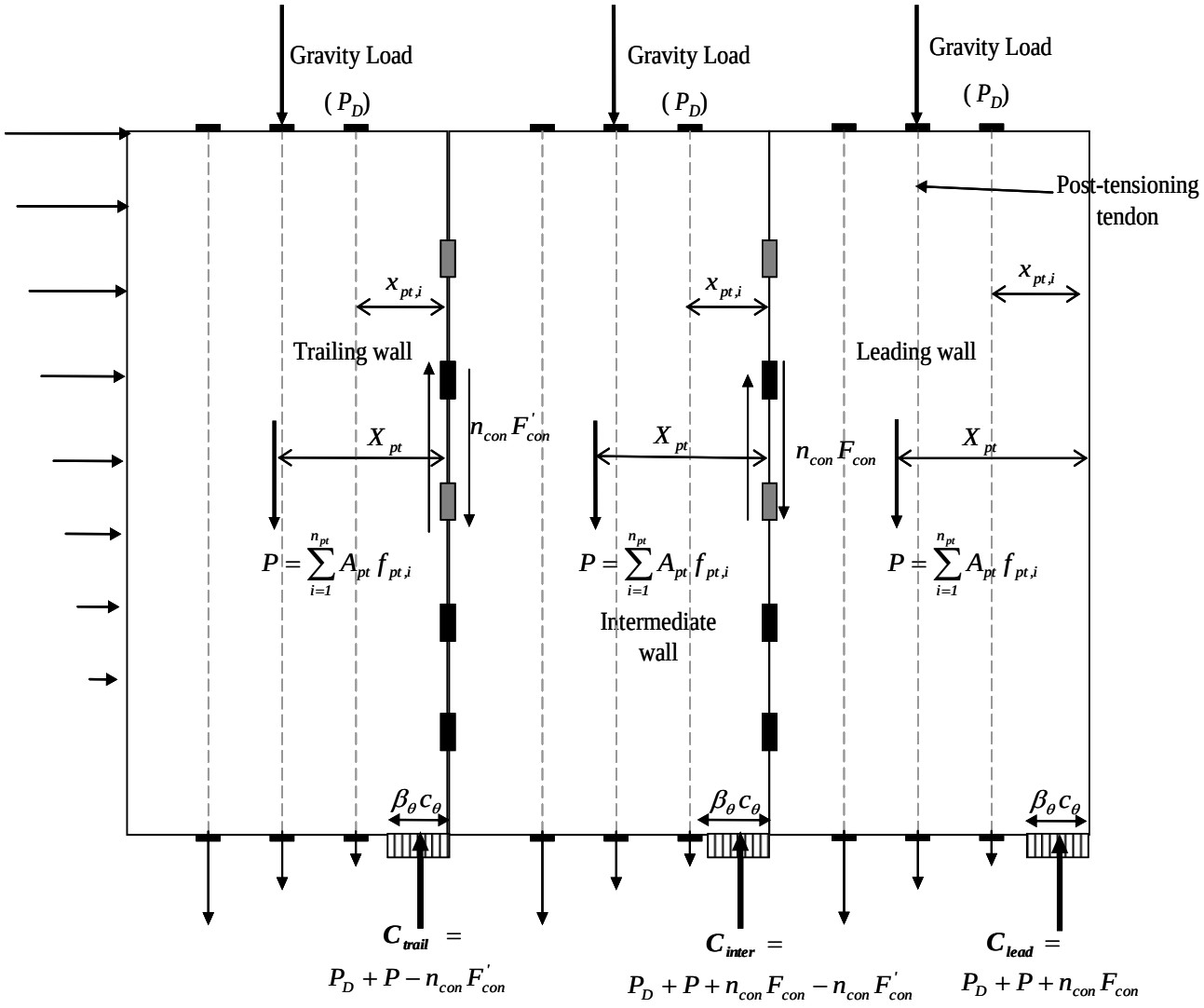

Figure 4.1 Various forces acting on a jointed three-wall system at base rotation θ.

Concrete Properties

f'_c = compressive strength of unconfined concrete,

f'_g = compressive strength of grout,

f'_{cc} = confined concrete strength,

ε_{cc}= concrete strain at f'_{cc},

ε_{cu} = strain capacity of confined concrete, and

γ_c = concrete density.

Connector Details:

n_{con} = number of connectors per joint,

F_{con} = downward connector force acting on the wall at a given displacement,

F'_{con} = upward connector force acting on the wall at a given displacement, and

Δ_{con} = deformation of the connector parallel to the vertical face of wall.

(Use a reliable force-displacement response of the connector to determine the values of F_{con} *and* F'_{con} for a given Δ_{con}, see an example in Figure 3.12.)

Step 2: Decompression point

In this step, the decompression point is established, which defines the beginning of a gap opening at the wall base and corresponds to the condition that makes the stress in the extreme concrete fiber furthest from the rocking edge of the wall reaching a value of zero. Assuming a linear strain distribution at the critical section due to the moment induced by the decompression force (F_{decomp}), the following equations are used to determine the corresponding moment resistance. The decompression moment capacity of the wall *j* ($M_{decomp,\ j}$) is calculated from the elastic flexural formula $\sigma = \frac{Mc}{I}$ and substituting the values for the neutral axis depth (c) and the moment of inertia (I):

$$M_{decomp,j} = \frac{\sigma_j I}{c} \tag{4.1}$$

where σ_j = stress in the wall *j* due to the initial prestress force (F_{po}) and the total gravity load (P_D) and I = moment of inertia of wall based on the gross section properties. Hence,

$$\sigma_j = \frac{P_D + \sum_{1}^{n_{pt}} f_{pi} A_{pt}}{l_w t_w} \tag{4.2}$$

$$I = \frac{1}{12} t_w l_w^3 \tag{4.3}$$

$$c = \frac{l_w}{2} \tag{4.4}$$

Hence, the decompression moment capacity of the wall system (M_{decomp}) is given by

$$M_{decomp} = \sum M_{decomp,j} = \sum_{j=1}^{n} \frac{1}{6} l_w \left[P_D + \sum_{1}^{n_{pt}} f_{pi} A_{pt} \right] \tag{4.5}$$

Step 3: Neutral Axis Depth at 2% Base Rotation

The neutral axis depth that satisfies the vertical direction force equilibrium at the wall base is found for each wall through an iteration process with an assumed neutral axis depth as the initial value. The following sub-steps are used in this process.

1. *Assume a neutral axis depth (c) for the selected wall*

2. *Determine the total gravity load on each wall (P_D)*

$$P_D = \gamma \, l_w \, t_w \, h_w + w_{floor} \, l_w \tag{4.6}$$

where w_{floor} is the uniform dead load acting on the wall.

3. *Determine the stresses and strains in the post-tensioning tendons*

- The elongation of the i^{th} post-tensioning tendon at 2% base rotation is:

$$\Delta_{p,i} = 0.02 * (x_{pt,i} - c) \tag{4.7}$$

- The strain in this post-tensioning tendon is:

$$\varepsilon_{p,i} = \frac{\Delta_{p,i}}{h_u} + \frac{f_{p0}}{E_p} \tag{4.8}$$

- Determine the corresponding stress in the i^{th} post-tensioning tendon ($f_{p,i}$) from the stress-strain curve of the post-tensioning steel. The above steps should be repeated until stresses in all post-tensioning tendons in the wall are obtained.
- The total post-tension force in the wall is, therefore,

$$P = \sum_{1}^{n_{pt}} f_{p,i} A_{pt} \tag{4.9}$$

4. *Determine the forces in the vertical connector*

- Estimate the connector deformation by equating it to the uplift at the wall end. Hence,

$$\Delta_{con} = 0.02*(l_w - c) \tag{4.10}$$

- Calculate the corresponding force in the vertical connector (F_{con}) from the force-displacement response of the connector (see an example in Figure 3.12).

5. *Determine the new neutral axis depth*

Assuming a uniform compressive stress acting at the wall base over a length of βc, where c is the neutral axis depth, the resultant compressive force is obtained as follows:

$$C = (\beta c)\left(\alpha f_{cc}^{'}\right) t_w \tag{4.11}$$

where α and β are the equivalent rectangular block constants and are given by

$\alpha \approx \dfrac{2*r*\left(0.98 - 0.0022*f_c^{'}\right)}{r - 1 + 2^r}$ and $r = 1.24 + 0.01*\left(\dfrac{f_c^{'} - 4.0}{0.25}\right)$; and

β = 0.96. (see Appendix A for justification of the recommended α and β values)

- Calculate the resultant compressive force from equilibrium of forces (see Fig. 4.1)

$C = C_{lead} = P + P_D + n_{con} F_{con}$ for the leading wall (4.11a)

$C = C_{inter} = P + P_D + n_{con} F_{con} - n_{con} F_{con}^{'}$ for an intermediate wall, and (4.11b)

$C = C_{trail} = P + P_D - n_{con} F_{con}^{'}$ for the trailing wall. (4.11c)

where $F_{con}^{'}$, which defines the upward connector force acting on the wall, used in Eqs. 4.11b and 4.11c is equal to F_{con} that is determined in the analysis of the previous wall at 2% base rotation.

- Calculate the neutral axis depth at the wall base

$$c = \frac{C}{\alpha\beta f_{cc}^{'} t_w} \tag{4.12}$$

Iterate the above sub-steps until c calculated in Eq. 4.12 converges to the assumed c value at the beginning of *Step 3*.

Step 4: Select a base rotation (θ)

Choose a value for θ in the range between zero and $\theta_{ultimate}$, where $\theta_{ultimate}$ may be taken as 3% or $1.5\theta_{design}$.

Step 5: Determine forces acting on the j^{th} wall at selected base rotation θ

1. *Determine the neutral axis depth c_θ corresponding to base rotation θ*

   From experimental data and analysis based on the MBA approach on precast walls with unbonded post-tensioning, including those in the jointed system of the PRESSS test building, it was found that the neutral axis depth does not significantly vary beyond an interface rotation of about 0.5% as illustrated in Figure 4.2 (See Section 4.3 for experimental confirmation). Consistent with this observation, the neutral axis depth determined at 2% base rotation in *Step 3* is, therefore, used in the simplified analysis procedure to establish a trilinear relation between the neutral axis depth and the interface rotation at the wall base. This is demonstrated in Figure 4.2, where Point 1 corresponds to the wall length at zero percent base rotation and Points 2 and 3 are defined at base rotations of 0.1 percent and 0.5 percent, respectively. The neutral axis depth (*c*) at point 3 is taken as that found at 2 percent rotation in *Step 3*, whereas the neutral axis depth is approximated 2c at Point 2.

2. *Determine stresses and strains in the post-tensioning steel*

   - The elongation of the post-tensioning tendon:

$$\Delta_{p,i} = \theta^{*}(x_{pt} - c_\theta) \tag{4.13}$$

   - The strain in the post-tensioning tendon:

$$\varepsilon_{p,i} = \frac{\Delta_{p,i}}{h_u} + \frac{f_{p0}}{E_p} \tag{4.14}$$

   - Determine the stress in the i^{th} post-tensioning tendon ($f_{p,i}$) from the stress-strain

curve of the post-tensioning steel. The above steps should be repeated to determine the stresses in all post-tensioning tendons.

- The total post-tensioning force in the wall at the selected base rotation θ

$$P = \sum_{1}^{n_{pt}} f_{p,i} A_{pt} \tag{4.15}$$

- Calculate the location of the resultant post-tensioning force from the rocking edge using Eq. 4.16 (see Figure 4.1).

$$X_{pt} = \frac{\sum_{1}^{n_{pt}} f_{p,i} A_{pt} x_{pt,i}}{P} \tag{4.16}$$

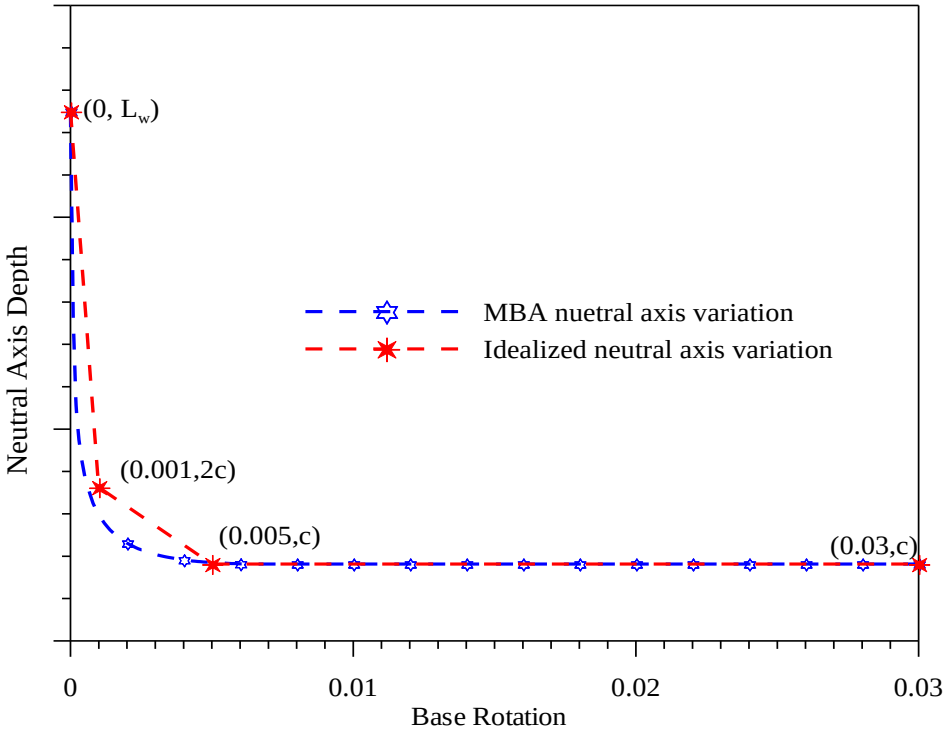

Figure 4.2 An illustration of trilinear idealization used for the neutral axis depth at the base of a wall with unbonded post-tensioning as a function of base rotation.

3. *Determine the forces in the vertical connector*

- Calculate the connector deformation by equating it to the uplift at the wall end

$$\Delta_{con} = \theta^{*}(l_w - c_\theta) \tag{4.17}$$

- Calculate the corresponding downward connector force (F_{con}) using an

appropriate force-displacement response envelope (see an example in Figure 3.12).

4. *Calculate the resultant concrete compressive force at the wall base*

From the equilibrium of forces in the vertical direction (see Fig. 4.1),

$C = C_{lead} = P + P_D + n_{con} F_{con}$ for the leading wall (4.18a)

$C = C_{inter} = P + P_D + n_{con} F_{con} - n_{con} F'_{con}$ for intermediate walls, and (4.18b)

$C = C_{trail} = P + P_D - n_{con} F'_{con}$ for the trailing wall. (4.18c)

where F'_{con}, which defines the upward connector force acting on the wall, used in Eqs. 4.18b and 4.18c is equal to F_{con} that is determined in the analysis of the previous wall at base rotation of θ.

Step 6: Compute the resisting moment of the wall

Taking the moment about the center of the wall (see Fig. 4.1),

For the leading wall,

$$M_{lead} = 0.5 l_w F_{con} + P(X_{pt} - 0.5 l_w) + C(0.5 l_w - 0.5 \beta_\theta c_\theta) \quad (4.19a)$$

For intermediate walls,

$$M_{inter} = 0.5 l_w (F_{con} + F'_{con}) + P(X_{pt} - 0.5 l_w) + C(0.5 l_w - 0.5 \beta_\theta c_\theta) \quad (4.19b)$$

For the trailing wall,

$$M_{trail} = 0.5 l_w F'_{con} + P(X_{pt} - 0.5 l_w) + C(0.5 l_w - 0.5 \beta_\theta c_\theta) \quad (4.19c)$$

In the above equations, $0.5 \beta_\theta c_\theta$ represents the distance to the resultant compression force from the rocking edge of the wall. At the decompression point, the compressive stress variation at the wall bases is expected to be triangular and hence the β_θ value is taken as 0.67 in order to locate the resultant compressive force at the appropriate location. Using Eq. 4.20e and assuming a linear variation for β_θ between the decompression point and θ of up to 0.1%, the value of β_θ is approximated for small θ values using Eq. 4.20d.

$$\beta_\theta = 0.66 + 146.9\theta \text{ for } \theta \le 0.001 \quad (4.20d)$$

For base rotations in the range of 0.1% and $\theta_{ultimate}$ (e.g., 3%), β_θ is obtained from Eq. 4.20e, which was based on Eq. A.11 and assuming a variation of $\varepsilon_{end}/\varepsilon_{cu}$ from 0.2 to 1.0 as θ increases from 0.1% to 3%.

$$\beta_\theta = 1.0 + 0.12\ln[27.6\theta + 0.1725] \text{ for } 0.001 < \theta \le 0.03 \quad (4.20e)$$

Once the moment resistance is calculated as per Eq. 4.19, estimates of critical concrete strains may be obtained. Although this information is not needed for characterizing the behavior of the precast wall system, strain estimates are needed in the design procedure for quantifying the confinement reinforcement. As such, an equation for estimating strains is included in Chapter 5 (see Eq. 5.12) and its validation is presented in Section 4.3.2.4.

Repeat *Steps 4* through *6* and obtain moment resistance of the wall for all θ values.

Repeat *Steps 3* through *6* until the moment resistance of each wall in the wall system is found as a function of the base rotation.

Step 7: Compute the resisting moment of the entire wall system

The moment resistance of the wall system as a function of base rotation may be obtained by summing the resistance of the individual walls at each selected value of θ using Eq. 4.21.

$$M_{wall\ system} = M_{lead} + \sum_{2}^{n-1} M_{inter} + M_{trail} \quad (4.21)$$

4.2.1 Applications to Other Wall Systems

Although the simplified procedure presented above is for the jointed wall systems with equal wall lengths, it can be equally applied to characterize the lateral load behavior of precast

single walls with unbonded post-tensioning and jointed wall systems with different wall lengths. For the single wall analysis, the connector force should be set to zero. For jointed systems walls with different wall lengths, appropriate wall lengths should be used to estimate the neutral axis depths, connector forces, and wall base moment resistance.

4.3 Experimental Validation

This section presents validation for the simplified analysis procedure presented in Section 4.2, by comparing selected analysis results with available experimental data. For this purpose, the wall direction response of the PRESSS test building and tests conducted by Perez et al. (2004) on single precast walls with unbonded tendons are primarily used. The selected responses include the envelopes of the base moment resistance as a function of the top floor lateral displacement, elongation in the post-tensioning steel, and the neutral axis depths at the wall bases.

4.3.1 PRESSS Jointed wall

Following the PRESSS building test, Thomas and Sritharan (2004) completed an investigation that quantified the actual lateral force resistance of the jointed wall system by separating its contribution from the wall direction response. During this investigation, they found that the wall direction response of the PRESSS building was significantly influenced by framing action resulting from the seismic columns and precast floors in the bottom three stories. By isolating the contribution of the framing action, they arrived at the experimental base moment vs. displacement response envelope for the wall system using data points recorded during testing at selected measured lateral displacements (see examples in Figures 2.2 to 2.4). Six displacement transducers measured the vertical displacements of the leading and trailing walls at the base with respect to the wall foundation. Using the data from these devices, the neutral axis depths (c) and the post-tensioning tendons elongations (Δ_p) were also established for the leading and trailing walls at the selected lateral displacements. Also estimated from the displacement devices was the wall end uplift ($\Delta_{end\ uplift}$) for the leading wall. The wall end uplift, which was assumed to be the same as the relative vertical displacement between the walls for the analysis procedure presented in the previous section,

was comparable to the measured relative vertical displacement between walls shown in Figures 2.6 and 2.8. By assuming a linear profile for the gap opening at the base, Thomas and Sritharan presented change in the post-tensioning force, post-tensioning elongation, the UFP connector displacement, and the neutral axis depth as a function of the top floor displacement for the PRESSS wall system. This information, along with the dimensions and properties reported by these researchers, is used to verify the applicability of the simplified analysis method for the PRESSS jointed wall system.

4.3.1.1 Base Moment Resistance

Figure 4.3 compares the base moment vs. the top lateral displacement established for the jointed wall with those calculated from the simplified analysis procedure. It is seen that the simplified analysis procedure provides a good estimate for the base moment vs. lateral displacement response envelope. At the top floor displacement of 11.5 inch, the calculated base moment resistance from the simplified analysis method is only 2.9% below the experimental value. At the design drift of 2%, the simplified analysis procedure underestimated the moment resistance of the jointed wall by 3.9%.

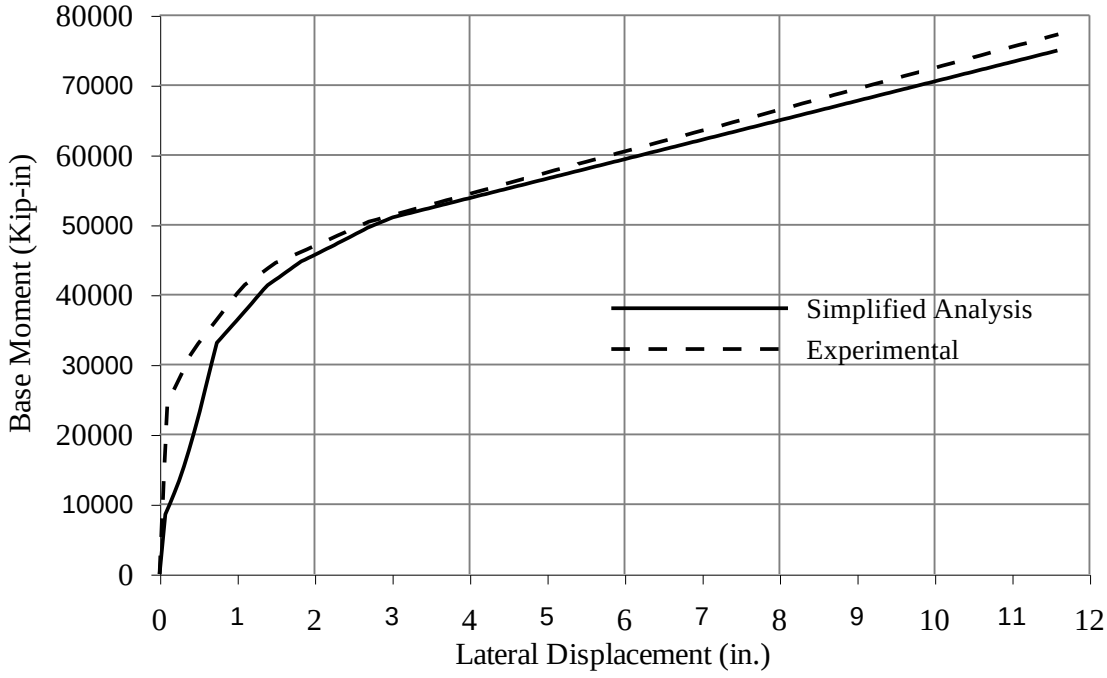

Figure 4.3 The base moment vs. top floor displacement for the PRESSS jointed wall system.

4.3.1.2 Neutral Axis Depth

The neutral axis depths calculated using the simple analysis procedure for the PRESSS jointed wall system are compared with those obtained from experimental data in Figures 4.4 and 4.5. It is seen from these figures that the simplified method provides a good estimate for the neutral axis depth for both leading and trailing walls. There are some differences that exist between the analytical and extracted neutral axis depths, which are largely responsible for the small underestimation in the elongation of the post-tensioning tendons in Figures 4.6 and 4.7 and the corresponding moment resistance in Figure 4.3. A more accurate estimate of the neutral axis depths will more accurately predict the elongations of the post-tensioning tendons. Furthermore, Figures 4.4 and 4.5 confirm that the assumption of using a constant neutral axis for base rotations above a small threshold value is acceptable.

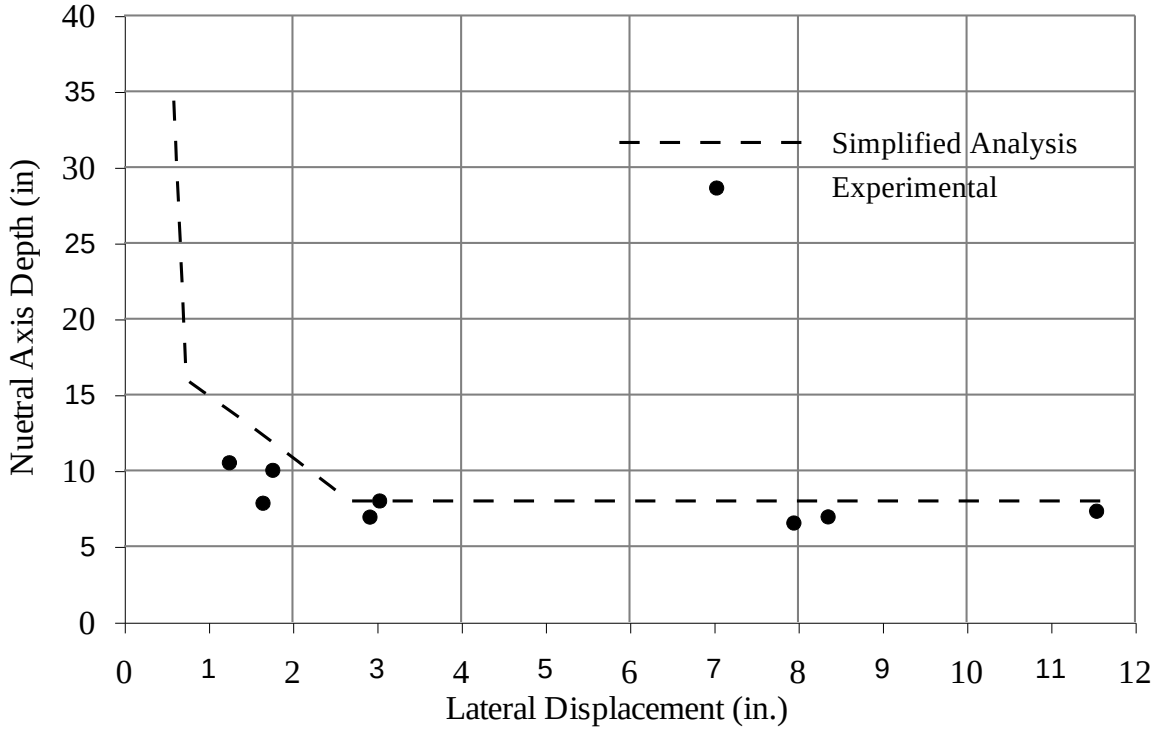

Figure 4.4 The change in the nuetral axis depth in the leading wall.

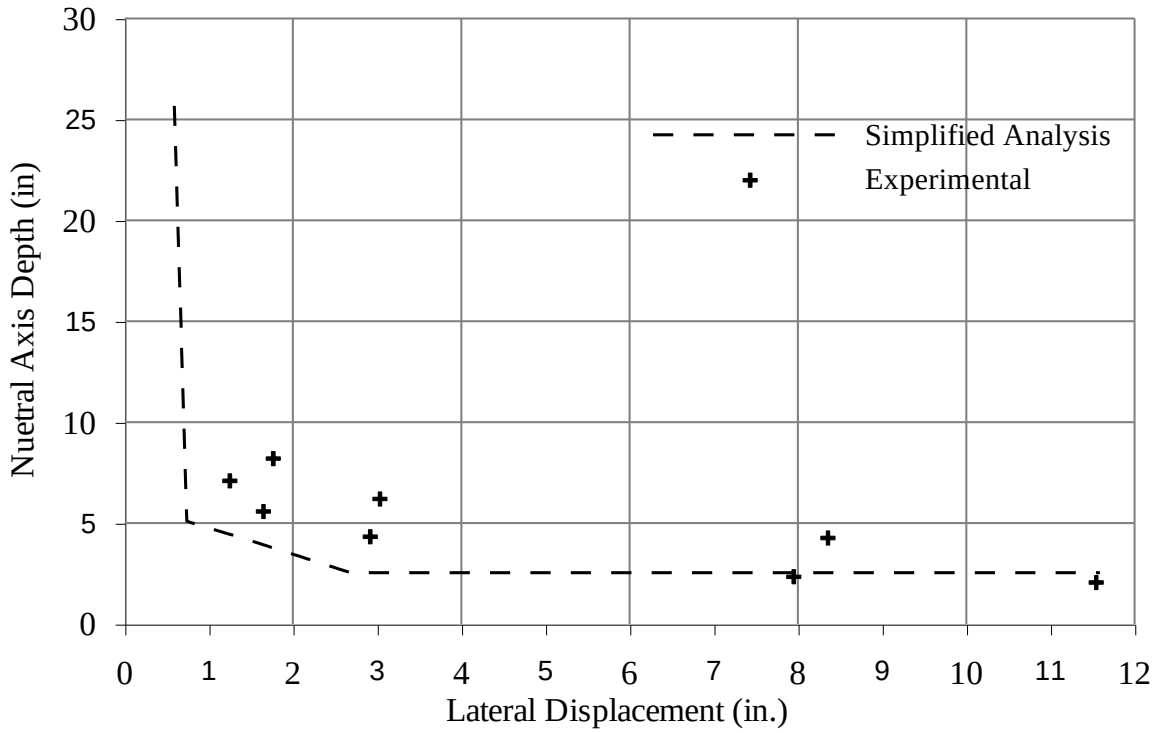

Figure 4.5 The change in the nuetral axis depth in the trailing wall.

4.3.1.3 Post-tensioning Elongation

Figures 4.6 and 4.7 compare the calculated post-tensioning steel elongation with the experimental data for both the leading and trailing walls as a function of lateral displacement. The elongation at the maximum top floor displacement of 11.5 in. (or 2.56% drift) in the leading wall was underestimated by 5.42% using the simplified procedure. Likewise, the elongation in the trailing wall was underestimated by 4.58% by the simplified procedure at the same drift level.

The jointed wall system was also analyzed using the MBA concept. The results of this analysis may be found in Thomas and Sritharan (2004). Overall the MBA analysis results provided somewhat better comparison with the experimental values. However the difference between the MBA and the simplified analysis results are insignificant.

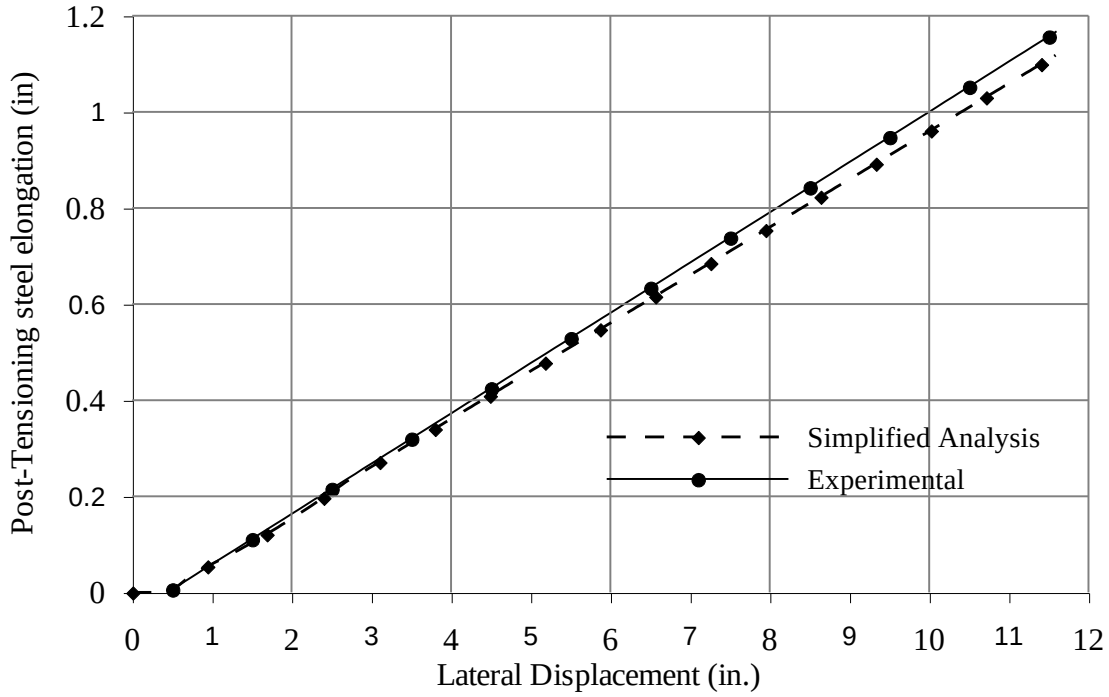

Figure 4.6 The change in the post-tensioning steel elongation in the leading wall.

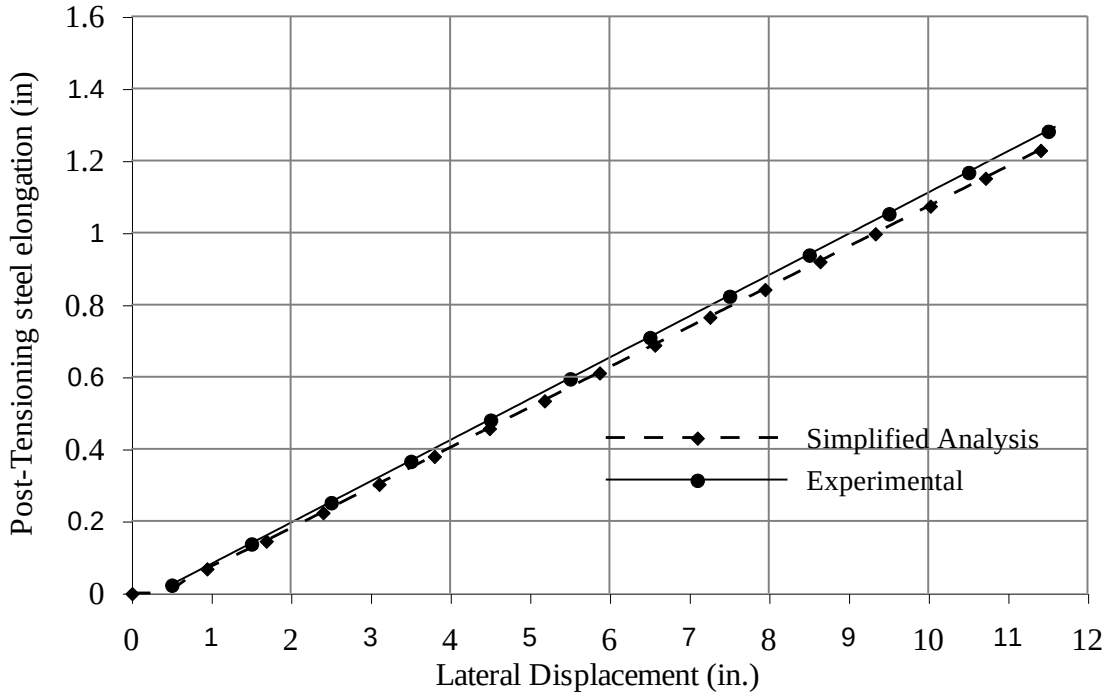

Figure 4.7 The change in the post-tensioning steel elongation in the trailing wall.

4.3.2 Single Walls with Unbonded Post-Tensioning

Perez et al. (2004) conducted a series of lateral load tests on single precast walls designed with unbonded post-tensioning. The test specimens chosen from this study for experimental validation were TW1, TW3 and TW5. Dimensions and properties of these test walls are summarized in Tables 4.1. The walls were subjected to lateral displacements to study their seismic behavior while maintaining a constant axial load in the center of the wall to simulate the gravity load effects. The lateral displacements to the walls were imposed using a hydraulic actuator connected to the top of the walls. TW1 was tested to a monotonically increasing lateral load while TW3 and TW5 were subjected to full reverse cyclic loads. The load sequence of TW3 consisted of three cycles each at the following drifts: 0.05%, 0.1%, 0.25%, 1%, 1.5%, 2% and 3%. In addition to following these cycles, TW5 was subjected to three cycles at 3.5%, 4%, 5% and 6%.

During each wall test, the lateral displacement of the loading block at the wall top, which provided the actual wall lateral displacement, was measured using four displacement devices: two string potentiometers (LB SP-N and LB SP-S) and two LVDTs (LB LVDT-N and LB LVDT-S), where N and S refer to the north and south sides of the test wall, respectively. The rotation at the wall base was measured using a rotation meter (RMB), which was positioned 9 inches above the base of each wall. A series of displacement devices mounted at 5 inches above the wall base measured the opening of the gap at the wall-to-foundation interface. Concrete strain gauges were attached to #4 reinforcing bars running vertically within the confined portions of the bottom wall panel. Assuming strain compatibility between concrete and steel, the measured strains were reported by the researchers to represent the confined concrete strains at the location of the gauges. Strain gauges were also attached to the post-tensioning steel to monitor the initial prestress as well as the variation resulting from the applied lateral load. More complete details of the test units and instrumentation may be found in Perez et al. (2004).

Presented below are comparisons between the experimental data and the analytical results obtained from the simplified analysis procedure using the properties summarized in

Table 4.1 The properties for unbonded precast single walls tested by Perez et al. (2004).

	Parameter	TW1	TW3	TW5
Wall Parameters	Length	100 in.	100 in.	100 in.
	Height	284.75 in.	284.75 in.	284.75 in.
	Unbonded Length	390 in.	390 in.	390 in.
	Thickness	6 in.	6 in.	6 in.
	Length of Confinement	26.75 in.	26.875 in.	26.875 in.
	Height of Confinement	130 in.	130 in.	130 in.
	Thickness of Confinement	4 in.	4.75 in.	4.75 in.
Prestress Parameters	Prestress Steel Area	7.5 in^2.	7.5 in^2.	3.75 in^2.
	Eccentricity	17.25 in.	17.25 in.	20 in.
	Initial Stress	88.5 ksi	88.5 ksi	44.3 ksi
	Initial Prestress Force	663.6 kip	663.6 kip	165.9 kip
	Initial Stress in Concrete	1.19 ksi	1.19 ksi	0.59 ksi
Properties of Spiral Confinement Reinforcement	Yield Strength	60 ksi	60 ksi	60 ksi
	Ultimate Strength	90 ksi	90 ksi	90 ksi
Concrete Properties and Confinement	Concrete Strength ($f_c^{'}$)	6.0 ksi	8 ksi	8 ksi
	$E_{concrete}$	4415 ksi	5098 ksi	5098 ksi
	Volumetric Ratio of Confinement Reinforcement	7.39 % (spiral reinforcement)	ρ_x = 2.47%; ρ_y = 1.75% (hoop reinf.)	ρ_x = 2.47%; ρ_y = 1.75% (hoop reinf.)
Load Parameters	Axial Load (N)	173.4 kips	173.4 kips	173.4 kips

Table 4.1. In addition to the global response of the walls defined by the base shear vs. lateral drift response envelope, the variations in the neutral axis depth, strains in the post-tensioning bars and the confined concrete strain as a function of lateral drift are examined.

4.3.2.1 Global Response Envelope

The measured and calculated lateral load response envelopes of walls TW1, TW3 and TW5 are presented by plotting the base shear vs. the lateral drift in Figures 4.8, 4.9 and 4.10, respectively. From these figures, it is clear that the simplified analysis procedure satisfactorily captured the overall response of all three walls except for TW3 at drifts above 2% due to premature failure of this wall. In each case, the initial stiffness and the ultimate shear capacity were calculated with sufficient accuracy. Table 4.2 summarizes the calculated and experimental base shear capacities of the walls at the maximum drift. It is seen that the analysis method overestimated the base shear capacities of walls TW3 and TW5 only by 5.2% and 2.8%, respectively, whereas the base shear capacity of TW1 was underestimated by 0.3%.

Table 4.2 Comparison of base shear capacities calculated for unbonded single precast walls.

	TW1 (kips)	**TW3 (kips)**	**TW5 (kips)**
Experimental	161.0	154.3	102.0
Simplified analysis method	160.6	162.3	104.8

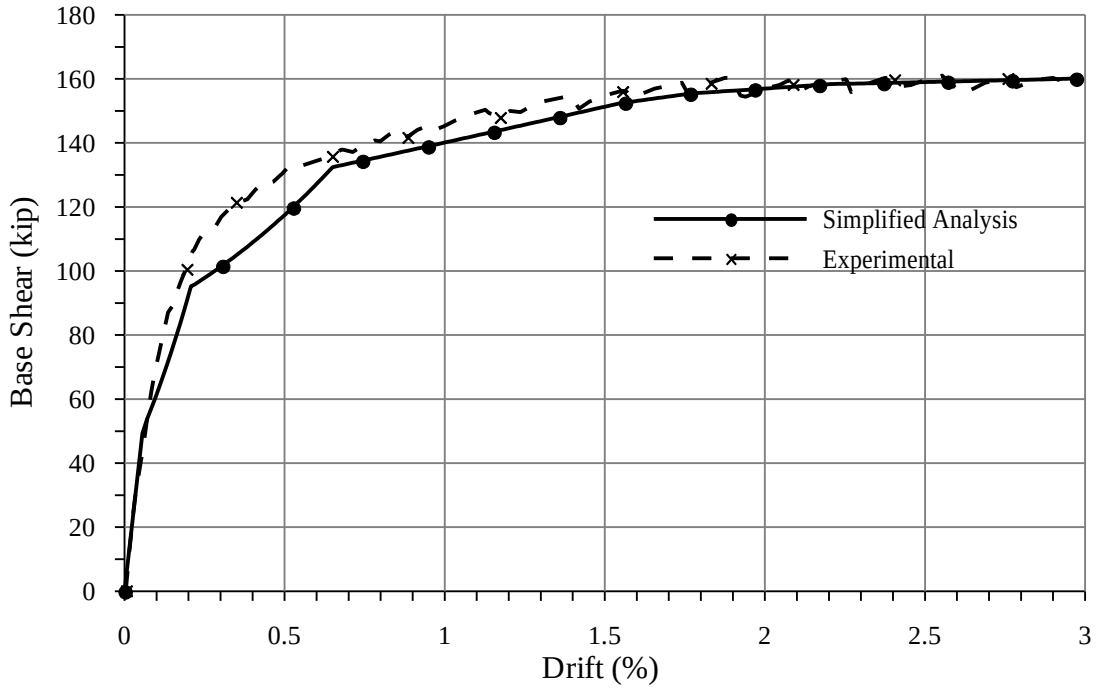

Figure 4.8 Base shear resistance vs. lateral drift response envelope for TW1.

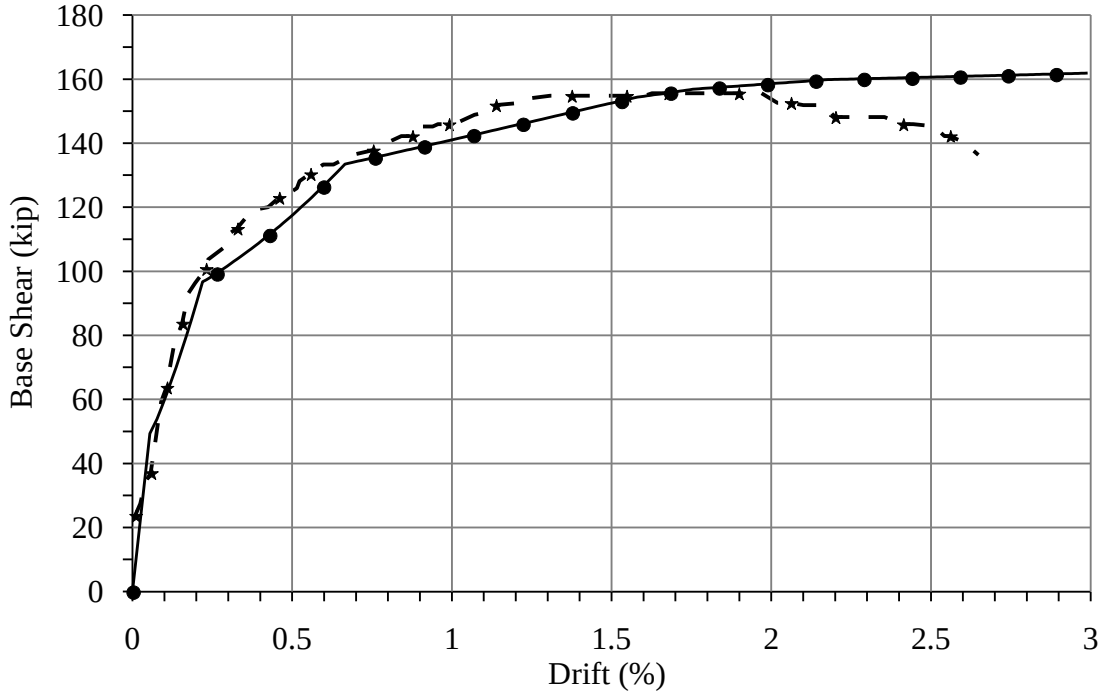

Figure 4.9 Base shear resistance vs. lateral drift response envelope for TW3.

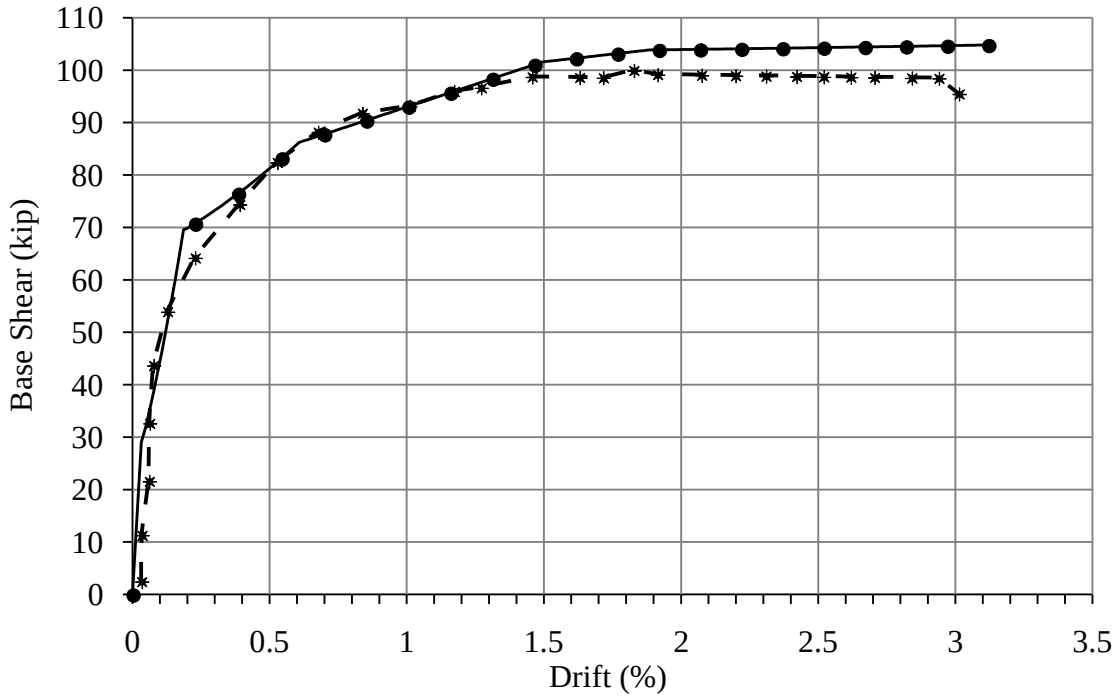

Figure 4.10 Base shear resistance vs. lateral drift response envelope for TW5.

4.3.2.2 Neutral Axis Depth

The neutral axis depths calculated by the simplified analysis method are compared with the experimental data in Figures 4.11 for TW1. Note that the x-axis in this figure represents the lateral drift rather than the rotation at the base of the wall. The comparison between the calculated and measured neutral axis depth is not only satisfactory, but also supports the tri-linear approximation with a constant neutral axis depth for base rotations above 0.5% as assumed in the simplified analysis procedure. In Table 4.3, the experimental and calculated neutral axis depths obtained at 2% drift are compared, which also seems adequate given the approximations made and the relatively small impact that the error in the neural axis depth has on predicting the other key response parameters (e.g., see Section 4.3.2.3). A graphical comparison for the neutral axis depth is not presented here for TW3 or TW5 because the researchers reported the neural axis depth only at a few selected drifts for these two walls.

Table 4.3 Comparison of neutral axis depths at 2% drift for unbonded single precast walls

	TW1	TW3	TW5
Experimental	20.37 in.	18.95 in.	14.02 in.
Simplified analysis method	22.51 in.	21.88 in.	13.02 in.

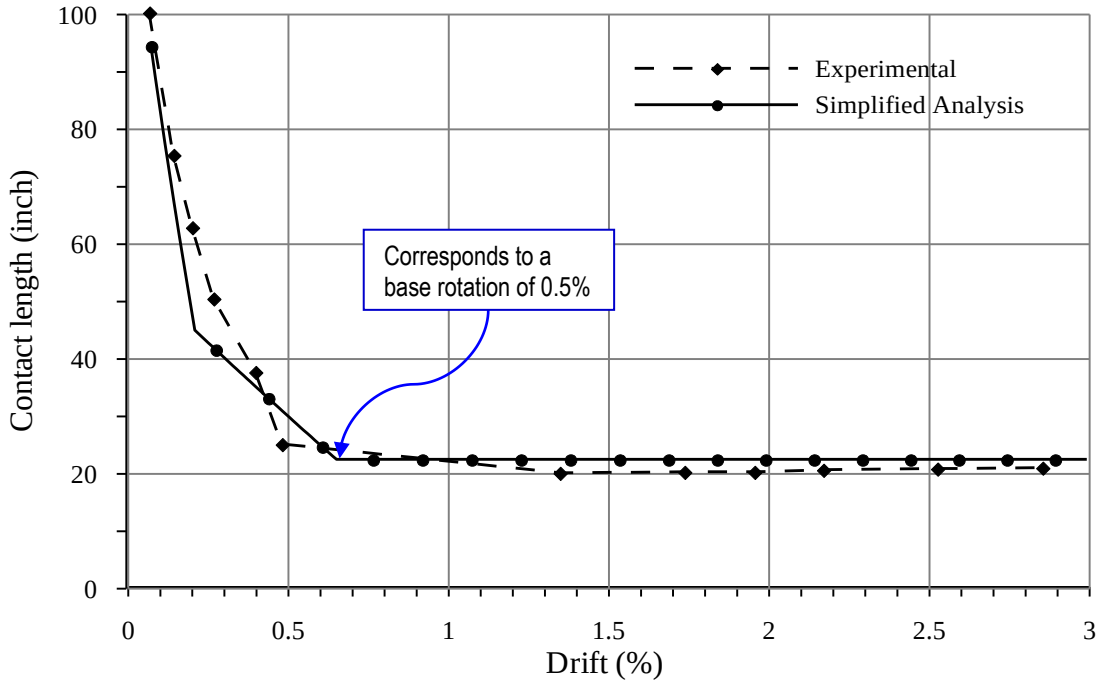

Figure 4.11 The neutral axis depth of TW1 as a function of lateral drift.

4.3.2.3 Elongation of Post-tensioning Steel

The change in post-tensioning steel stress was calculated as a function of lateral drift for bars positioned at different locations in TW1, TW3 and TW5 and they are compared with experimental data in Figures 4.12, 4.13 and 4.14, respectively. Overall, the simplified analysis method estimated the variation in the stress of the post-tensioning steel satisfactorily, and it also predicted the yielding of the post-tensioning steel that occurred at a drift of about 1.5% for the most critical bar. These comparisons also confirm that the small differences seen in the neural axis depth comparisons in Table 4.3 did not significantly affect the calculated variation of strain in the post-tensioning steel.

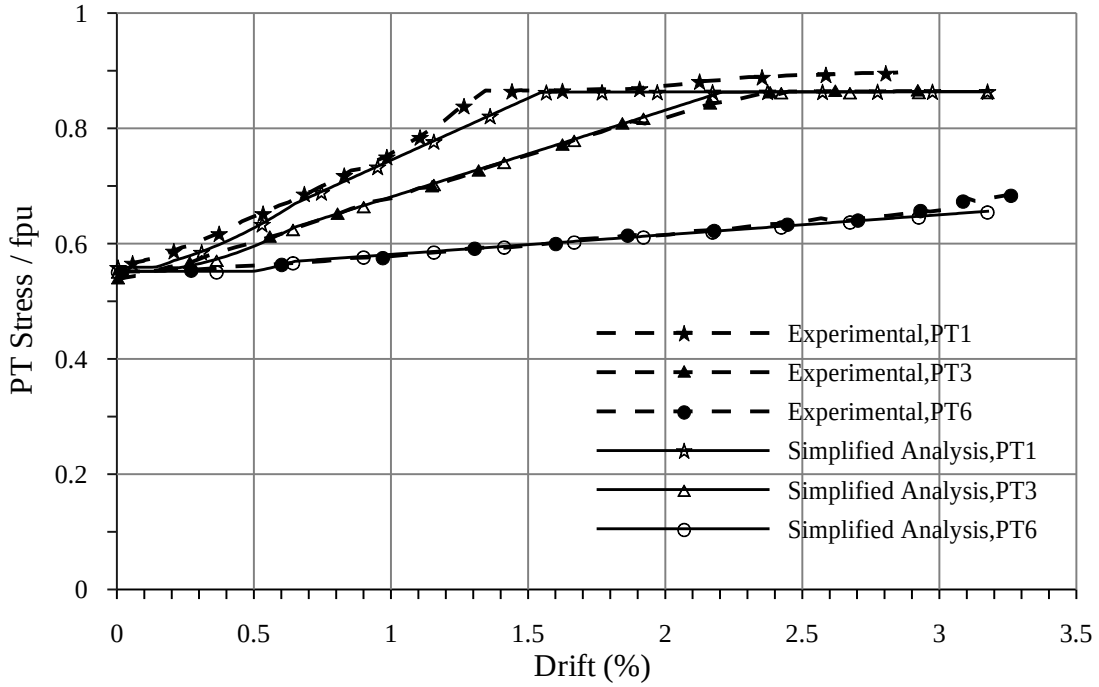

Figure 4.12 Variation of post-tensioning steel stress in TW5 with lateral drift.

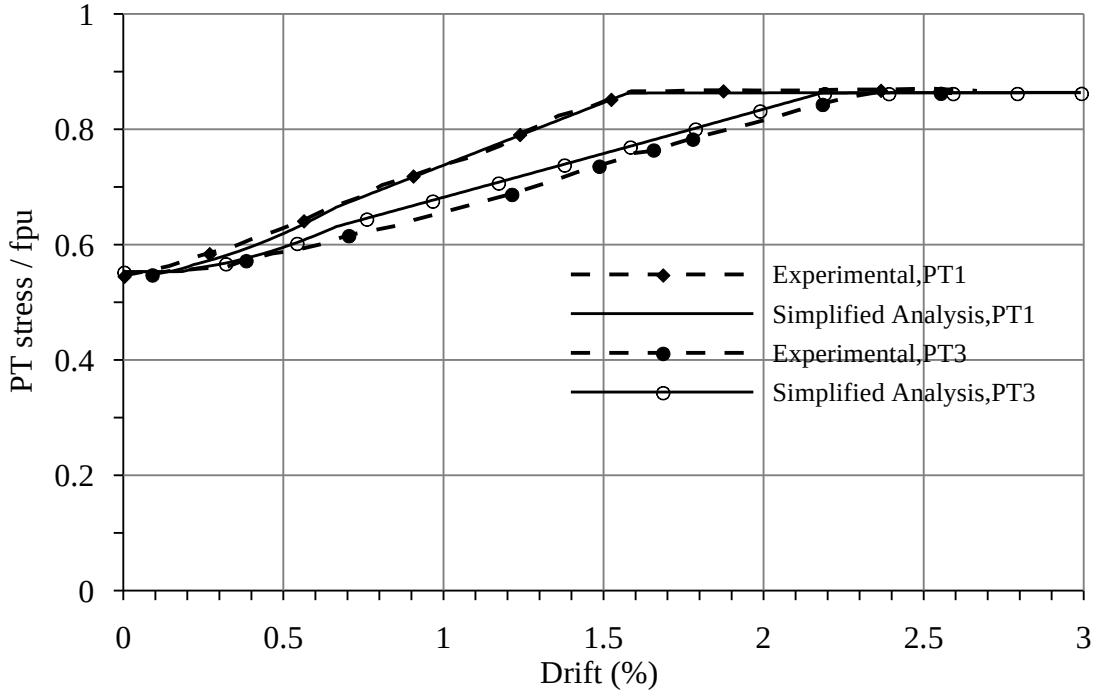

Figure 4.13 Variation of post-tensioning steel stress in TW3 with lateral drift.

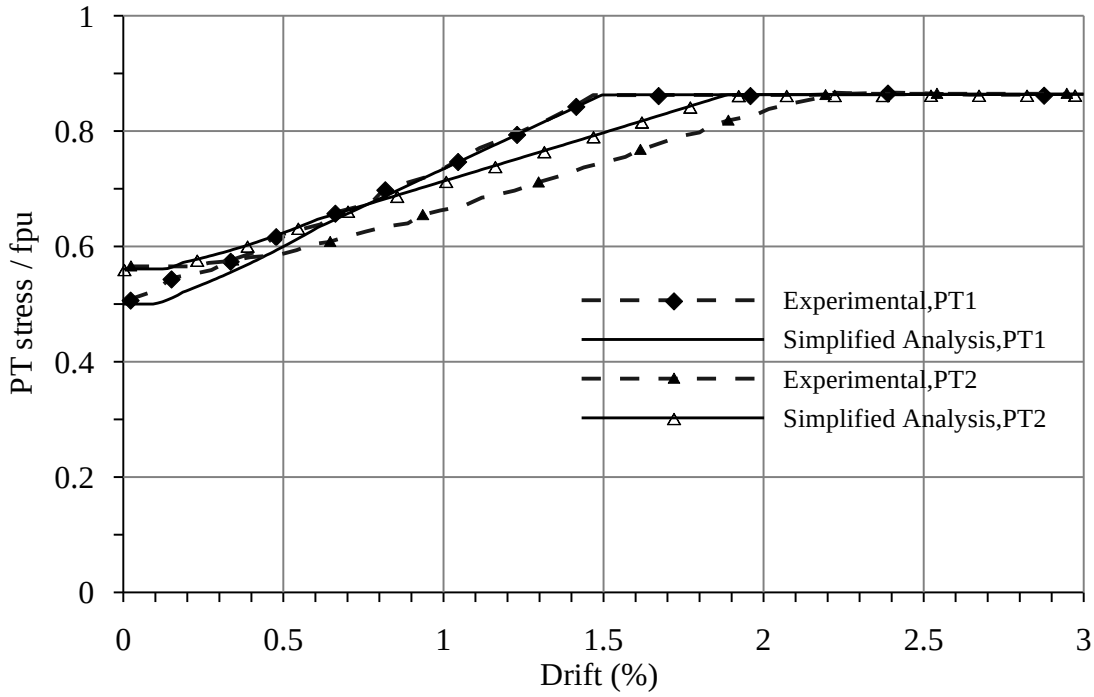

Figure 4.14 Variation of post-tensioning steel stress in TW5 with lateral drift.

4.3.2.4 Concrete Confinement Strain

The strain data obtained from a concrete gauge in TW1 is compared with the analysis results in Figure 4.15, in which the analytical values were obtained using Eq. 5.12. This concrete gauge was located in the confined concrete region at a distance of 4.5 in. from the compression wall end and at a height of 5 in. from the wall base. Given the simplicity used in the analysis approach, the comparison between the measured and calculated strains is remarkably good. At large drifts, the estimated strains by the analysis are underestimated. However, this is not of serious concern for two reasons: 1) given the complexity associated with the behavior of jointed connections, Eq. 5.12 is established to obtain estimates not the actual strains, and 2) the confined concrete models are inherently conservative and thus basing the confinement reinforcement on the estimated strains will provide reserve strain capacity as much as 50% above the maximum strains expected based on the theoretical confinement models. The analysis and design methods are targeted to obtain more accurate results at a design base rotation of 2% (corresponding to a drift of slightly above 2%). It is

observed in Figure 4.15 that the measured and estimated strains show excellent agreement at lateral displacements near the design drift.

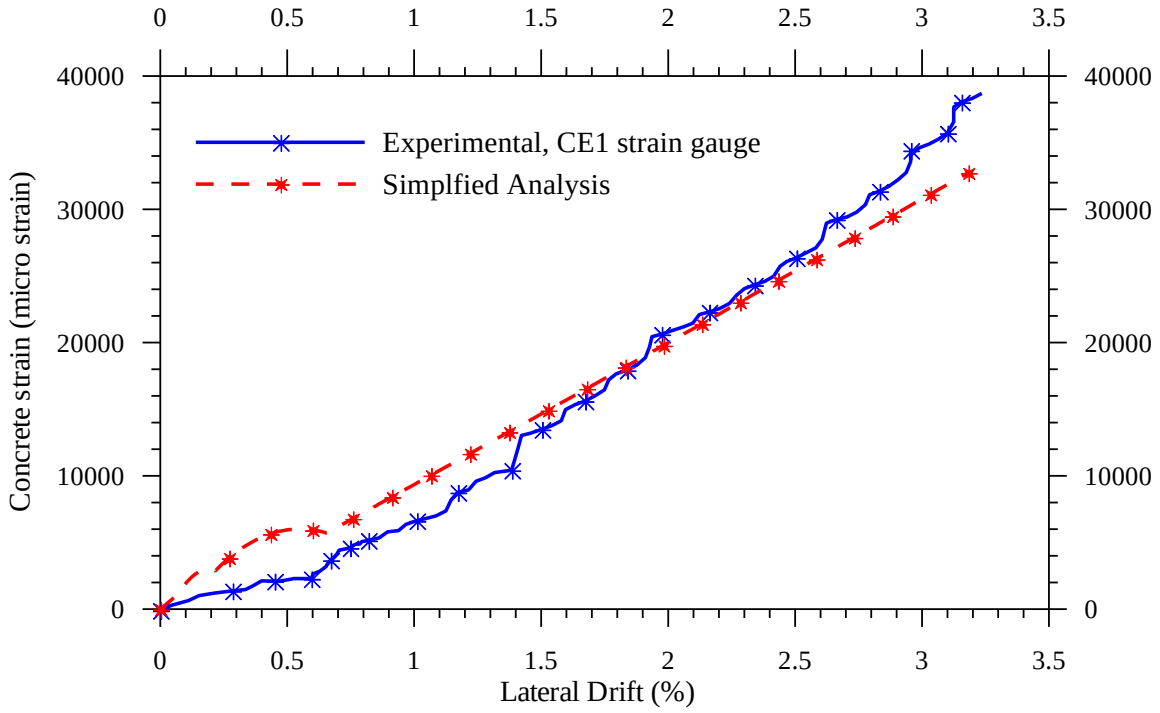

Figure 4.15 Comparison of concrete strains in the confined region of TW1.

Intentionally blank

CHAPTER 5: DESIGN METHODOLOGY

5.1 Introduction

This chapter presents a seismic design procedure for unbonded post-tensioned jointed wall systems that have multiple walls with identical dimensions. As noted previously, at the completion of the PRESSS program, Stanton and Nakaki (2002) published a set of guidelines for the design of all five precast structural systems tested in the PRESSS building. Subsequently, the guidelines proposed for the precast jointed wall system were examined by Thomas and Sritharan (2004) using the data from the PRESSS test building. The design methodology summarized in this chapter generally follows that proposed by Stanton and Nakaki (2002) and addresses the shortcomings of the methodology identified by Thomas and Sritharan. A critical issue that was not addressed in the original design method was how the design base moment determined for the wall system should be divided up between the individual precast walls. The proposed methodology not only addresses this issue, but proposes a simplification in the methodology by requiring the design of only the most critical wall. The remaining walls in the jointed system are detailed with essentially the same post-tensioning and connector details. The proposed methodology is also demonstrated through two sets of design examples.

5.2 Jointed Wall System

In a jointed wall system considered in this chapter, multiple precast walls with identical dimensions, as illustrated in Figure 5.1, are used. Each wall is anchored to the foundation using unbonded post-tensioned tendons that are concentrated at the center of the wall. Furthermore, the walls are connected to each other using special connectors along the vertical joints. As described previously, the basic concept of the wall system is such that it will allow the walls to rock individually at the base when the wall system is subjected to a lateral force and return to its original vertical position when the force is removed. The post-tensioned tendons are typically designed to remain elastic up to the design-level earthquake loading. As a result, the post-tensioning tendons provide sufficient restoring force for the

jointed wall even when the vertical connectors experience inelastic action due to the earthquake load. This restoring force helps to minimize the residual displacements of the wall system when the lateral load is removed. The restoring capacity of the jointed wall depends on the amount of post-tensioning steel, the number of vertical connectors, initial prestressing force, and the cyclic behavior of the vertical connector. The shear transfer from the wall to the foundation at the base utilizes a friction mechanism.

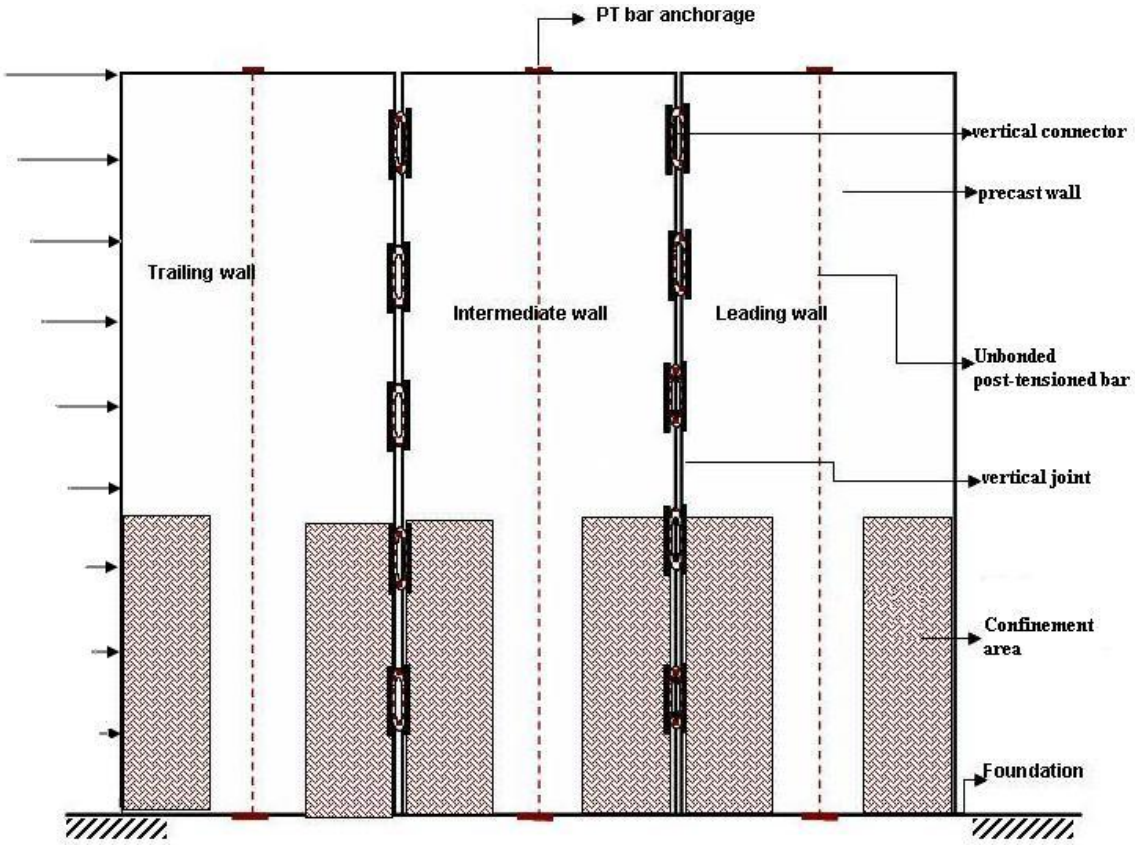

Figure 5.1 Details of a precast jointed wall system.

5.3 Summary of Parametric Study

Lateral load resistance of a jointed wall system at a given drift depends on the geometry and number of walls in the system, the amount of post-tensioning steel, the number of vertical connectors, initial prestressing force, and the force-displacement response of the vertical connector. To understand the effects of several of these design parameters on the

response of jointed wall systems, a parametric study was conducted involving jointed systems consisting of two, three, and four precast walls (Aaleti, 2005). All wall systems were assumed to satisfy the aforementioned assumptions. From this study, the following conclusions were drawn:

1. In a jointed two-wall system, the leading wall will provide about 2/3rd of the total lateral force resistance, but the actual moment resistance of the leading wall will be dependent on the force transmitted through the vertical connectors. This conclusion is consistent with the response of the jointed wall system in the PRESSS building.

2. In a jointed wall system having more than two walls, each of the intermediate walls will provide a larger moment resistance than the leading or the trailing wall. The percentage contribution of an intermediate wall towards the total base moment resistance will depend on the number of walls in the jointed system as well as the force transmitted through the connectors.

3. As suggested by Thomas and Sritharan (2004), the post-tensioning steel in the trailing wall would first reach the yield limit state in a jointed wall system, which should dictate the initial design stress for the post-tensioning steel. However, the wall providing the largest moment resistance should be used to design the required area of the post-tensioning steel.

5.4 Methodology

Incorporating the findings from the parametric study summarized in Section 5.3, a procedure for seismic design of precast post-tensioned jointed walls is presented in this section.

5.4.1 Design Assumptions

Consistent with the recommendations of Stanton and Nakaki (2002), the following assumptions are made for the design of jointed precast wall systems:

- The wall will undergo in-plane deformations only. Torsion and out-of-plane deformations are prevented by providing adequate out-of-plane bracing.

- All individual walls are assumed to have identical dimensions, reinforcement details, and the initial prestressing force.

- All the vertical joints contain an equal number of identical connectors and a dependable force vs. displacement response envelope is available for the connector (e.g., see Fig. 3.12).

- All walls undergo the same lateral displacement at the floor and roof levels due to the rigid floor assumption.

- The post-tensioning steel is located at the center of each wall.

- The strength of fiber grout that is placed between the wall base and foundation is greater than the strength of concrete in the walls.

- The post-tensioning steel reaches the yield strain at the design drift. The corresponding rotation at the wall base is assumed to be θ_{design}, which may be taken as 2%. Alternatively, use an acceptable wall design drift to estimate a suitable value for $\theta_{design.}$

5.4.2 Design Steps

The following seven steps are recommended for the design of the jointed wall systems.

Step 1: Material Properties and Wall Dimensions

- Select the following material properties.

  Prestressing tendon: Modulus of elasticity (E_p) and yield strength (f_{py}).

  Concrete: Unconfined concrete strength ($f_c^{'}$), elastic modulus of concrete (E_c) which may be approximated to $58{,}000\sqrt{f_c^{'}(psi)}$ or $4800\sqrt{f_c^{'}(MPa)}$, and appropriate coefficient of friction between the precast wall base and foundation (μ).

  Connector: Force vs. displacement response envelope.

- Establish the wall dimensions.

  Select the total length of the wall system (L_s) or length of a single wall (L_w), wall height (H_w), wall thickness (t_w), and the number of walls (n). The height and length of the wall system can be determined from the architectural drawings or from preliminary design calculations.

  When deciding the number of walls in each system, use a smallest possible value for n with a suitable H_w/L_w ratio. Stanton and Nakaki (2002) suggest that H_w/L_w should be more than 2.0 to ensure flexural dominant behavior by each wall. Consequently, if the length of each wall or the total length of the wall system is known, the other variable can be determined from Eq. 5.1.

$$L_w = \frac{L_s}{n} \tag{5.1}$$

  The following guidance may be used to determine an initial value for the wall thickness:

  1. select a value in the range of $h_{story}/16$ to $h_{story}/25$, where h_{story} is the story height (Englekirk 2003);

2. ensure that the selected wall thickness should be sufficient to limit the shear stress in the wall to the permissible limit specified in the current building standard (e.g., ACI 318-05 2005); and

3. the selected wall thickness should be sufficient to accommodate the required confinement reinforcement at the wall ends without causing any construction difficulties.

Step 2: Required Design Moment Resistance

Using a force-based design (FBD) or direct displacement-based design (DDBD) procedure, arrive at the required base moment resistance for the wall system (M_{design}). Hence, the precast wall system should be designed such that

$$\phi M_n \geq M_{design} \tag{5.2}$$

where ϕ is the flexural strength reduction factor and M_n is the nominal moment capacity of the wall system at the design drift.

Step 3: Force Resisted by the Connector

- Assuming a vertical relative displacement between two adjacent walls to be $0.9L_w\theta_{design}$, estimate the force in the connector (F_{con}) at the design drift from the force-displacement envelope curve available for the connector (see an example in Figure 3.12).

- For the wall systems described above, a symmetric lateral response is expected when they are subjected to symmetric cyclic loading. For such systems, the hysteretic energy dissipation can be correlated to equivalent viscous damping using Eq. 5.3.

$$\zeta_{eq} = \frac{2}{\pi}\frac{A_{loop}}{A_{rect}} \tag{5.3}$$

where A_{loop} is the area enclosed by a symmetric hysteresis loop at the design drift and A_{rect} is the area of the rectangle circumscribing the hysteresis loop.

- The number of connectors should be determined such that a desired level of equivalent damping is incorporated in the wall system. If UFP connectors, as successfully used in the PRESSS wall, are chosen, then the required number of connectors may be established from Eq. 5.4 to ensure that the wall system would have a desired level of equivalent damping (Galusha 1999).

$$N_{con} = \frac{\pi\zeta_{eq}M_n}{1.25(n-1)F_{con}L_w} \tag{5.4}$$

where N_{con} is the number of connectors in each vertical joint between the precast walls and ζ_{eq} is the required level of equivalent viscous damping, which should be in the 15 to 20 percent range to ensure that the wall system will have adequate damping.

Step 4: Required Area of the Post-tensioning Steel

- In a jointed wall system containing walls with equal dimensions, the design moment for the wall that would provide the largest moment resistance can be determined from Eq. 5.5.

$$M_{design,wall} = \Omega\frac{M_{design}}{n\phi} \tag{5.5a}$$

$$\Omega = 1 + \frac{\lambda\phi N_{con}F_{con}L_w}{M_{design}} \tag{5.5b}$$

where Ω is the moment contribution factor and λ is a constant. When $n = 2$, $\lambda = 0.9$ and $M_{design,wall}$ will correspond to the moment demand in the leading wall (i.e., $M_{design,lead}$). When $n \geq 3$, $\lambda = 1.05$ and the $M_{design,wall}$ will correspond to the moment in an intermediate wall (i.e., $M_{design,inter}$). The derivation of Eq. 5.5 and suitable values for λ are presented in Appendix B.

- If the jointed system contains only two walls (i.e., $n = 2$), design the area of the post-tensioning steel, A_p, using Eq. 5.6, which uses the moment equilibrium of forces acting on the base of the leading wall (see Figure 5.2).

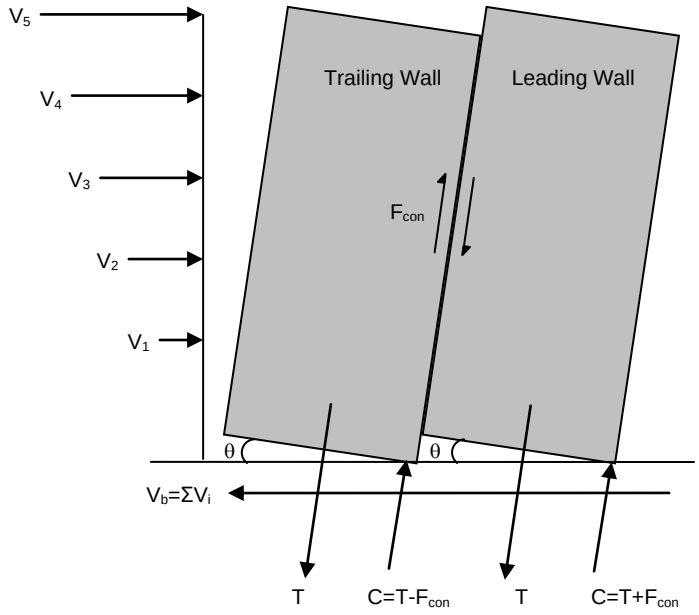

Figure 5.2 Forces acting on a jointed two-wall system at base rotation θ (C = resultant compressive force and $T = P_D$ + *force in the prestressing tendons*)

$$M_{design,lead} = \left(P_D + 0.95 f_{py} A_p\right) * \left(\frac{L_w}{2} - \frac{P_D + 0.95 f_{py} A_p + N_{con} F_{con}}{2 * (\alpha . f_{cc}^{'}) t_w} \right) + N_{con} F_{con} * \left(L_w - \frac{P_D + 0.95 f_{py} A_p + N_{con} F_{con}}{2 * (\alpha . f_{cc}^{'}) t_w} \right) \quad (5.6)$$

where P_D, the summation of the wall self weight and superimposed live load, is equated to ($\gamma_c L_w t_w H_w$ + W_{floor} L_w), γ_c is the unit weight of concrete, W_{floor} is the distributed superimposed live load at the base of wall from all floors, $0.95f_{py}$ represents the expected stress in the post-tensioning steel in the critical wall at the design drift, and $\alpha.f_{cc}^{'}$ approximates the expected confined concrete strength of the equivalent rectangular stress block with $f_{cc}^{'}$ representing the strength of the confined concrete. Based on the minimum confinement reinforcement requirement of ACI as detailed in *Step 7*, it is suggested that the value of $f_{cc}^{'}$ is taken as $1.35f_c^{'}$ with a suitable value for α from Eq. 5.7. A more accurate value for $f_{cc}^{'}$ may be used after completing *Step 7*, which will optimize the amount of prestressing steel in the walls.

$$\alpha = \frac{2*r*\left(0.98 - 0.0022*f_c^{'}\right)}{r - 1 + 2^r} \tag{5.7a}$$

where $$r = 1.24 + 0.01*\left(\frac{f_c^{'} - 4.0}{0.25}\right) \tag{5.7b}$$

It is noted that the effects of cover concrete were not separately accounted for in Eq. 5.6. Instead, the entire compression region is treated as a confined region to simplify the design procedure. A similar approach should be followed in conjunction with the recommended design procure.

When substituting for all known variables, Eq. 5.6 will lead to a quadratic equation in A_p and the small positive root should be used as the design value for A_p.

- Similarly for a multi-wall system with $n \geq 3$ (see Figure 5.3), the required area of the post-tensioning steel is established using the moment equilibrium of forces acting at the base of an intermediate wall, as detailed in Eq. 5.8.

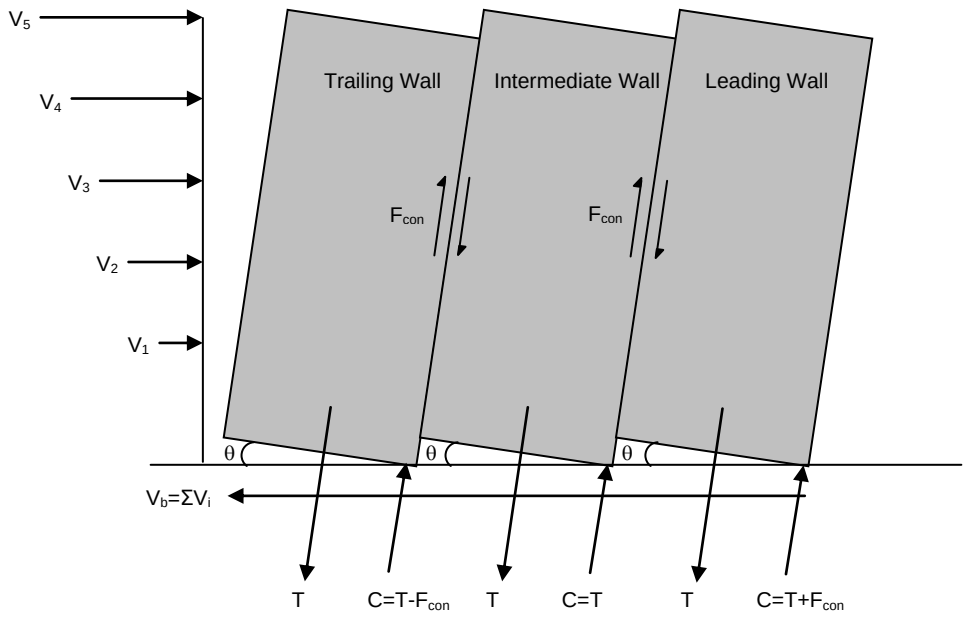

Figure 5.3 Forces acting on a jointed three-wall system at base rotation θ (C = resultant compressive force and $T = P_D$ + *force in the prestressing tendon*)

$$M_{design,inter} = \left(P_D + 0.95 f_{py} A_p\right) * \left(\frac{L_w}{2} - \frac{P_D + 0.95 f_{py} A_p}{2 * (\alpha . f_{cc}^{'}) t_w} \right) + N_{con} F_{con} L_w \qquad (5.8)$$

The connector forces acting on both sides of an intermediate wall will not be equal (see Section 4.2). However, they are assumed to be the same in Eq. 5.8 to simplify the design procedure. The value of $f_{cc}^{'}$ may be approximated to $1.35 f_c^{'}$ with a suitable value for α from Eq. 5.7. As with the leading wall design in Eq. 5.6, Eq. 5.8 will lead to a quadratic equation in A_p and the small positive root should be taken as the design value for A_p.

- Once the area of the post-tensioning tendons (A_p) is estimated, the connector force (F_{con}) should be revised using a better estimate for the connector deformation (Δ_{con}) from Eq. 5.9. This equation, which estimates the connector deformation using the uplift of the leading wall, can be satisfactorily used for the design of both two-wall

and multiple-wall jointed systems. With a revised value for F_{con}, a new value for $M_{design,wall}$ and the corresponding A_p should be obtained from Eqs. 5.5 – 5.8.

$$\Delta_{con} = \theta_{des}\left(L_w - \frac{P_D + 0.95 f_{py} A_p + N_{con} F_{con}}{(\alpha . f_{cc}^{'})t_w}\right) \tag{5.9}$$

Step 5: Design the Initial Stress for the Post-tensioning Steel

- Using Eq. 5.10, estimate the neutral axis depth at the base of the trailing wall at the design drift.

$$c_{design,trail} = \frac{P_D + f_{py} A_p - N_{con} F_{con}}{\beta * (\alpha . f_{cc}^{'})t_w} \tag{5.10}$$

where the value of β can be approximated to 0.96 (see Appendix A).

- Assuming that the post-tensioning tendons reach the yield limit state in the trailing wall at the design drift, the initial stress in the post-tensioning steel is established from Eq. 5.11.

$$f_{pi} = f_{py} - \frac{\left(0.5L_w - c_{design,trail}\right)\theta_{design} E_p}{H_w} \tag{5.11}$$

Step 6: Estimate the Moment Capacity

The connector details, area of the post-tensioning steel and the initial prestress designed in the previous steps are recommended for use in all walls in the jointed system, which would simplify the design instead of designing the walls individually as postulated by Stanton and Nakaki (2002). Using the analysis procedure presented in Chapter 4, estimate the total base moment resistance of the jointed wall system and ensure that Eq. 5.2 is satisfied. Based on the examples investigated to date by the authors, the proposed design method

appears to adequately satisfy Eq. 5.2 and no further iteration was found to be necessary. However, if Eq. 5.2 is not satisfied in a design problem, it is recommended that wall dimensions be altered in order to improve the design.

Step 7: Design of Confinement Reinforcement

With the jointed connection between the wall and foundation, strain concentrations are expected at the compressive regions of the wall toes. A realistic maximum strain demand has not been successfully established from experiments or analyses. However, using the data from the PRESSS test building and recognizing that the leading wall would experience the largest resultant compressive force at the base for all values of θ, Eq. 5.12 has been suggested for estimating the maximum concrete strain demand in the compressive regions of the wall toes (Sritharan and Thomas 2003) and a validation of this equation may be seen in Figure 4.15.

$$\varepsilon_{conc} = c_{max,lead}\left(\frac{M_{max,lead}}{E_c I_{gross}} + \frac{\theta_{max}}{0.06 H_w}\right) \tag{5.12}$$

where $M_{max,lead}$ is the base moment resistance of the leading wall at the maximum expected drift, the corresponding base rotation is θ_{max}, which may be taken as $1.5*\theta_{design}$, I_{gross} is the gross moment of inertia of the wall and is equal to $\frac{t_w L_w^3}{12}$, and $c_{max,lead}$ is the neutral axis depth at the base of the leading wall at θ_{max}. The value of $c_{max,lead}$ may be established as part of the analysis of the wall system in Step 6. Following an estimate for ε_{conc} from Eq. 5.12, quantify the required amount of confinement reinforcement in the wall toes using an appropriate confinement model. If the model proposed by Mander et al. (1988) is selected as in Appendix A, then Eq. 5.13 will be used to determine the required amount of confinement reinforcement.

$$\rho_s = \frac{(\varepsilon_{conc} - 0.004) f'_{cc}}{1.4 f_{yh} \varepsilon_{su}} \tag{5.13}$$

where ρ_s is the volumetric ratio of the required confinement steel, f_{yh} and ε_{su} are, respectively, the yield strength and ultimate strain capacity of the confinement reinforcement, and f'_{cc} is the ultimate strength of the confined concrete. Since f'_{cc} is dependent on the value of ρ_s, an iterative approach would be necessary to solve Eq. 5.13. For the first step in the iteration, f'_{cc} may be approximated to $1.35 f'_c$. This is because the selected confinement reinforcement should also satisfy all seismic design provisions prescribed in the current building standard for the design of transverse reinforcement in the plastic hinge region of a concrete wall. This includes the minimum hoop reinforcement requirement of ACI Eq. 21-4 (2005), which can be interpreted as demanding minimum confinement reinforcement of $0.09 f'_c / f_y$ in both major and minor axis directions of the wall sections. The corresponding effective confinement pressure is $0.09 k_e f'_c$, where k_e is the effective confinement coefficient. With a value of 0.6 for k_e, this minimum confinement pressure will provide a f'_{cc} value of about $1.35 f'_c$.

Finally, using the friction coefficient of μ, the shear resistance at the base of the wall should be ensured using a shear friction mechanism. If an interface material such as grout is placed between the precast walls and foundation, this should be reflected in the value of μ. Since the stress in the post-tensioning steel and the connector force increase with drift, it will be necessary to perform this check at both θ_{design} and θ_{max}.

5.5 Design Examples

The application of the design methodology presented above is demonstrated using two sets of design examples. The wall systems used in these examples are not meant to provide the most economical design solutions, but rather suitable for examining the design methodology over a wide range of critical design variables.

5.5.1 Example Set 1

In the first set, a two-wall, three-wall and four-wall jointed system are designed to resist a design base moment of 75780 kip-in. The length of each wall and total number of UFP connectors in each wall system are assumed to be the same as those used in the PRESSS test building (i.e., L_w *= 108 in.* and N_{con} *= 20*). Furthermore, the properties selected for the examples are those of the PRESSS wall system, except for the unconfined concrete strength, which is taken as 6 ksi. Given that change in concrete strength has a relatively small impact on the design outcome, the two-wall design example is expected to be comparable to the wall system used in the PRESSS test building.

Solution: Presented below are step-by-step solutions to the three different examples.

Step 1: Material Properties and Wall Dimensions

Material Properties

Concrete strength ($f_c^{'}$) = 6 ksi.

Concrete density (γ_c) = 150 pcf.

Yield strength of post-tensioning bars (f_{py}) =140 ksi.

Young's modulus of post-tensioning bars (E_p) =27700 ksi.

The force-displacement response of the UFP connector shown in Figure 3.12 is used.

Wall dimensions

Length of a single wall (L_w) =108 in.

Thickness of the wall (t_w) = 8 in.

Height of the wall (H_w) =450 in.

Step2: Design Moment

Given that the design moment (M_{design}) = 75780 kip-in.

Step 3: Force in the Connector

Assume the wall base rotation at design drift (θ_{des}) = 0.02.

At θ_{des}, force transmitted through each connector, F_{con} = 11.2 kip.

The total number of connectors in the wall system = 20 (taken the same total number as used in the PRESSS wall)

Table 5.1 shows the number of connectors per vertical joint for various wall systems.

Table 5.1 Number of connectors in each vertical joint between two adjacent walls.

Example	Wall system	N_{con} (No. of connectors per joint)
1	Two-wall	20
2	Three-wall	10
3	Four-wall	7

Step 4: Required Area of the Post-tensioning Bars

From Eq. 5.5,

$$M_{design,wall} = \Omega \frac{M_{design}}{n\phi}$$

$$\Omega = 1 + \frac{\lambda \phi N_{con} F_{con} L_w}{M_{design}}$$

Table 5.2 demonstrates the estimation of $M_{design,wall}$ for the three wall systems after revising F_{con} as per Eq. 5.9.

By solving Eq. 5.6 for the two-wall system and Eq. 5.8 for three- and four-wall systems, Table 5.3 shows determination of suitable A_p values are obtained. In each case, the smaller positive root is taken as the design value for A_p.

Table 5.2 Estimation of $M_{\text{design,wall}}$ for each wall system.

Parameter	Two-wall system	Three-wall system	Four-wall system
n	2	3	4
ϕ	0.9	0.9	0.9
λ	0.9	1.05	1.05
L_{w}	108 in.	108 in.	108 in.
F_{con}	11.15 kips	11.25 kips	11.25 kips
M_{design}	75780 kip-in.	75780 kip-in.	75780 kip-in.
Ω	1.26	1.15	1.11
$M_{design,lead}$	52938 kip-in.	–	–
$M_{design,inter}$	–	32319 kip-in.	23282 kip-in.

Step 5: Design of Initial stress in the Post-tensioning Bars

Eqs. 5.10 and 5.11 presented in the design procedure are used to determine the required initial stress in the post-tensioning bars and the details are given in Table 5.4.

Step 6: Estimated Moment Capacity

Following the analysis procedure presented in Chapter 4, the moment capacities of the three wall systems are determined at θ_{des} using the designed values for A_p and f_{pi}. The results are presented in the Table 5.5, which shows that a) the calculated moment resistance of the critical wall in each wall system is greater than or nearly equal to the corresponding design moment, and b) ϕM_n *is greater* than M_{design} for all three wall systems. These comparisons, shown graphically in Fig 5.4 and 5.5, confirm that the design procedure presented in this chapter for precast jointed wall systems is satisfactory.

Table 5.3 Area of the required post-tensioning steel for the three wall systems.

	Roots of the quadratic equation	**Design solution**
Two-wall system	A_{p1} = 4.44 in^2	A_p = 4.44 in^2
	A_{p2} = 38.84 in^2	
Three wall system	A_{p1} = 2.56 in^2	A_p = 2.56 in^2
	A_{p2} = 43.31 in^2	
Four wall system	A_{p1} = 1.69 in^2	A_p = 1.69 in^2
	A_{p2} = 44.42 in^2	

Table 5.4 Design of the initial stress in the post-tensioning bars.

Example	**Neutral axis depth of trailing wall at θ_{des} (in.)**	**Initial stress (f_{pi}) (ksi)**
Two-wall system	8.23	83.66
Three wall system	5.51	80.30
Four wall system	3.95	78.40

Table 5.5 Comparison of calculated and design moments for the three wall systems.

Example	**Calculated capacity (kip-in)**	**Design moment (kip-in)**
Two-wall system	$M_{n,lead}$ = 51491 kip-in	$M_{design,lead}$ = 52938 kip-in.
	ϕM_n = 76415 kip-in	M_{design} = 75780 kip-in.
Three wall system	$M_{n,inter}$ = 32375 kip-in	$M_{design,inter}$ = 32319 kip-in.
	ϕM_n = 76145 kip-in	M_{design} = 75780 kip-in.
Four wall system	$M_{n,inter}$ = 23353 kip-in	$M_{design,inter}$ = 23283 kip-in
	ϕM_n = 76192 kip-in	M_{design} = 75780 kip-in.

Step 7: Confinement Reinforcement

For the design of confinement reinforcement, θ_{max} is taken as 0.03 and the corresponding moment capacities (M_{max}) for the leading wall are taken from the analysis conducted in *Step 6*. The $M_{max,,lead}$ and the required concrete strain capacity values are shown in Table 5.6. Note that the required ρ_s is less than $\rho_{s,min}$ discussed in *Step 7* of the design procedure, which is $0.09 f_c^{'} / f_y + 0.09 f_c^{'} / f_y = 0.018$. Hence, the minimum required confinement reinforcement should be provided.

Table 5.6 Design of confinement steel ratios for the wall systems.

Example	**$M_{max\ lead}$ (base moment of the leading wall at θ_{max})**	**$c_{max,lead}$ (neutral axis depth)**	**ε_{conc} (required concrete strain capacity)**	**Required ρ_s**
Two-wall system	56365 kip-in.	15.45 in.	0.0174	0.0092
Three wall system	34245 kip-in.	9.31 in.	0.0104	0.0041
Four wall system	24909 kip-in.	6.67 in	0.0075	0.0021

5.5.2 Example Set 2

Design a two-wall, three-wall, and four-wall jointed system to resist a base moment of 75780 kip-in. For this example set, assume the total length and the total number of UFP connectors to be nearly the same as those used in the PRESSS test building. In addition, the properties selected for the examples are those of the PRESSS wall system, except for the unconfined concrete strength, which is taken as 6 ksi.

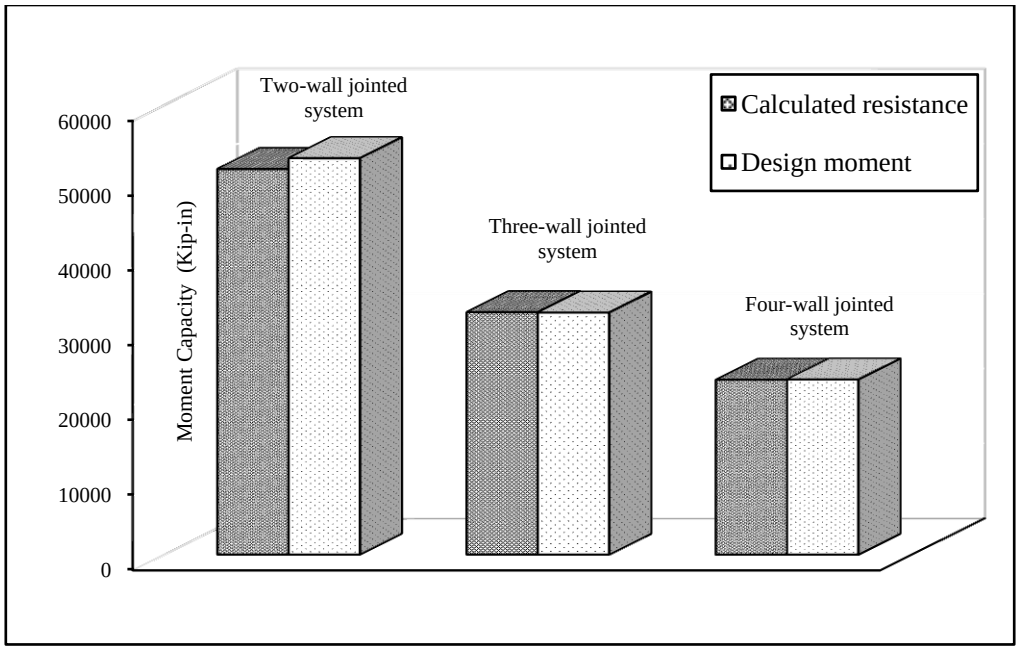

Figure 5.4 Comparison between $M_{design,wall}$ and $M_{n,wall}$ for the critical wall that determined the area of post-tensioning bars in each wall system.

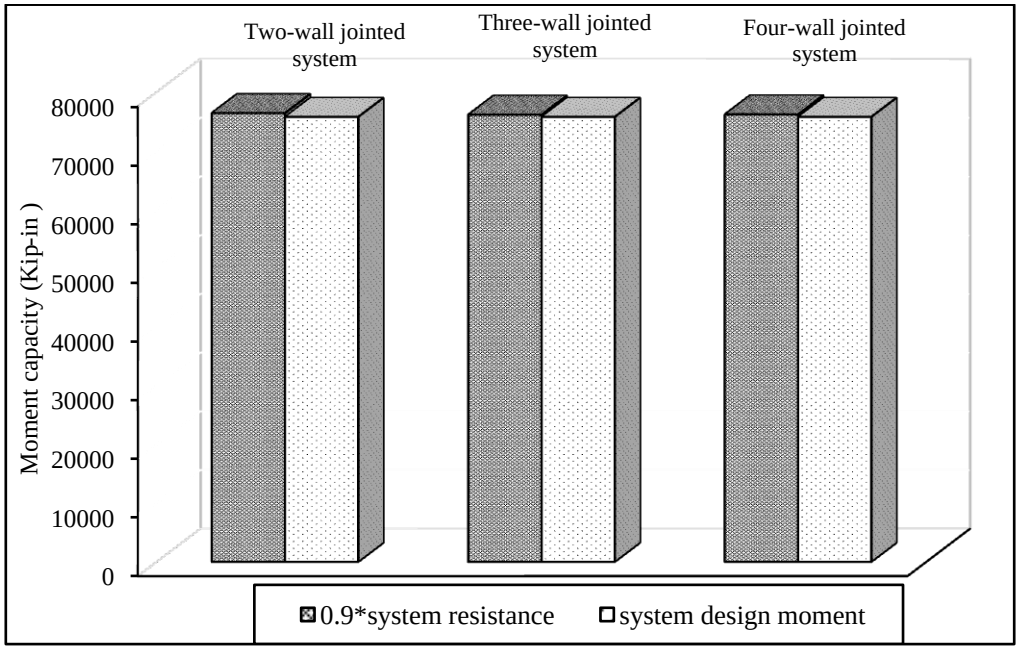

Figure 5.5 Comparison between ϕM_n and M_{design} for the three wall systems.

Solution:

Step 1: Material Properties and Wall Dimensions

Material Properties

Concrete strength ($f_c^{'}$) = 6 ksi.

Concrete density (γ_c) = 150 pcf.

Yield strength of post-tensioning bars (f_{py}) =140 ksi.

Young's modulus of post-tensioning bars (E_p) =27700 ksi.

The force-displacement response of the UFP connector shown in Figure 3.12 is used.

Wall dimensions

Length of the wall system (L_s) = 216 in.

Thickness of the wall (t_w) = 8 in.

Height of the wall (H_w) = 450 in.

The length of individual wall in each wall system is obtained from Eq. 5.1 and is provided in Table 5.7.

Table 5.7 Length of each wall in different wall systems.

Example	L_w (Length of each wall)
Two-wall	108 in.
Three-wall	72 in.
Four-wall	54 in.

Step2: Design Moment

As stated in the problem statement, the design moment (M_{design}) = 75780 kip-in.

Step 3: Force in the Connector

Assume the rotation at the wall base at the design drift (θ_{des}) = 0.02. The total number of connectors in each wall system is kept approximately at 20. Table 5.8 shows the number of connectors per vertical joint and the force transmitted through each connector (F_{con}) for the three wall systems.

Table 5.8 Number of connectors in each vertical joint between two adjacent walls and the estimated force transmitted by each connector at θ_{des}.

Example	N_{con} (No. of connectors per joint)	F_{con} (kips)
Two-wall system	20	11.2
Three-wall system	10	10.5
Four-wall system	7	10.2

Step 4: Required Area of Post-tensioning Bars

From Eq. 5.5,

$$M_{design,wall} = \Omega \frac{M_{design}}{n\phi}$$

$$\Omega = 1 + \frac{\lambda \phi N_{con} F_{con} L_w}{M_{design}}$$

Table 5.9 demonstrates the estimation of $M_{design,wall}$ for the different examples with revised values for F_{con} as per Eq. 5.9. By solving the Eq. 5.6 or Eq. 5.8 presented in the design procedure for the calculated $M_{design,wall}$ values, design values of A_p are obtained in Table 5.10. The smaller positive root is taken as the required area of post-tensioning bars in each wall system.

Step 5: Design of Initial stress in the Post-tensioning Bars

Eqs. 5.10 and 5.11 presented in the design procedure are used to determine the required initial stress in the post-tensioning bars and the details are given in Table 5.11.

Table 5.9 Estimation of $M_{design,\ wall}$ for the three different wall systems.

Parameter	Two-wall system	Three-wall system	Four-wall system
n	2	3	4
ϕ	0.9	0.9	0.9
λ	0.9	1.05	1.05
L_w	108 in.	72 in.	54 in.
F_{con}	11.15 kip.	10.35 kip.	9.8 kip.
M_{design}	75780 kip-in.	75780 kip-in.	75780 kip-in.
Ω	1.26	1.09	1.05
$M_{design,lead}$	52938 kip-in.	-	-
$M_{design,inter}$	-	30675 kip-in.	22022 kip-in.

Table 5.10 Area of the required post-tensioning bars in each wall system.

	Roots of the quadratic equation	Design solution
Two-wall system	A_{p1} = 4.44 in.^{2}	A_p = 4.44 in.^{2}
	A_{p2} = 38.84 in.^{2}	
Three wall system	A_{p1} = 5.81 in.^{2}	A_p = 5.81 in.^{2}
	A_{p2} = 24.39 in.^{2}	
Four wall system	A_{p1} = 7.48 in.^{2}	A_p = 7.48 in.^{2}
	A_{p2} = 15.12 in.^{2}	

Table 5.11 Design values for the initial stress in the post-tensioning tendons.

Example	Neutral axis depth of trailing wall at θ_{des} (in.)	Initial stress (f_{pi}) (ksi)
Two-wall system	8.23	83.66
Three wall system	13.5	112.3
Four wall system	18.21	129.2

Step 6: Estimated Moment Capacity

Following the analysis procedure presented in Chapter 4, the moment capacities of the three wall systems are determined at θ_{des} using the designed values for A_p and f_{pi}. The results are presented in the Table 5.12, which shows that a) the calculated moment resistance of the critical wall in each wall system is greater than or nearly equal to the corresponding design moment, and b) ϕM_n *is greater* than M_{design} for all three wall systems. These comparisons, shown graphically in Fig 5.6 and 5.7, confirm that the design procedure presented in this chapter for precast jointed wall systems is satisfactory.

Table 5.12 Comparison of calculated and design moments for the three wall systems.

Example	Calculated capacity (kip-in)	Design moment (kip-in)
Two-wall system	$M_{n,lead}$ = 51491 kip-in	$M_{design,lead}$ = 52938 kip-in.
	ϕM_n = 76415 kip-in	M_{design} = 75780 kip-in.
Three wall system	$M_{n,inter}$ = 30725 kip-in	$M_{design,inter}$ = 30675 kip-in.
	ϕM_n = 76108 kip-in	M_{design} = 75780 kip-in.
Four wall system	$M_{n,inter}$ = 21928 kip-in	$M_{design,inter}$ = 22022 kip-in
	ϕM_n = 75542 kip-in	M_{design} = 75780 kip-in.

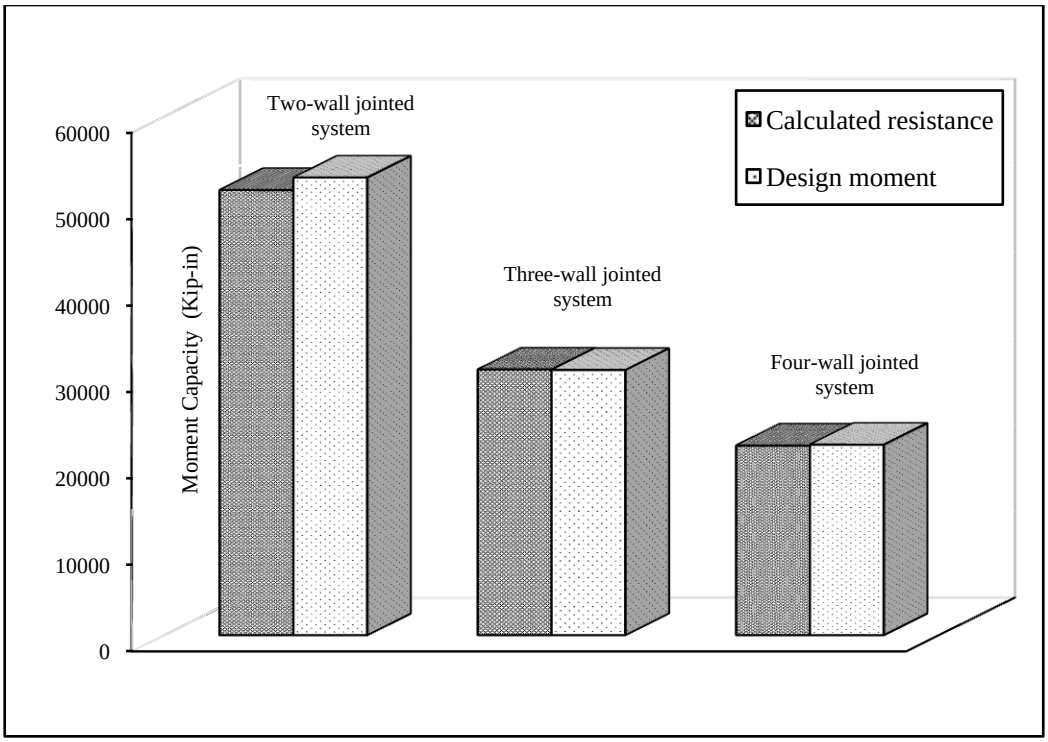

Figure 5.6 Comparison between $M_{design,wall}$ and $M_{n,wall}$ for the critical wall that determined the area of post-tensioning bars in each wall system.

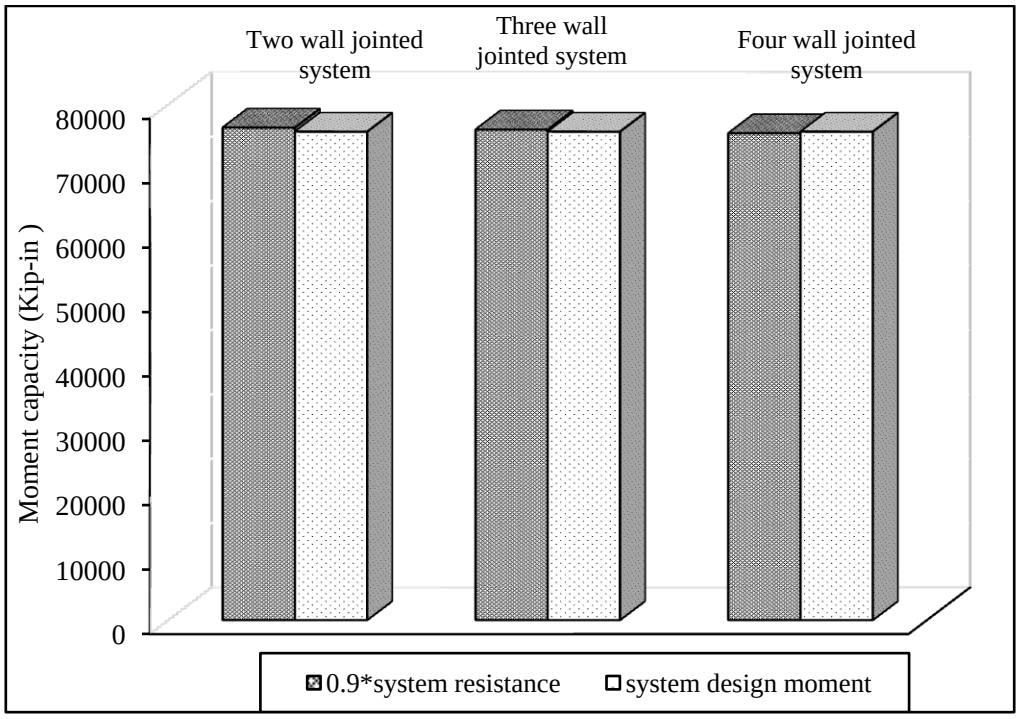

Figure 5.7 Comparison between ϕM_n and M_{design} for the three wall systems.

Step 7: Confinement Reinforcement

For the design of confinement reinforcement, θ_{max} is taken as 0.03 and the corresponding moment capacities (M_{max}) for the leading wall are taken from the analysis conducted in *Step 6*. The $M_{max,,lead}$ and the required concrete strain capacity values are shown in Table 5.12. Note that the required ρ_s is less than $\rho_{s,min}$ discussed in *Step 7* of the design procedure, which is $0.09 f_c^{'} / f_y + 0.09 f_c^{'} / f_y = 0.018$. Hence, the minimum required confinement reinforcement should be provided.

Table 5.12 Design of confinement steel ratios for the wall systems.

Example	**$M_{max,\ lead}$ (base moment of the leading wall at θ_{max})**	**$c_{max,lead}$ (neutral axis depth)**	**ε_{conc} (required concrete strain capacity)**	**Required ρ_s**
Two-wall system	56365 kip-in.	15.45 in.	0.0174	0.0092
Three wall system	30312 kip-in.	16.80 in.	0.0192	0.011
Four wall system	20652 kip-in.	19.27 in	0.0223	0.0137

Intentionally blank

CHAPTER 6: SUMMARY AND CONCLUSIONS

6.1 Summary

Following a presentation on seismic performance of a jointed two-wall system included in the PRESSS building based on the corrected test data, an analysis procedure and a design method suitable for this system are presented in this report. In these types of systems, the precast walls are secured to the foundation using unbonded post-tensioning. Consequently, a section level analysis as used for monolithic walls cannot be performed for the walls in the jointed system due to the strain incompatibility introduced by the use of unbonded post-tensioning steel. This challenge has led to recommendations of design and analysis methods for jointed wall systems and single precast walls consisting of unbonded post-tensioning. These methods approximate the strength of confined concrete and use the equivalent rectangular stress block concept for predicting the neutral axis depth in design calculations and predicting structural behavior of the jointed wall. Although simplifications are maintained in the proposed analysis and design methods, which can be applied to both jointed wall systems and single precast walls designed with unbonded post-tensioning, several notable improvements are made to increase the accuracy of these methods and address the drawbacks of the previously proposed approaches. Validations for the analysis method and example problems demonstrating the accuracy of the design methodology have been presented.

Also included herein are experimental findings from testing of U-shaped flexural plate (UFP) connectors; UFPs were used as the connector in the PRESSS jointed wall system, in which the connectors primarily provided the energy dissipation capability while the unbonded post-tensioning in the precast walls ensured the self-centering capability. In consideration of the isotropic hardening of the stainless steel material used for the UFPs, a force-displacement response suitable for characterizing the behavior of UFPs in design calculations has been established. In this process, it was important to adequately address the influence of the strain history on the performance of UFPs and this was addressed by using the test data collected during the wall direction seismic testing of the PRESSS building.

6.2 Conclusions

The conclusions drawn from the study are as follows:

1. Seismic performance of the jointed wall system in the PRESSS building was excellent and it produced dependable seismic response, minimal structural damage and recentered within 0.1% of lateral drift at the end of pseudodynamic seismic tests despite the short-durations of input motions.
2. Despite subjecting to a displacement of 2.7 in., the performance of the UFP connectors was good and dependable, and they contributed to sufficient amount of damping needed for the PRESSS building in the wall direction of testing.
3. Equivalent viscous damping of the PRESSS wall system increased with increasing lateral drift and then remained constant at large lateral displacements. When subjected to earthquake input motions representing designing level and greater intensity of input motions, the wall system produced an equivalent viscous damping of about 18 percent.
4. The unbonded post-tensioning bars in the PRESSS wall system remained essentially elastic even though the maximum average lateral drift experienced by the wall exceeded 2.5%. In the design of the wall system, the post-tensioning bars were designed to yield at a lateral drift 2%. However, yielding should not be expected at this drift level due to the assumptions and conservatism built into the design procedure.
5. The test observations and limited measured strain data confirmed that walls in the PRESSS jointed system included more than an adequate amount of confinement reinforcement.
6. Cyclic testing on UFP connectors confirmed that their behavior will be dependent on the strain history and that their cyclic behavior will be difficult to predict due to the isotropic hardening of stainless steel used for manufacturing the UFPs. However, for design purposes, a force-displacement response for the UFP has been established through testing, in which the influence of the strain history is adequately accounted for.
7. A simplified procedure has been established for analyzing precast walls designed with unbonded post-tensioning. Verification of the analysis procedure confirmed that the established procedure will satisfactorily predict the monotonic response of jointed wall systems and single walls designed with unbonded post-tensioning. In adding to characterizing the lateral force vs. displacement behavior, several other parameters,

including the variation in the neutral axis depth and elongation of the post-tensioning steel, can be quantified accurately. This procedure approximates the change in the neutral axis depth using a trilinear curve and account for the effects of confinement on equivalent rectangular concrete stress block.

8. A seismic design procedure has been established for precast jointed wall systems, which can be easily extended to design single precast walls with unbonded post-tensioning. By completing example problems, it has been shown that the proposed procedure will
    a. adequately quantify the design moments of walls in jointed multiple-wall systems;
    b. adequately represent the variation in the neural axis depth at the wall bases as a function of base rotation;
    c. ensure that yielding of the post-tensioning steel would not occur before a chosen target lateral drift is achieved;
    d. satisfactorily account for the contribution of stainless steel UFPs if they are chosen as the connectors to join the individual walls;
    e. adequately account for the confinement effects of concrete; and
    f. estimate the expected maximum concrete strain sufficiently to quantify the appropriate amount of confinement reinforcement.

REFERENCES

Aaleti, S., Seismic Analysis and Design of Unbonded Post-tensioned Precast Concrete Wall Systems, *MS Thesis*, Iowa State University, Ames, IA, 2005.

ACI Committee 318, *Building Code Requirements for Structural Concrete (ACI 318-05)*, American Concrete Institute, Farmington Hills, MI.

ACI Innovation Task Group 5, "Acceptance Criteria for Special Unbonded Post-Tensioned Precast Structural Walls Based on Validation Testing (ACI ITG 5.1-07) and Commentary (ACI ITG R5.1-07)," American Concrete Institute, Farmington Hills, MI, 2007.

ASTM Committee E-28, Standard Test Methods of Tension Testing of Metallic Materials, E 8-91, *Annual Book of ASTM Standards*, American Society for Testing and Materials, 1991.

Celik. O. and S. Sritharan, "An Evaluation of Seismic Design Guidelines Proposed for Precast Concrete Hybrid Frame Systems", *ISU-ERI-Ames Report ERI-04425*, Department of Civil Engineering, Iowa State University, 2004.

Conley J., Sritharan, S. and M. J. N. Priestley, "Wall Direction Response. PRESSS-3: The Five-Story Precast Test Building (Vol. 3-5)', *Report No. SSRP - 99/19*, Structural Systems Research Project, University of California, San Diego, California, 2002.

Englekirk, R. E., *Seismic Design of Reinforced and Precast Concrete Buildings*, John Wiley & Sons, Hoboken, NJ, 2003.

Galusha III, J. G., "Precast, Post-Tensioned Concrete Walls Designed to Rock", *M.S. thesis, Department of Civil Engineering*, University of Washington, 1999.

Ghosh, S.K. "Earthquake Resistant Precast Buildings", *MC magazine*, Winter 2001.

Ghosh, S. K., "Seismic Design Provisions in U.S. Codes and Standards: A Look Back and Ahead", *PCI Journal*, Jan-Feb 2002.

Fintel, M., "Ductile Structural Walls in Earthquake Resistant Multistory Buildings", ACI Structural Journal, June 1974.

Fintel, M. "Performance of Buildings with Structural Walls in Earthquakes of the Last Thirty Years", *PCI Journal*, May-June 1995.

Fintel, M. "Shear walls: An Answer for Seismic Resistance?", *Concrete International*, Vol.13, No.7, July 1991.

International Building Code (IBC), *International Code council*, Virginia, USA, 2003.

Kurama, Y., R. Sause, S. Pessiki, and L. W. Lu, "Lateral Load Behavior and Seismic Design of Unbonded Post-Tensioned Precast Concrete Walls", *ACI Structural Journal*, July-Aug 1999, pp. 622-632.

Kurama, Y., S. Pessiki, R. Sause, and L. W. Lu, "Seismic Response Evaluation of Unbonded Post Tensioned Precast Walls", *ACI Structural Journal*, Sept-Oct 2002.

Kurama, Y., S. Pessiki, R. Sause, and L. W. Lu, "Seismic Behavior and Design of Unbonded Post-Tensioned Precast Concrete Walls", *PCI Journal*, Vol.44, No.3, May-June 1999.

Nakaki, S.D., Stanton, J.F., and S. Sritharan, "An Overview of the PRESSS Five-Story Precast Test Building", *PCI Journal*, March-April 1999.

Naaman, A. E., *Prestressed Concrete Analysis and Design*, Second Edition, Techno Press 3000, Ann Arbor, MI.

Building Seismic Safety Council, NEHRP Recommended Provisions for Seismic Regulations for New Buildings and Other Structures, National Earthquake Hazard Reduction Program, Washington, D. C., 1997.

Mander, J. B., M. J. N., Priestley and R. Park, "Theoretical Stress-Strain Model for Confined Concrete", *ASCE Journal of Structural Engineering*, Vol.114, No.8, Aug 1988.

Pampanin, S., Priestley, M. J. N. and S. Sritharan, "Analytical Modeling of the Seismic Behaviour of Precast Concrete Frames Designed with Ductile Connections", *Journal of Earthquake Engineering*, Vol. 5, No. 3, 2001.

Park, R. "A Perspective on the Seismic Design of Precast Concrete Structures in New Zealand". PCI Journal, Vol. 40, No.3, May-June 1995.

Perez, F. J., Pessiki, S. and R. Sause, "Experimental and Analytical Lateral Load Response of Unbonded Post-tensioned Precast Concrete Walls", *ATLSS Report No. 04-11*, Department of Civil Engineering, Lehigh University, May 2004.

Priestley, M. J. N., "Overview of PRESSS Research Program", PCI Journal, Vol.36, No.4, 1991, pp.50-57.

Priestley, M. J. N., Sritharan, S., Conley, J., and Pampanin, S. "Preliminary Results From the PRESSS Five-Story Precast Concrete Test Building", *PCI Journal*, Nov-Dec 1999.

Sritharan, S., Pampanin, S., Conley, J. "Design Verification, Instrumentation and Test Procedures, PRESSS-3: The Five Story Precast Test Building", Vol. 3-3, Department of Civil and Construction Engineering, Iowa state University, Ames, IA.

Sritharan, S. and D. J. Thomas, "Analysis of a Jointed Precast Wall System Subjected to Seismic Actions", *In Proceedings of the FIB-Symposium*, 2003, Athens, Greece.

Stanton, J. F., Nakaki, S.D. "Design Guidelines for Precast Concrete Seismic Structural Systems", *PRESSS Report No. SM 02-02*, Department of Civil Engineering, University of Washington, February 2002.

Thomas D. J. and S. Sritharan, "An Evaluation of Seismic Design Guidelines Proposed Precast Jointed Wall Systems", *ISU-ERI-Ames Report ERI-04643, Department of Civil and Construction and Environmental Engineering*, Iowa State University, Ames, Iowa, 2004.

Uniform building Code, International Conference of Building Officials, Whittier, CA, 1997.

Vernu S. and S. Sritharan, "Section, Member and System Level Analyses for Precast Concrete Hybrid Frames", *ISU-ERI-Ames Report ERI-04635, Department of Civil and Construction and Environmental Engineering*, Iowa State University, Ames, Iowa, 2004.

APPENDIX A: EQUIVALENT RECTANGULAR STRESS BLOCK FOR CONFINED CONCRETE

A.1 Introduction

The compressive strength and strain capacity of concrete increase as the confinement reinforcement increases. The stress-strain behavior of confined concrete can be described using the model proposed by Mander et al. (1988). Using this model, an equivalent rectangular block representation is examined for the confined concrete in this appendix. It is shown that the effective concrete strength ($\alpha.f_{cc}^{'}$) and the location of the resultant compression force ($0.5\beta c$) vary with the unconfined concrete strength, the amount of confinement reinforcement and the maximum compression strain in the extreme compression fiber.

A.2 Confined concrete model

According to Mander et al., the stress-strain behavior of confined concrete can be described as shown below (see Figure A.1)

$$f_c = \frac{f_{cc}^{'} xr}{r - 1 + x^r} \tag{A.1}$$

$$f_{cc}^{'} = f_c^{'}\left(2.254\sqrt{1+\frac{7.94\,f_l^{'}}{f_c^{'}}} - 2\frac{f_l^{'}}{f_c^{'}} - 1.254\right) \tag{A.2}$$

$$x = \frac{\varepsilon_c}{\varepsilon_{cc}} \qquad r = \frac{E_c}{E_c - E_{\sec}} \qquad E_{\sec} = \frac{f_{cc}^{'}}{\varepsilon_{cc}} \tag{A.3}$$

$$\varepsilon_{cc} = 0.002\left(1 + 5\left[\frac{f_{cc}^{'}}{f_{c}^{'}} - 1\right]\right) \tag{A.4}$$

$$\varepsilon_{cu} = 0.004 + \frac{1.4\rho_s f_{yh}\varepsilon_{su}}{f_{cc}^{'}} \tag{A.5}$$

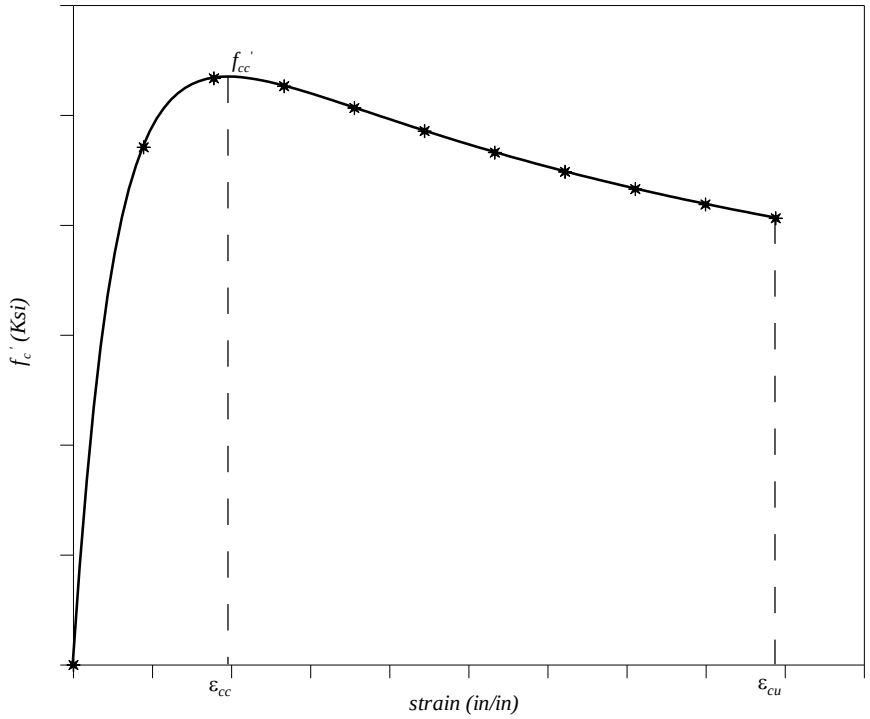

Figure A.1 A schematic view exhibiting the behavior of confined concrete according to the model proposed by Mander et al. (1988).

Note that $f_l^{'} = 0.5\rho_s f_{yh} k_e$ and thus $\rho_s f_{yh}$ can be replaced with $\frac{2 f_l^{'}}{k_e}$ in Eq. A.5, which leads to

$$\varepsilon_{cu} = 0.004 + \frac{2.8 f_l^{'}\varepsilon_{su}}{k_e f_{cc}^{'}} \tag{A.6}$$

Where f_c is the confined concrete stress at strain of ε_c,

$f_{cc}^{'}$ is the peak confined concrete strength,

E_c is the young's modulus of concrete and is approximated to $57000\sqrt{f_c^{'}(psi)}$,

E_{sec} is the secant modulus of concrete as per Eq. A.3,

ε_{cc} is the strain corresponding to $f_{cc}^{'}$,

ε_{cu} is the strain corresponding to crushing of confined concrete,

f_{yh} is the yield strength of hoop reinforcement,

ε_{su} is the ultimate strain capacity of hoop reinforcement,

$f_l^{'}$ is the effective lateral confining stress, and

k_e is the confinement effectiveness coefficient and is taken as 0.6 for rectangular wall sections.

For rectangular concrete sections, $\rho_s = \rho_x + \rho_y$, where ρ_x and ρ_y are the transverse reinforcement ratios in the directions parallel to the major and minor axes of the section.

A.3 Estimation of equivalent rectangular block constants

In this section, an attempt is made to determine suitable constants to define an equivalent rectangular stress block for confined concrete. In accordance with Figure A.2, constants α and β are found by imposing the following conditions:

- the area under the confined concrete curve should be equal to the area of the equivalent rectangular block, and
- the moment contribution of forces (or the location of the resultant forces) should be the same in both cases.

These two conditions can be mathematically expressed as follows:

$$\alpha\beta = \frac{\int_0^{\varepsilon_{end}} f_c d\varepsilon}{f_{cc}^{'}\varepsilon_{end}} \qquad \text{(A.7)}$$

$$\alpha\beta(1-0.5\beta) = \frac{\int_0^{\varepsilon_{end}} f_c \varepsilon d\varepsilon}{f_{cc}^{'} \varepsilon_{end}^2} \tag{A.8}$$

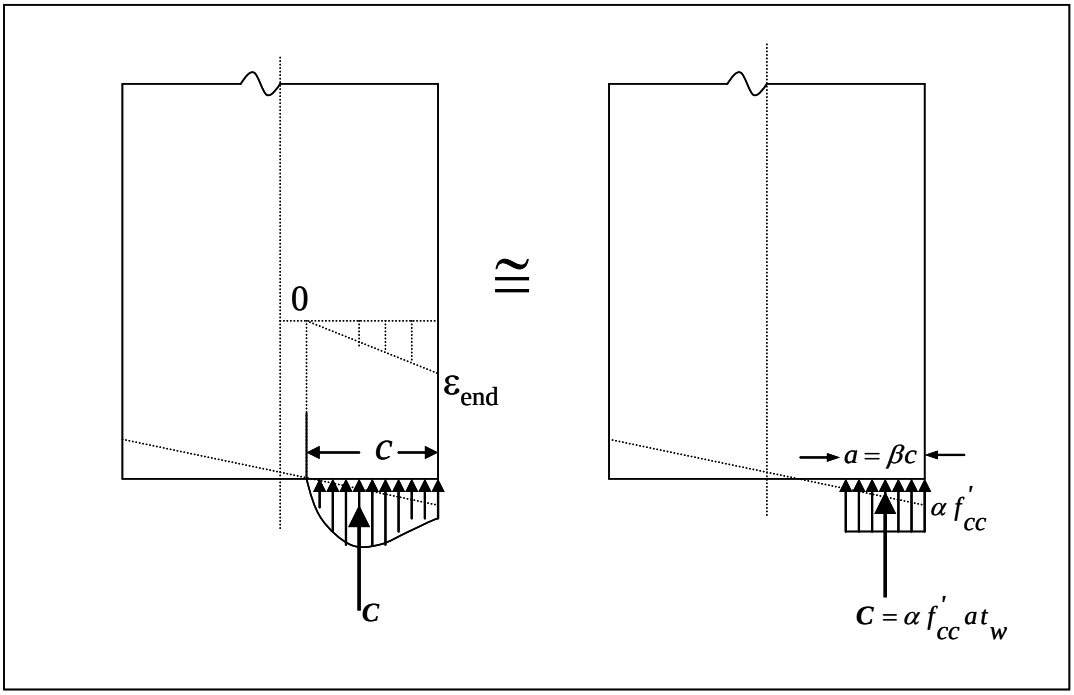

(a) Actual stress and strain distributions (b) Equivalent stress block

Figure A.2 Equivalent rectangular block approximation for confined concrete.

Substituting for $\alpha\beta$ from Eq. A.7 into A.8

$$\beta = 2 - 2 * \frac{1}{\varepsilon_{end}} * \frac{\int_0^{\varepsilon_{end}} f_c \varepsilon d\varepsilon}{\int_0^{\varepsilon_{end}} f_c d\varepsilon} \tag{A.9}$$

By solving Eqs. A.7 and A.9, the constants α and β can be found for a given problem. However, as seen in the above equations, the values of α and β will depend on the concrete strength, the amount of confinement, and the value of ε_{end}, where ε_{end} defines the compressive strain in the extreme fiber of the confined concrete (see Fig. A.2a).

In order to understand the influence of unconfined concrete strength and confinement pressure on α and β, a parametric study was conducted, in which the unconfined concrete strength was varied from 4 ksi to 8.5 ksi in increments of 0.25 ksi whereas the effective confinement pressure ($f_l^{'}$) expressed in terms of the unconfined concrete strength was varied from 0.09 $f_c^{'}$ to 0.18 $f_c^{'}$ in increments of 0.01 $f_c^{'}$. Selected results from this study are presented in Figures A.3 – A.12, in which the effect of varying the value of ε_{end} on α and β is also addressed.

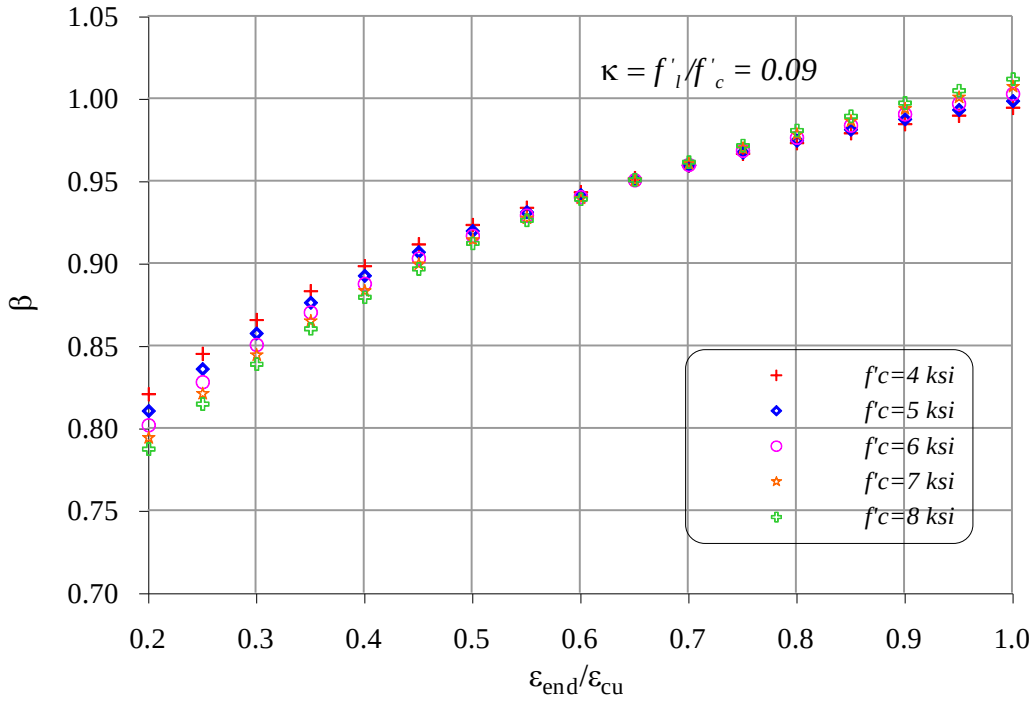

Figure A.3 Variation β as a function of unconfined concrete strength and $\varepsilon_{end} / \varepsilon_{cu}$ ratio.

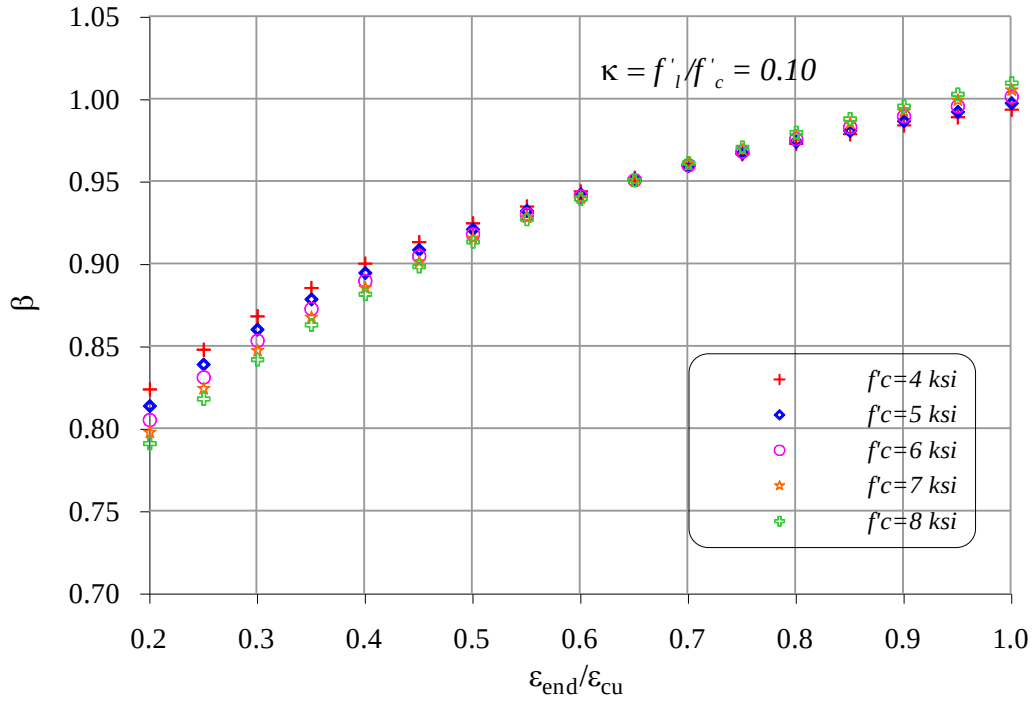

Figure A.4 Variation of β as a function of unconfined concrete strength and $\varepsilon_{end} / \varepsilon_{cu}$ ratio.

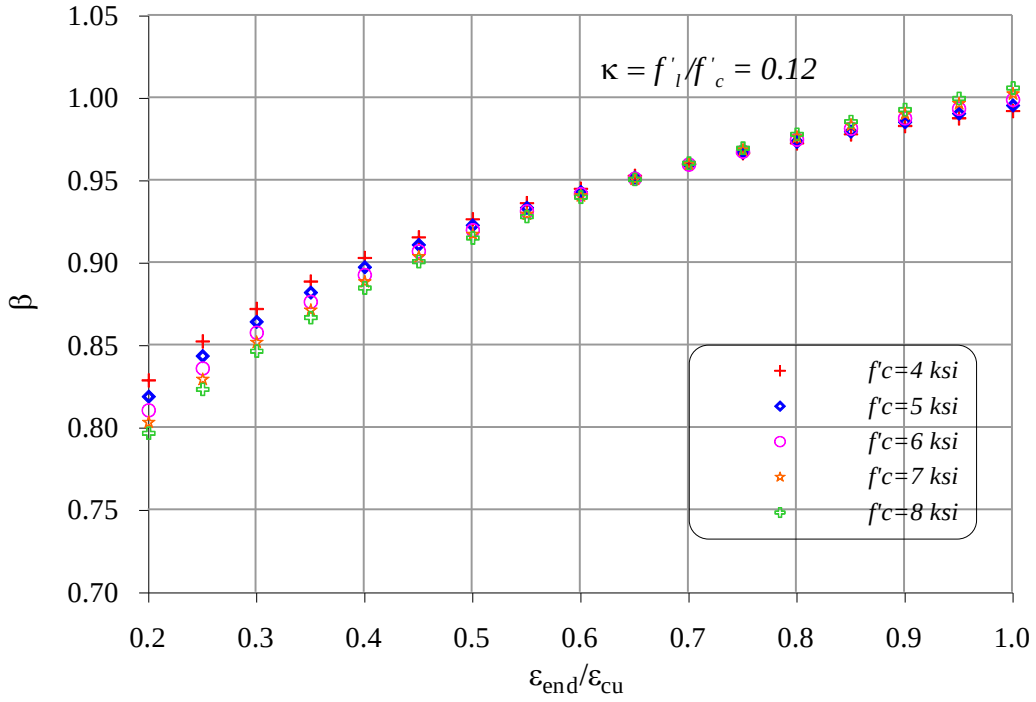

Figure A.5 Variation of β as a function of unconfined concrete strength and $\varepsilon_{end} / \varepsilon_{cu}$ ratio.

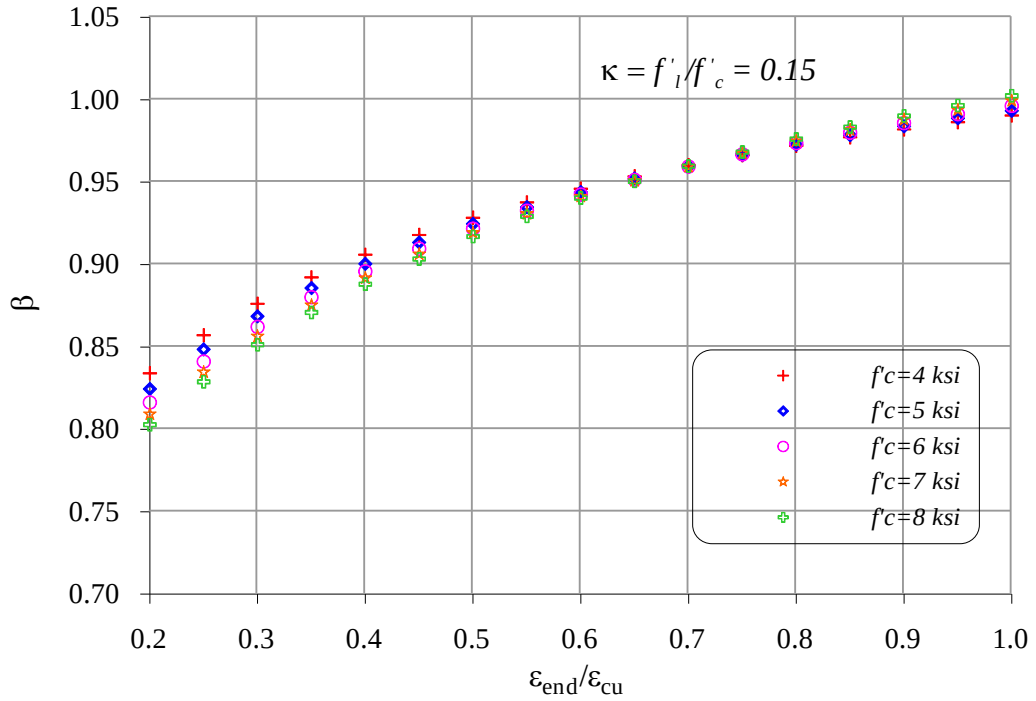

Figure A.6 Variation of β as a function of unconfined concrete strength and $\varepsilon_{end} / \varepsilon_{cu}$ ratio.

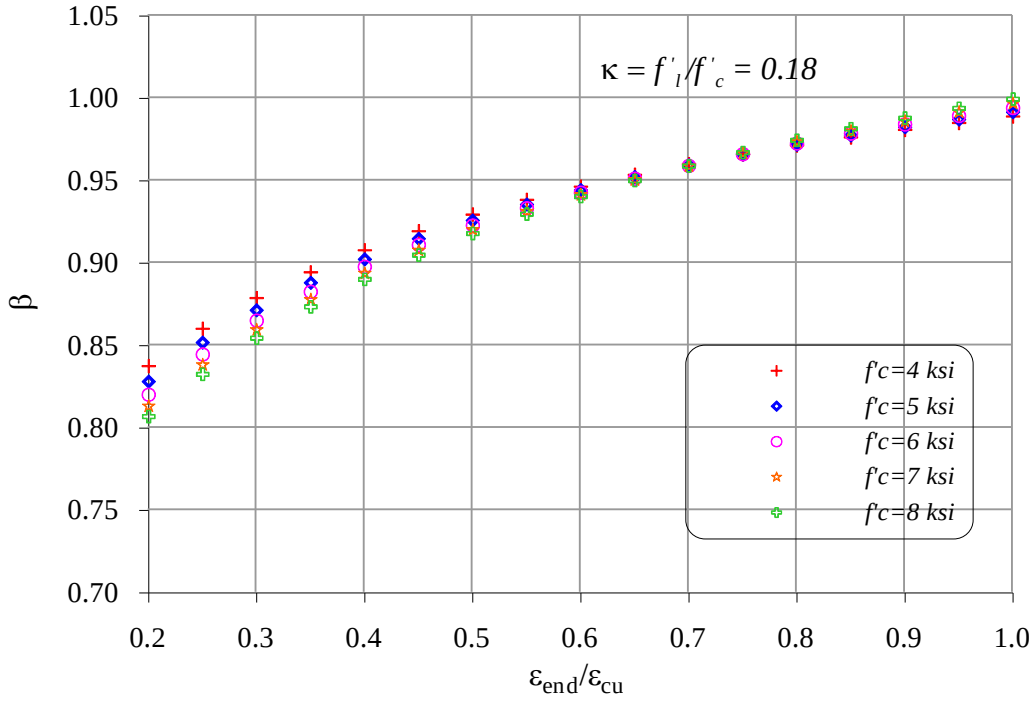

Figure A.7 Variation of β as a function of unconfined concrete strength and $\varepsilon_{end} / \varepsilon_{cu}$ ratio.

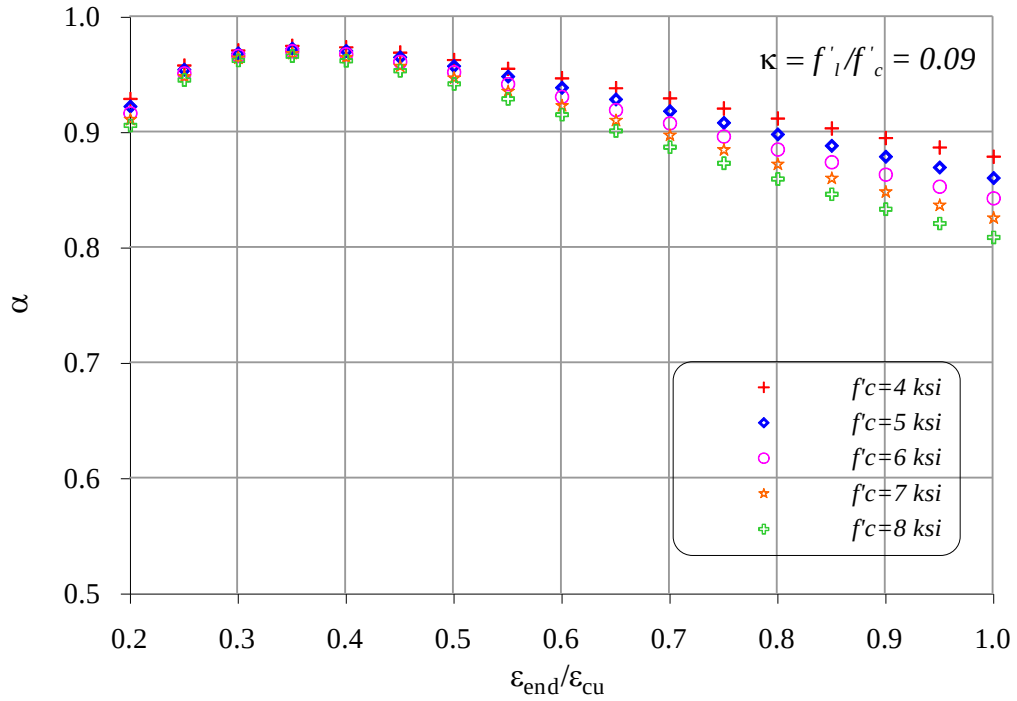

Figure A.8 Variation of α as a function of unconfined concrete strength and $\varepsilon_{end} / \varepsilon_{cu}$ ratio.

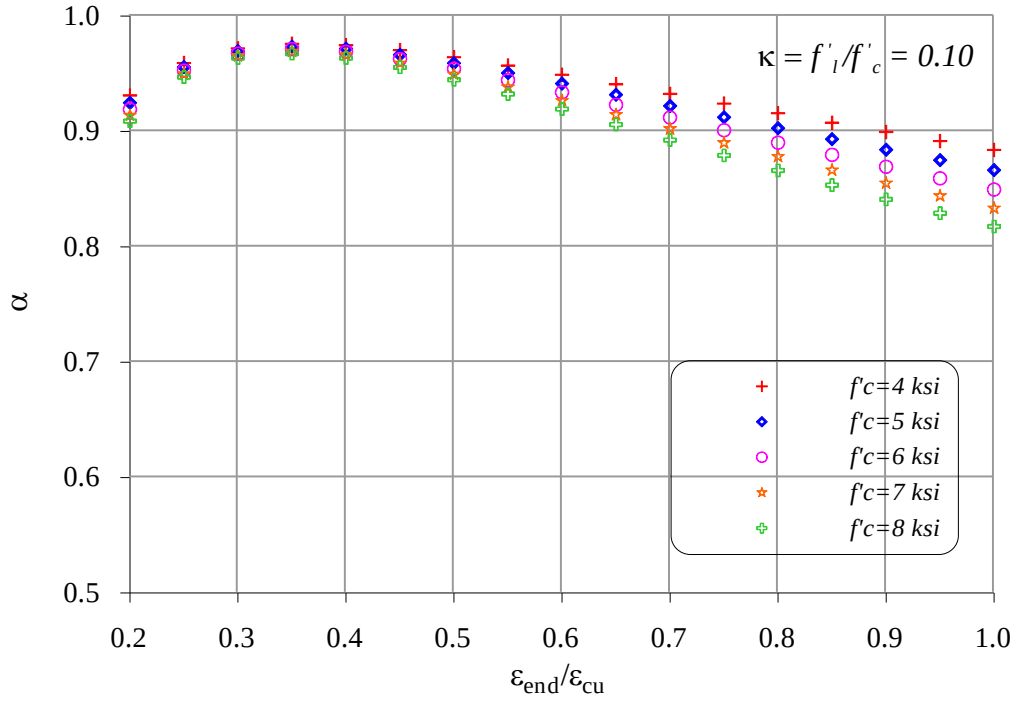

Figure A.9 Variation of α as a function of unconfined concrete strength and $\varepsilon_{end} / \varepsilon_{cu}$ ratio.

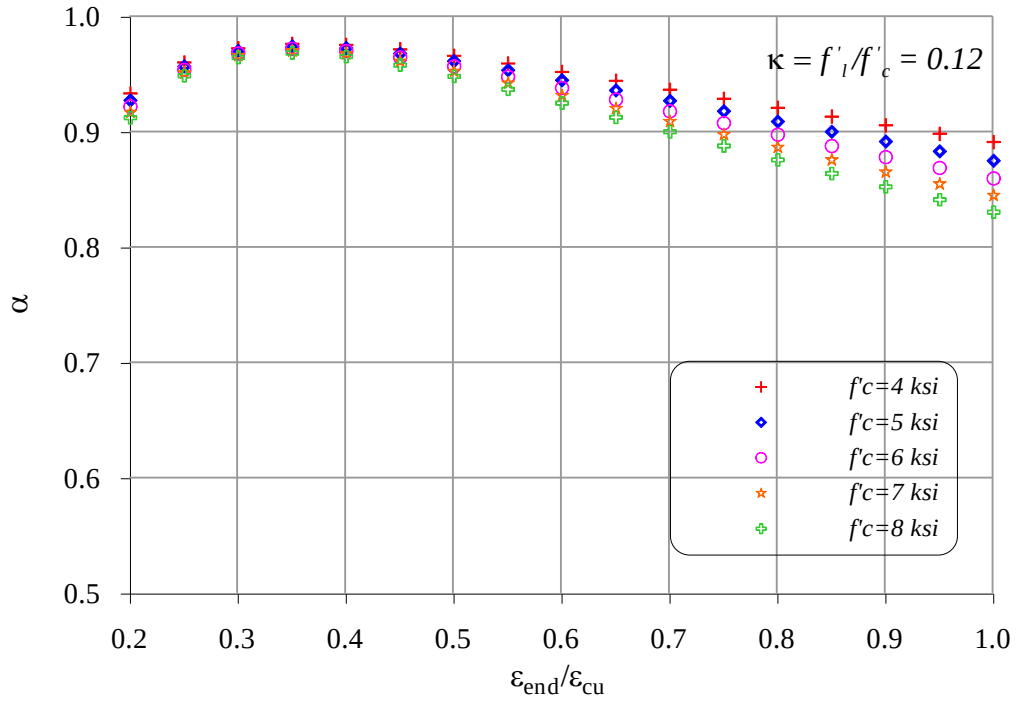

Figure A.10 Variation of α as a function of unconfined concrete strength and $\varepsilon_{end} / \varepsilon_{cu}$ ratio.

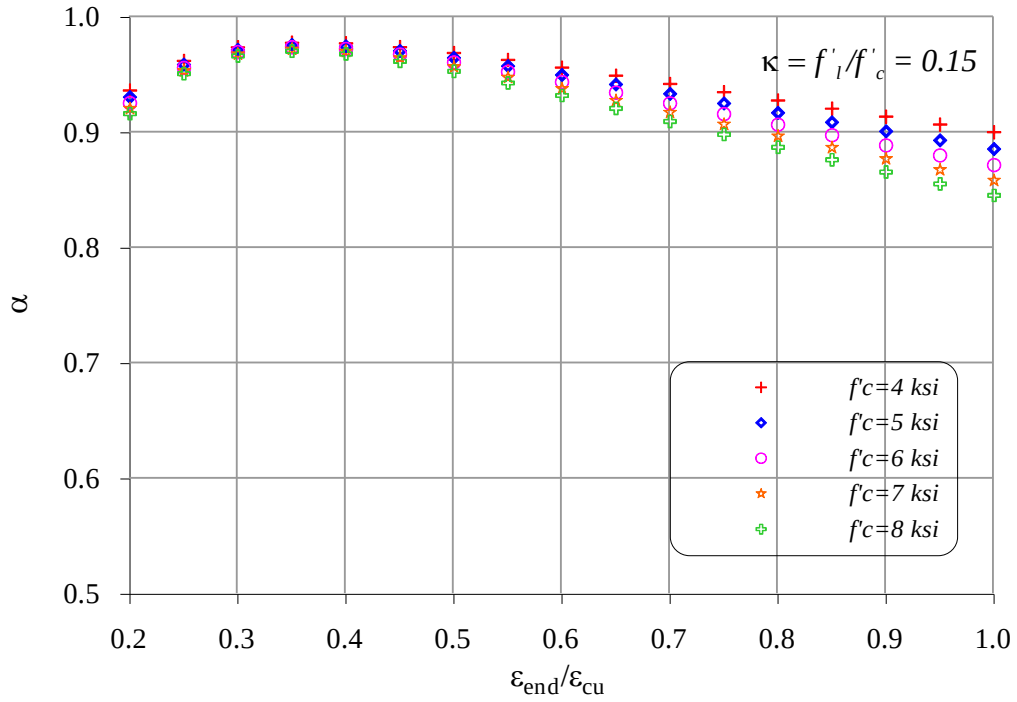

Figure A.11 Variation of α as a function of unconfined concrete strength and $\varepsilon_{end} / \varepsilon_{cu}$ ratio.

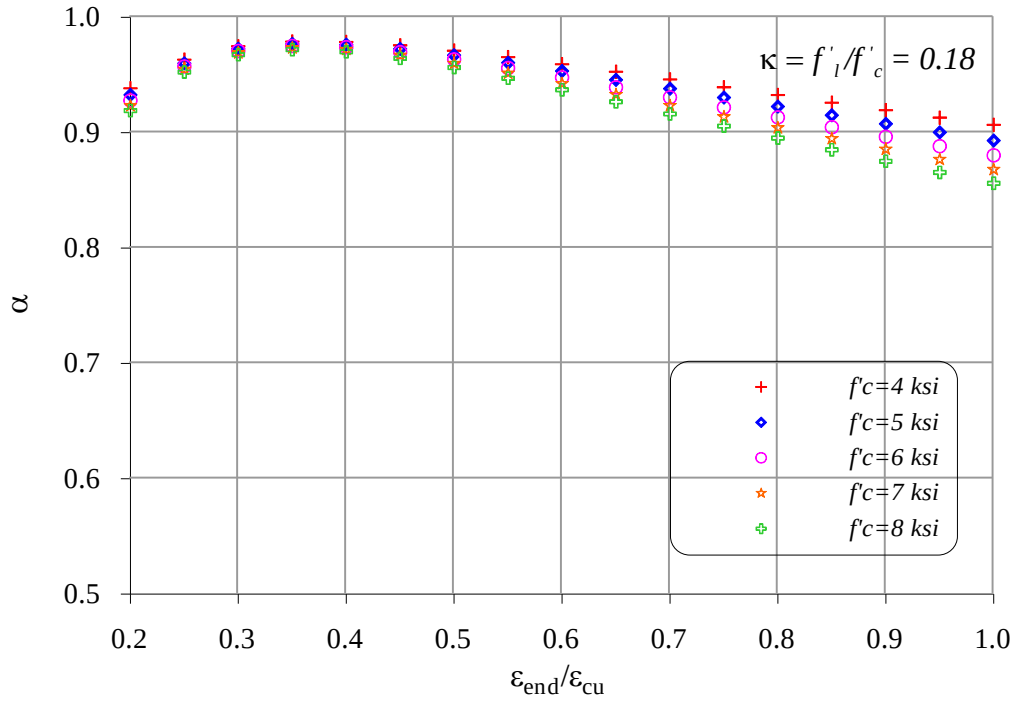

Figure A.12 Variation of α as a function of unconfined concrete strength and $\varepsilon_{end} / \varepsilon_{cu}$ ratio.

Figures A.3 – A.12 clearly show that the value of α and β depend on all three parameters: concrete strength, confinement pressure and the extreme fiber compressive strain. The value calculated for β falls in the range between *0.81* and *1.04* while α varies from *0.75* to *0.96*. Based on the various observations on α and β from different figures, the following conclusions have been drawn:

- In an analysis utilizing an equivalent stress block for confined concrete, using constant values for α and β is inappropriate when ε_{end} varies as part of the analysis.

- When confined concrete is represented by an equivalent stress block, the value of α as a function of $f_c^{'}$ and ($\varepsilon_{end}/\varepsilon_{cu}$) and value of β as a function of ($\varepsilon_{end}/\varepsilon_{cu}$) may be adequately represented using Eqs. A.10 and A.11, respectively. Note that it was found that both equations could be expressed independent of $f_l^{'}$. In addition, it is recognized that the value of β is almost insensitive to $f_c^{'}$ as seen in Figures A.3 – A.7. Figures A.13 – A.16 demonstrate the accuracy of Eqs. A.10 and A.11 for the two extreme values of the

confinement pressures, in which the predicted values of α and β using the equations below are within *±5%* of their actual values.

$$\alpha = \frac{\alpha_0 r\left(\frac{\varepsilon_{end}}{0.35 * \varepsilon_{cu}}\right)}{r - 1 + \left(\frac{\varepsilon_{end}}{0.35 * \varepsilon_{cu}}\right)^r} \tag{A.10a}$$

$$\text{where} \quad \alpha_0 = 0.98 - 0.0022 * f_c^{'}, \quad \textit{and} \tag{A.10b}$$

$$r = 1.24 + 0.01 * \left(\frac{f_c^{'} - 4.0}{0.25}\right) \tag{A.10c}$$

$$\beta = 0.12 \ln\left(\frac{\varepsilon_{end}}{\varepsilon_{cu}}\right) + 1.0 \tag{A.11}$$

- In a design method, where the value of $f_c^{'}$ is fixed and ε_{end} is likely to be in the range of $0.65\varepsilon_{cu}$ to $0.75\varepsilon_{cu}$, constant values may be used for α and β. Considering the values that are typical in current practice (i.e., $f_c^{'}$ = 4 – 6 ksi and $\varepsilon_{end} \approx 0.7\varepsilon_{cu}$), the values of α and β can be taken as follows:

$$\alpha \approx \frac{2 * r * \left(0.98 - 0.0022 * f_c^{'}\right)}{r - 1 + 2^r}, \text{ and} \tag{A.12}$$

$$\beta \approx 0.96 \tag{A.13}$$

To maintain simplicity in design, the value of α may be further approximated to *0.92* with $\alpha * \beta = 0.88$. This simplification should not affect the design significantly because a flexural strength reduction factor of 0.9 is used and that the area of the post-tensioning

steel will be rounded off. However, in the design procedure presented in Chapter 5, Eqs. A.12 and A.13 are used.

- More accurate values for α and β can be used in both design and analysis by using the values directly from the appropriate graphs.

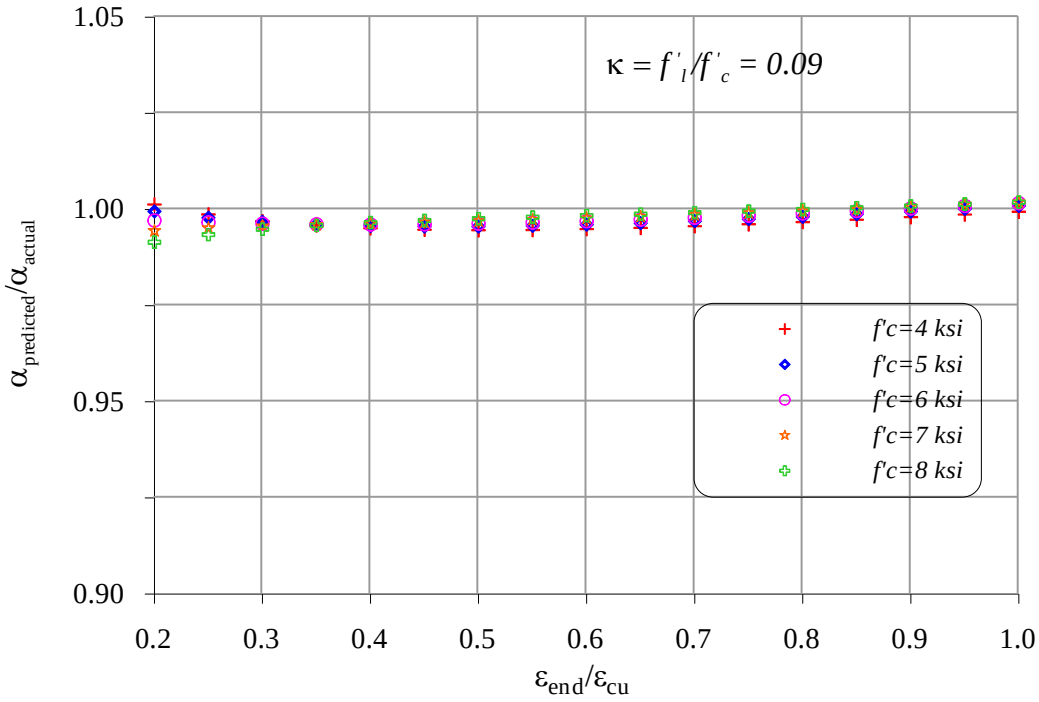

Figure A.13 The $\alpha_{predicted}/\alpha_{actual}$ ratio as a function of unconfined concrete strength and $\varepsilon_{end} / \varepsilon_{cu}$ ratio.

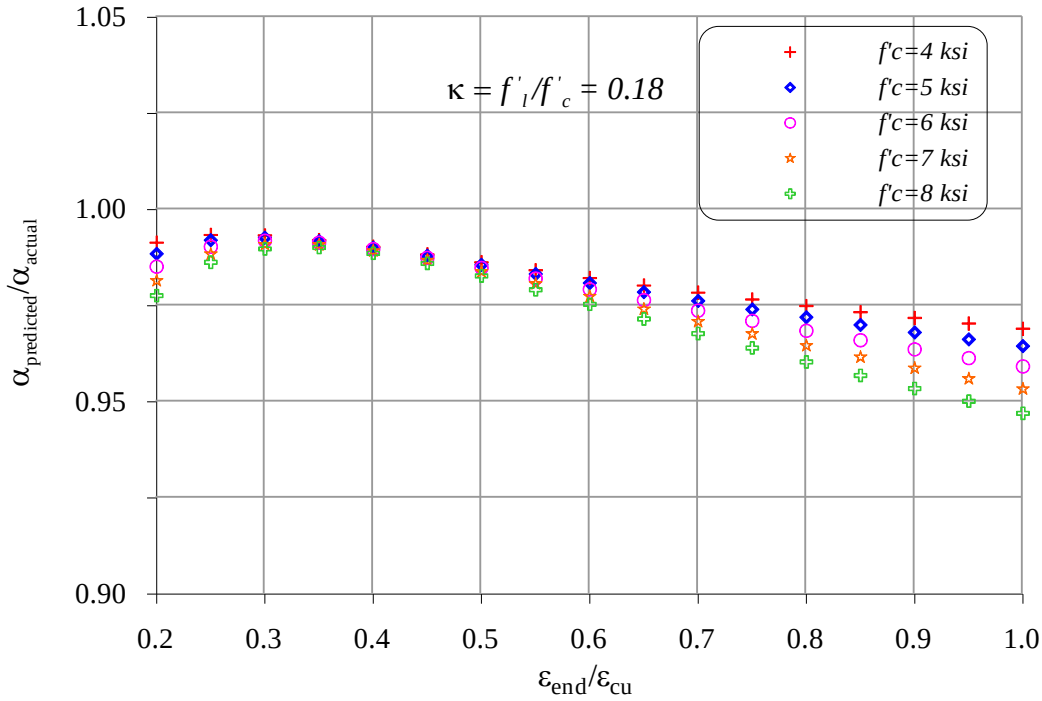

Figure A.14 The $\alpha_{predicted}/\alpha_{actual}$ ratio as a function of unconfined concrete strength and $\varepsilon_{end} / \varepsilon_{cu}$ ratio.

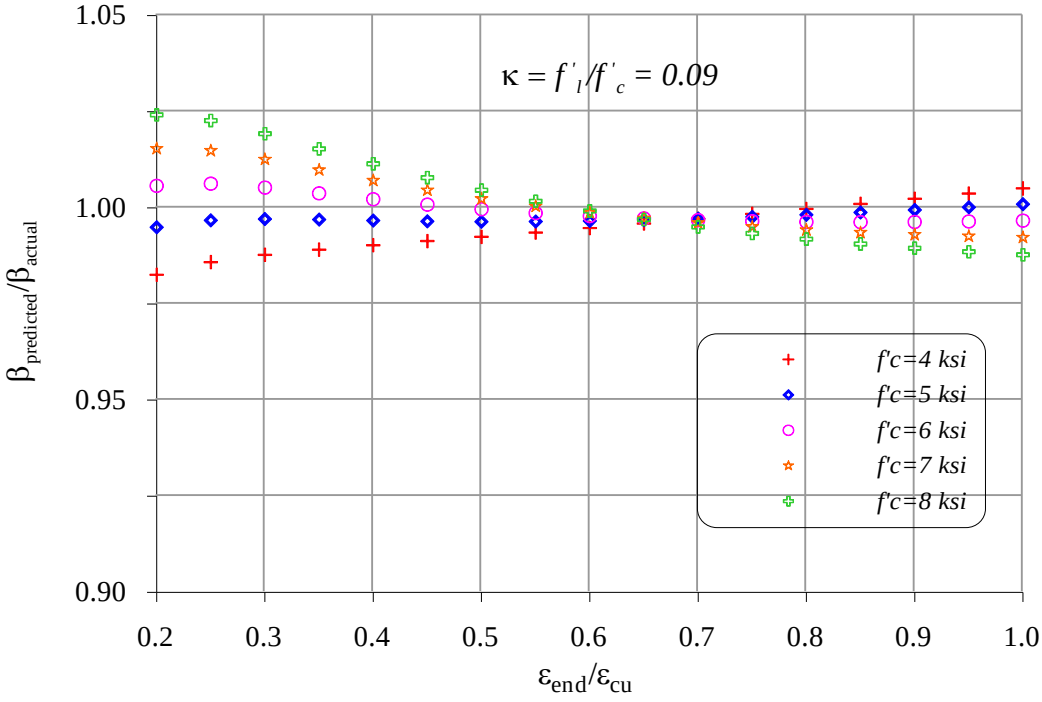

Figure A.15 The $\alpha_{predicted}/\alpha_{actual}$ ratio as a function of unconfined concrete strength and $\varepsilon_{end} / \varepsilon_{cu}$ ratio.

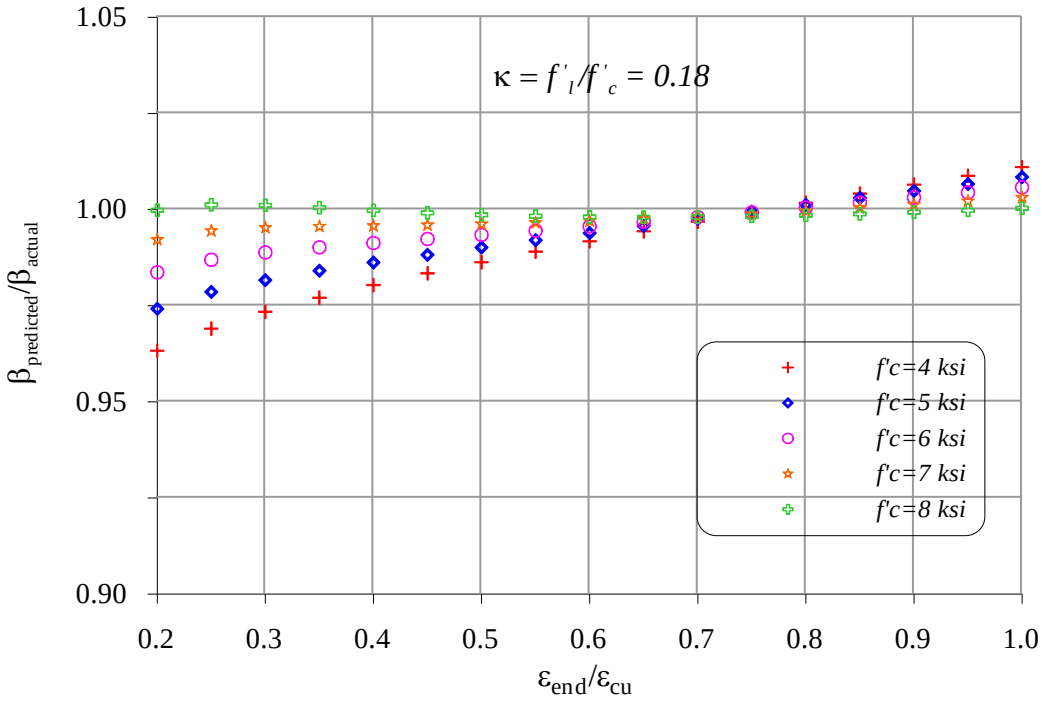

Figure A.16 The $\alpha_{predicted}/\alpha_{actual}$ ratio as a function of unconfined concrete strength and $\varepsilon_{end} / \varepsilon_{cu}$ ratio.

APPENDIX B: DERIVATION OF EQUATIONS TO QUANTIFY THE DESIGN MOMENT OF THE CRITICAL WALL

B.1 Introduction

This appendix presents the derivation of equations that can be used to quantify the design moment for the critical wall in a jointed wall system. It has been stated in Section 5.3 that the leading wall will be the critical wall in a two-wall jointed system, while the intermediate wall will be the critical wall in a jointed system containing three or more precast walls. Consequently, two different derivations are presented.

B.2 Assumptions

To derive the equations to determine the design moments of critical walls, the following assumptions are used.

- All walls in the jointed system have the same geometric properties as well as the same amounts of post-tensioning tendons and initial post-tensioning stress.
- The post-tensioning tendons are located at the center of each wall in the jointed system.
- The post-tensioning tendons in the trailing wall reach the yield stress when the rotation of wall at the base reaches 0.02 radians. Note that all walls are assumed to be subjected to the same rotation at the wall base.
- All vertical joints in the wall system contain an equal number of connectors and all the vertical joints transfer the same amount of shear force at the design drift. (Note that this assumption may not be accurate for an analysis procedure and thus the forces induced by connectors on the wall faces are appropriately taken into account in the analysis.)

B.3 Notation

The following notations are used in the derivation of equations.

A_p = area of post-tensioning tendons in each wall,

c_{lead} = neutral axis depth of the leading wall at design drift,

c_{inter} = neutral axis depth of the intermediate wall at design drift,

c_{trail} = neutral axis depth of the trailing wall at design drift,

E_p = Elastic Modulus of post-tensioning tendons,

f_{yield} = yield strength of the post-tensioning tendons,

f_{lead} = stress in post-tensioning steel in the leading wall at design drift,

f_{inter} = stress in post-tension steel in intermediate wall at design drift,

f_{trail} = stress in post-tensioning steel in trailing wall at design drift,

F_{con} = force in each connector at the design drift,

l_w = length of each wall in a jointed system,

M_{design} = design moment of the jointed wall system,

$M_{design,\ lead}$ = design moment of the leading wall,

$M_{design,\ trail}$ = design moment of the trailing wall,

$M_{design,\ inter}$ = design moment of the intermediate wall,

n = number of walls in a jointed system,

n_{con} = number of connectors in each vertical joint, and

P_D = total dead load acting on each wall.

B.4 Two-wall jointed system

For a two-wall jointed system, the design moment can be expressed as follows.

$$M_{design} = M_{design,lead} + M_{design,trail} = 2M_{design,lead} - (M_{design,lead} - M_{design,trail}) \quad \text{(B.1)}$$

Hence,

$$M_{design,lead} = \frac{M_{design} + (M_{design,lead} - M_{design,trail})}{2} \quad \text{(B.2)}$$

Taking the moment about the location of the resultant compression force in each wall (see Fig. B.1),

$$M_{design,lead} = (P_D + A_p f_{lead})\frac{(l_w - \beta c_{lead})}{2} + F_{con} n_{con}(l_w - 0.5\beta c_{lead}) \quad \text{(B.3)}$$

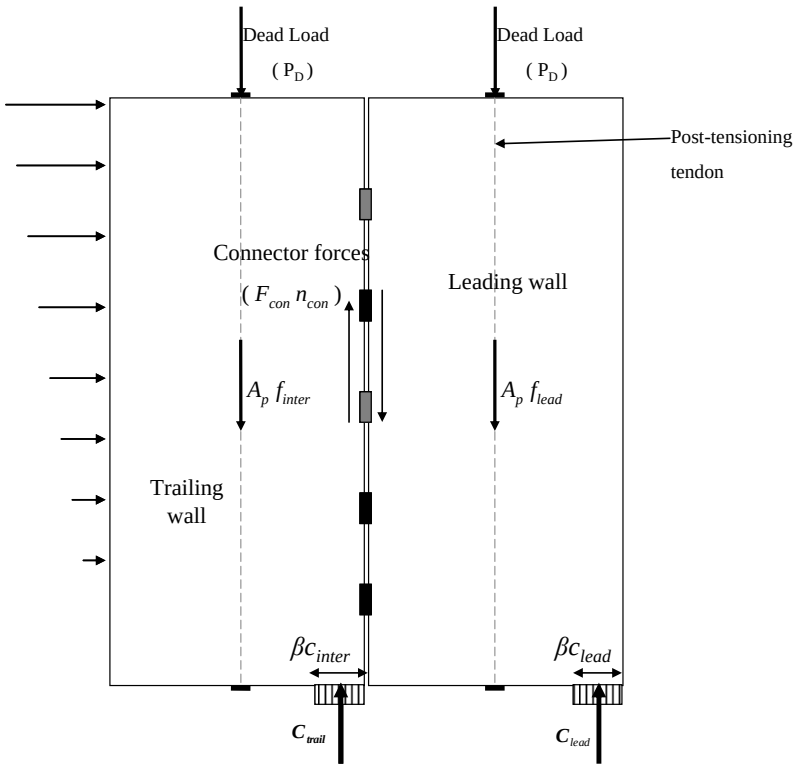

Figure B.1 Magnitudes and location of forces acting on a jointed two-wall system at a design drift.

$$M_{design,trail} = (P_D + A_p f_{trail}) \frac{(l_w - \beta c_{trail})}{2} + 0.5 F_{con} n_{con} \beta c_{trail} \qquad \text{(B.4)}$$

From Eq. (B.3) – Eq. (B.4)

$$M_{design,lead} - M_{design,trail} = F_{con} n_{con} l_w - \beta P_D \frac{(c_{lead} - c_{trail})}{2} + A_p l_w \frac{(f_{lead} - f_{trail})}{2} - F_{con} n_{con} \frac{(c_{trail} + c_{lead})}{2} + \beta A_p \frac{(c_{trail} f_{trail} - c_{lead} f_{lead})}{2} \qquad \text{(B.5)}$$

Lateral load resistance of a jointed wall system at a given drift depends on the geometry and number of walls in the system, the amount of post-tensioning steel, the number of vertical connectors, initial prestressing force, and the cyclic behavior of the vertical connector. To understand the effects of several of these design parameters on the response of jointed wall systems, a parametric study was conducted involving jointed systems consisted of two, three, and four precast walls (Aaleti, 2005). All wall systems were assumed to satisfy the

aforementioned assumptions. From this study, the approximations given in Eqs. (B.6) and (B.7) were established, which are graphically shown in Figures B.2 and B3, respectively.

$$f_{trail} - f_{lead} = \frac{E_p \theta_{des} (c_{lead} - c_{trail})}{h_{wall}} \approx 0.05 f_{yield} \tag{B.6}$$

$$(c_{lead} f_{lead} - c_{trail} f_{trail}) \approx 0.04 f_{yield} l_w \tag{B.7}$$

Furthermore, considering the forces acting on the leading wall, the following condition may be used to ensure recentering of the wall system (Stanton and Nakaki, 2002),

$$A_p f_{yield} \frac{l_w}{2} \geq n_{con} F_{con} l_w \tag{B.8}$$

By substituting Eqs. (B.6 – B.8) into Eq. (B.5),

$$\begin{aligned} M_{design,lead} - M_{design,trail} = {} & F_{con} n_{con} l_w - \beta P_d \frac{(c_{lead} - c_{trail})}{2} \\ & - 0.045 A_p l_w f_{yield} - \beta F_{con} n_{con} \frac{(c_{trail} + c_{lead})}{2} \end{aligned} \tag{B.9}$$

Using Eq. B.8,

$$M_{design,lead} - M_{design,trail} \leq 0.91 F_{con} n_{con} l_w - \beta P_d \frac{(c_{lead} - c_{trail})}{2} - \beta F_{con} n_{con} \frac{(c_{trail} + c_{lead})}{2} \tag{B.10}$$

Recognizing that the two negative terms on the right hand side of the above equation are relatively small compared to the positive term, the design moment of the leading wall is established as follows.

From Eq. B.8,

$$M_{design,lead} - M_{design,trail} \leq 0.9 F_{con} n_{con} l_w \tag{B.11}$$

Substituting Eq. B11 into B.2,

$$M_{design,lead} \le \frac{M_{design} + 0.9F_{con}n_{con}l_w}{2} \quad \text{(B.12)}$$

Conservatively, the design moment is approximated using Eq. B.13.

$$M_{design,lead} = \frac{M_{design} + 0.9F_{con}n_{con}l_w}{2} \quad \text{(B.13)}$$

B.5 Jointed system with more than two walls

Similar to the two-wall jointed system, the design moment of a three-wall jointed system can be expressed as follows.

$$\begin{aligned} M_{design} &= M_{design,lead} + M_{design,trail} + M_{design,inter} \\ &= 3M_{design,inter} - (M_{design,inter} - M_{design,lead}) - (M_{design,inter} - M_{design,trail}) \end{aligned} \quad \text{(B.14)}$$

The critical wall in a multiple wall system having more than two walls is the intermediate wall. Therefore, the critical design moment from Eq. B.14 is,

$$M_{design,inter} = \frac{M_{design} + (M_{design,inter} - M_{design,lead}) + (M_{design,inter} - M_{design,trail})}{3} \quad \text{(B.15)}$$

Taking the moment about the location of the resultant compression force for each wall (see Fig. B.4),

$$M_{design,inter} = (P_D + A_p f_{l\,inter}) \frac{(l_w - \beta c_{inter})}{2} + F_{con}n_{con}l_w \quad \text{(B.16a)}$$

$$M_{design,lead} = (P_D + A_p f_{lead}) \frac{(l_w - \beta c_{lead})}{2} + F_{con}n_{con}(l_w - 0.5\beta c_{lead}) \quad \text{(B.16b)}$$

$$M_{design,trail} = (P_D + A_p f_{trail}) \frac{(l_w - \beta c_{trail})}{2} + 0.5 F_{con} n_{con} \beta c_{trail} \quad \text{(B.16c)}$$

From Eq. B.16,

$$\begin{aligned}(M_{design,inter} - M_{design,lead}) + (M_{design,inter} - M_{design,trail}) \\ = \beta A_p \frac{(c_{trail} f_{trail} + c_{lead} f_{lead} - 2c_{inter} f_{inter})}{2} \\ + F_{con} n_{con} (l_w + 0.5\beta c_{lead} - 0.5\beta c_{inter}) \\ + 0.5 A_p l_w (2 f_{inter} - f_{lead} - f_{trail})\end{aligned} \quad \text{(B.17)}$$

Assuming that $f_{lead} \approx f_{inter}$, and $(c_{lead} f_{lead} + c_{trail} f_{trail} - 2c_{inter} f_{inter}) \approx 0$, and using Eqs. B.6 and B.8

$$\begin{aligned}(M_{design,inter} - M_{design,lead}) + (M_{design,inter} - M_{design,trail}) \\ \approx F_{con} n_{con} l_w + 0.025 A_p l_w f_y \\ \approx F_{con} n_{con} l_w + 0.05 F_{con} n_{con} l_w\end{aligned} \quad \text{(B.18)}$$

Hence,

$$(M_{design,inter} - M_{design,lead}) + (M_{design,inter} - M_{design,trail}) \approx 1.05 F_{con} n_{con} l_w \quad \text{(B.19)}$$

Substituting B.19 into B.13,

$$M_{design,inter} \approx \frac{M_{design} + 1.05 F_{con} n_{con} l_w}{3} \quad \text{(B.20)}$$

Therefore, the design moment of the critical wall may be estimated using Eq. B.21.

$$M_{design,lead} = \frac{M_{design} + 1.05 F_{con} n_{con} l_w}{3} \quad \text{(B.21)}$$

Eq. 19 can now be extended to jointed system consisting of n walls as follows:

$$M_{design} = M_{design,lead} + M_{design,trail} + (n-2)M_{design,inter} = nM_{design,inter} - (M_{design,inter} - M_{design,lead}) - (M_{design,inter} - M_{design,trail}) \quad \text{(B.22)}$$

$$M_{design,inter} = \frac{M_{design} + (M_{design,inter} - M_{design,lead}) + (M_{design,inter} - M_{design,trail})}{n} \quad \text{(B.23)}$$

Using Eq. B.19, the critical design moment of the wall system can be established from Eq. B.23.

$$M_{design,inter} = \frac{M_{design} + 1.05F_{con}n_{con}l_w}{n} \quad \text{(B.24)}$$

B.6 Conclusions

- In a design of a two-wall jointed system, the critical design moment corresponding to the leading wall can be estimated as

$$M_{design,lead} = \frac{M_{design} + 0.9F_{con}n_{con}l_w}{2}$$

- In a design of a multiple-wall jointed system containing n walls (where n > 3), the critical design moment corresponding to an intermediate wall can be estimated as

$$M_{design,inter} = \frac{M_{design} + 1.05F_{con}n_{con}l_w}{n}$$

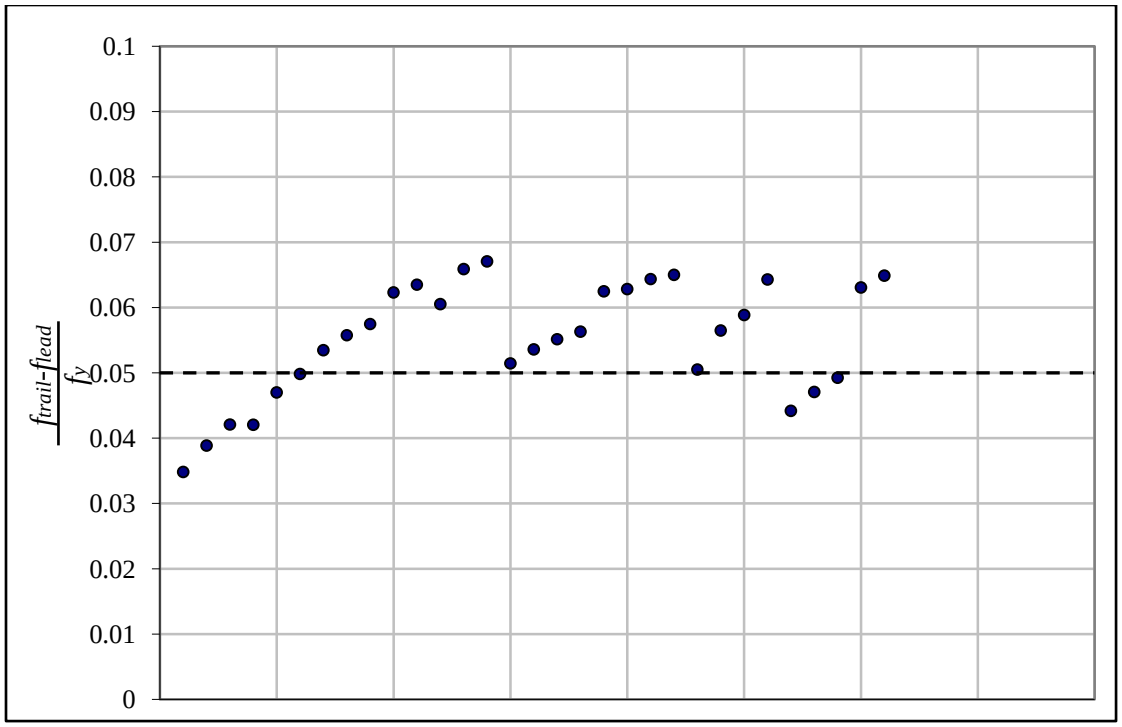

Figure B.2 Approximating $(f_{trail} - f_{lead})/f_y$ using results from different jointed walls used in a parametric study (Aaleti, 2005).

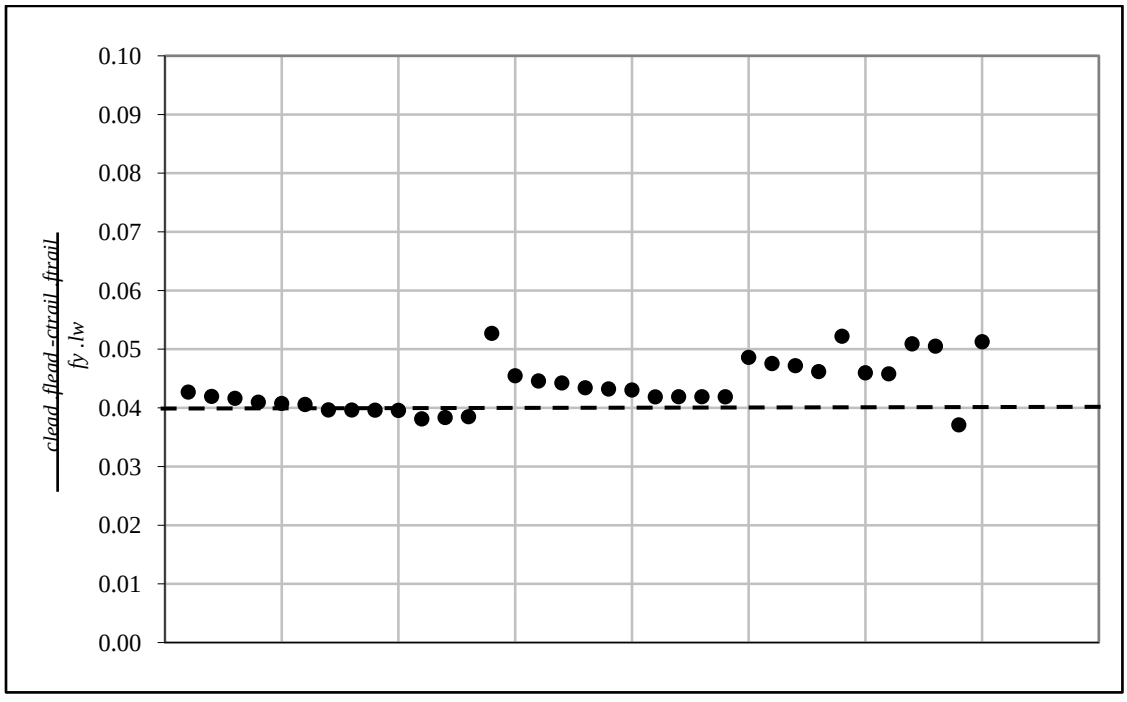

Figure B.3 Approximating $(c_{lead} f_{lead} - c_{trail} f_{trail})/f_y l_w$ using results from different jointed walls used in a parametric study (Aaleti, 2005).

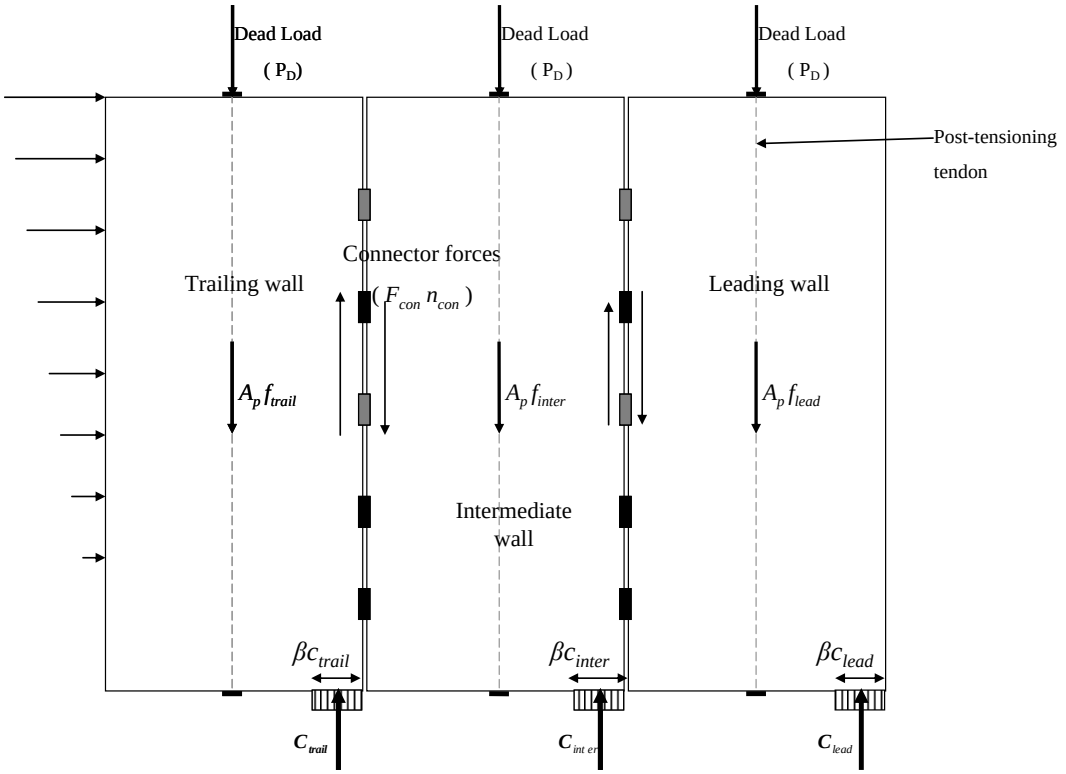

Figure B.4 Magnitudes and location of forces acting on a jointed three-wall system at a design drift.

Intentionally blank